Force Reflecting Hand Controller for Manipulator Teleoperation

Final Techncial Report

Contract #NAS7-1069

Mark D. Bryfogle

Meridian Corporation
4300 King Street
Alexandria, VA 22303-1508

December 31, 1991

1/13/92

Abstract

A force reflecting hand controller based upon a six degree of freedom fully parallel mechanism often termed a Stewart Platform has been designed constructed and tested as an integrated system with a slave robot manipulator test bed. A force reflecting hand controller comprises a kinesthetic device capable of transmitting position and orientation commands to a slave robot manipulator while simultaneously representing the environmental interaction forces of the slave manipulator back to the operator through actuators driving the hand controller mechanism. The Stewart Platform was chosen as a novel approach to improve force reflecting teleoperation because of its inherently high ratio of load generation capability to system mass content and the correspondingly high dynamic bandwidth. An additional novelty of the program was to implement closed loop force and torque control about the hand controller mechanism by equipping the handgrip with a six degree of freedom force and torque measuring cell. The mechanical, electrical, computer and control systems are discussed and system tests are presented.

Contents

List of Figures

List of Tables

Chapter 1

Introduction and Program Synopsis

This final report documents a Small Business Innovation Research (SBIR) Phase II program to develop a hardware testbed of a novel approach to a force reflecting hand controller for manipulator teleoperation. This report covers research from July 1989 to July 1991. The Phase I program ran from March 1988 to August 1988.

1.1 Technical Background and Program Motivation

This research falls within the general realm of manipulator teleoperation and the human machine interface. A manipulator is a mechanical motion generating device. Manipulator teleoperation can be defined as the command and control of the manipulator from a distance or position far removed from the manipulator. In particular we are interested in the manipulator end effector when viewed as a rigid body independent of any grippers or fingers mounted on the end effector. In this context, the commands can take the form of position and orientation (pose), force and torque, or combinations of the above.

The questions arise as to the method of command formulation for the manipulator and the means by which the human operator expresses his command intentions to the manipulator system. This means is referred to as the man machine interface. Humans are endowed with five senses as delineated in Table 1.1. The sense of touch is subdivided into the tactile and kinesthetic capabilities. The tactile sense embodies pressure and heat discrimination, while the kinesthetic sense embodies the knowledge of the position of body parts from nerves in the musculature. Humans have the additional capability of speech which can justifiably be classified under the tactile or kinesthetic sense since speech is modulated through pressure or muscle tension sensing in the vocal cords. In the table, senses are classified according to input and output capability relative to the human. The

Sense	Manifestations	Input Capability	Output Capability	Degrees of Freedom
Touch - Kinesthetic	Hand Pose	Yes	Yes	6
Touch - Tactile	Fingertip Contact	Yes	Yes	1 per digit
Touch - Kinesthetic	Retina Orientation	No	Yes	2
Touch - Kinesthetic	Speech	No	Yes	Multiple
Sight	Viewing	Yes	No	Multiple
Taste	Tasting	Yes	No	Multiple
Smell	Smelling	Yes	No	Multiple
Hearing	Hearing	Yes	No	Multiple

Table 1.1: Human Sensor Capabilities

output capability is necessary to formulate commands to the manipulator. The input capability can be used strategically to provide the operator the necessary information to formulate command decisions.

Of the eight sensing manifestations cited in the table, only the first four are candidates for manipulator command formulation. The first entry, hand pose, has the most immediate usefulness to the teleoperation problem since it is bilateral and works in six degrees of freedom (DOF). Fingertip touch is also useful, for example in typing numerical pose entries on a keyboard or working with a touchscreen or robot teach pendant. For sophisticated applications with multiple DOF, fingertip touch breaks down due to the inherent slow speed of formulating commands with individual finger strokes. Retinal tracking has capabilities for command formulation, however it is limited to two DOF. Voice has potential for flexible command formulation, however it is also slow and limited by the human time to express his commands vocally, and the time associated with a computer interpreting the speech image. The last four entries have no capability for command formulation and are included only for the benefit of demonstrating a complete argument.

Excluding direct computer interpretation of human thought or brain waves, the pose of the operator's hand represents the ultimate method through which the human can express the desired pose and environmental interaction forces to a manipulator. A one to one correspondence exists between the six DOF pose of the hand and that of the manipulator end effector. The human need not translate his desire into words or key strokes which in turn must be mapped back to pose coordinates by the computer controlling the manipulator. The kinesthetic sense or eye hand coordination is highly developed in humans. A baseball player hardly considers the path coordinates of the bat while striking the ball. Rather he concentrates on the target ball path, and the muscles respond accordingly as if preprogrammed. Accessing the kinesthetic sense of the hand is therefore highly desirable for commanding manipulators.

Now consider the problem of detecting the pose of the operator's hand. Two basic

methods are available, isometric and large motion range devices. The isometric devices constrain the hand and sense only small motion deviations from center through the mechanical displacement of the constraining structure and a suitable displacement transducer. These devices necessarily saturate the input portion of the hand pose comprising the operator's ability to sense forces and torques through his hand. The large motion range device conversely requires passive sensing of the hand pose.

The sensing can directly or indirectly measure the hand pose. In the direct case the transducing options include electromagnetic such as laser reflection or capacitive probes, or acoustic. These approaches often suffer in accuracy and generally do not allow the possibility for force feedback to the operator. It is conceivable that the operator could grasp an electric or magnetic dipole which could interact with a corresponding capacitive or inductive grid to simultaneously sense and drive the dipole. However this would require a very high resolution switching grid, consume a large amount of electric power, and create enormous amounts of electromagnetic noise in sensitive environments. As a closure to the direct measurement approach, one should consider the interesting but distant future possibility of directly measuring the hand pose while simultaneously creating the illusion of force in the operators hand through some sophisticated form of neural stimulation.

The indirect measurement means requires that the operator grasp a mechanical linkage equipped with passive position transducers at the mechanical joints. The mechanical linkage allows the opportunity to incorporate actuators which can be driven to produce an arbitrary force and torque state at the operator's hand. Such a device is termed a force reflecting hand controller and represents the object of this research program. Force feedback is highly desirable in teleoperation applications and has been shown to dramatically reduce task completion times [M1].

The force reflecting hand controller has the advantages of allowing pose sensing and force feedback. It has the disadvantage of introducing mass into the system. Mass has the undesirable attributes of inertia and friction forces, both of which can be mistaken by the operator as forces experienced by the manipulator while interacting with the environment. Additionally, mass introduces gravitational forces which must be compensated by the actuators.

The force reflecting hand controller has application in both teaching manipulator motions which can be played back at a later time and in direct "on line" continuous teleoperation. The need for teleoperation has been attacked with the argument that supervisory control is the optimum method for manipulator control. Under supervisory control, a multitude of manipulation tasks are preprogrammed. The operator accomplishes his work assignment by merely selecting the appropriate program at the appropriate time. This argument is countered by the notion of the impossibility of accurately predicting every possible manipulation task, and the need for flexibility when accidents and the like have altered the previously highly structured environment. Supervisory control incurs the expense of painstakingly structuring the environment. At a minimum, the force reflecting hand controller can be very usefully employed in developing programs for supervisory control. At the maximum, it offers extreme flexibility to respond to dynamically changing environments.

Manipulator teleoperation has the most immediate application in manipulator teaching, and in space, undersea, radioactive and chemically toxic environments which represent dangers to human well being. Programming manipulators represents a significant cost barrier to their application to industrial manufacturing environments. The United States, European, and Japanese ambitions to construct permanently manned space stations will require manipulators for construction and maintenance. The United States is actively beginning the remediation of the chemical and nuclear wastes associated with fifty years of weapon manufacture. Eastern Europe is known to have massive industrial waste zones requiring remediation. All these applications make teleoperation a very worthy candidate for research investment.

1.2 Current Systems and Research Initiatives

In discussing the research initiatives, it is appropriate to first discuss the currently available systems. To the best of the author's knowledge, two isometric input devices are available on the open market. The first is offered by Norwalk Systems, located in Norwalk, Connecticut. The second was designed by Dr. Gerhard Herzinger under the auspices of DLR [H1]. Both devices feature six DOF command capability through strain gauge sensing.

Two kinesthetic devices have been developed. The first by the Jet Propulsion Laboratory [B1] features an electric, direct current, cable driven, six axis mechanism with the kinematic structure depicted in Figure 1.1. The second device is manufactured by Kraft Robotics and features alternating current electric motors with gearing and an all revolute joint kinematic structure with six DOF depicted in Figure 1.2.

Both of these devices occupy large volumes of space. Speaking qualitatively, the JPL device has a very smooth feel. The JPL device balances gravitational forces by incorporating an elaborate set of moving masses at the expense of additional inertia content and the potential for mechanical vibration modes associated with these masses. The Kraft robotics device incorporates large gear reductions at each joint and therefore develops a very large inertia with respect to the handgrip such that the system approaches non backdriveablility with respect to the handgrip. The large forces associated with accelerating the mass content of the motors can be confused by the operator with forces experienced by the manipulator and therefore degradates the fidelity of the force feedback.

This program introduced two primary research initiatives:

- The force reflecting hand controller mechanism would utilize a fully parallel six DOF mechanism commonly referred to as the "Stewart Platform," [S1] shown in Figure 1.3,
- The hand controller mechanism would be equipped with a six DOF force/torque sensing cell in the handgrip to provide closed loop feedback around the hand controller mechanism.

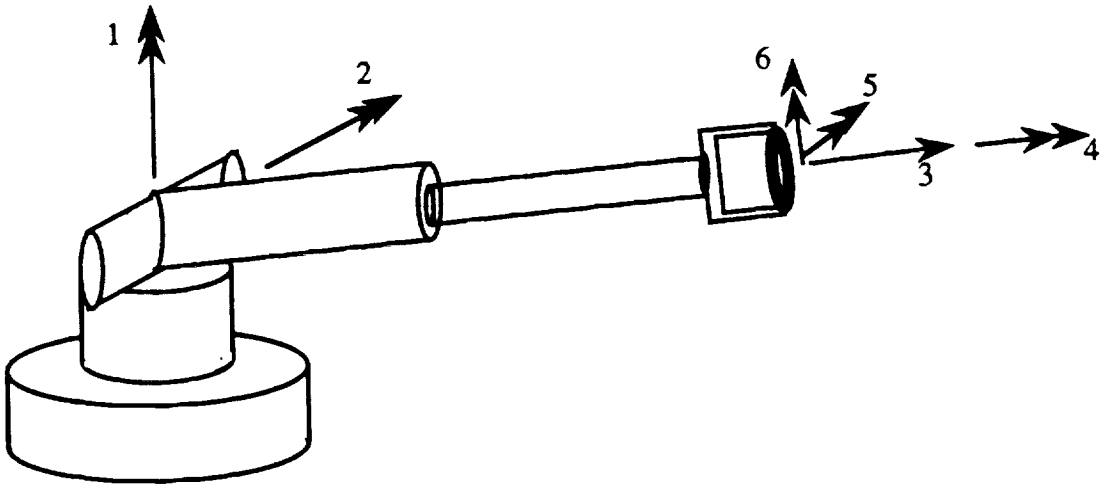

Figure 1.1: Kinematic Structure of the JPL Hand Controller

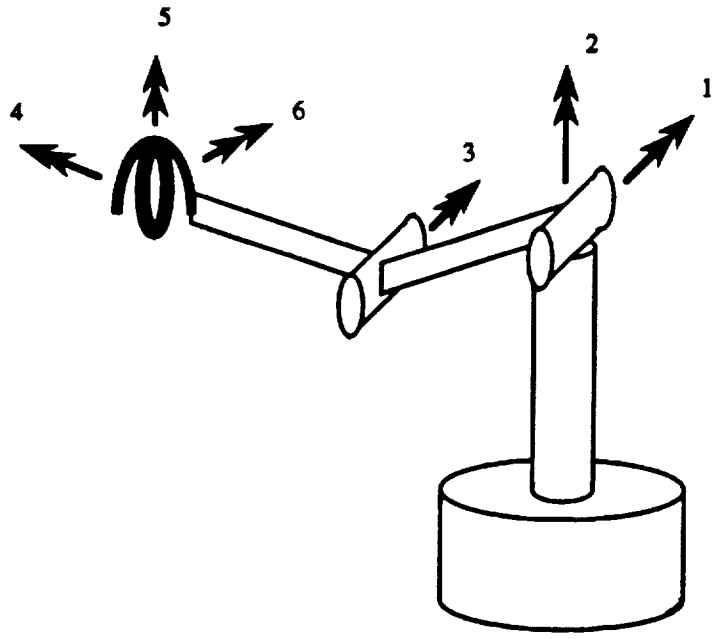

Figure 1.2: Kinematic Structure of the Kraft Robotics Hand Controller

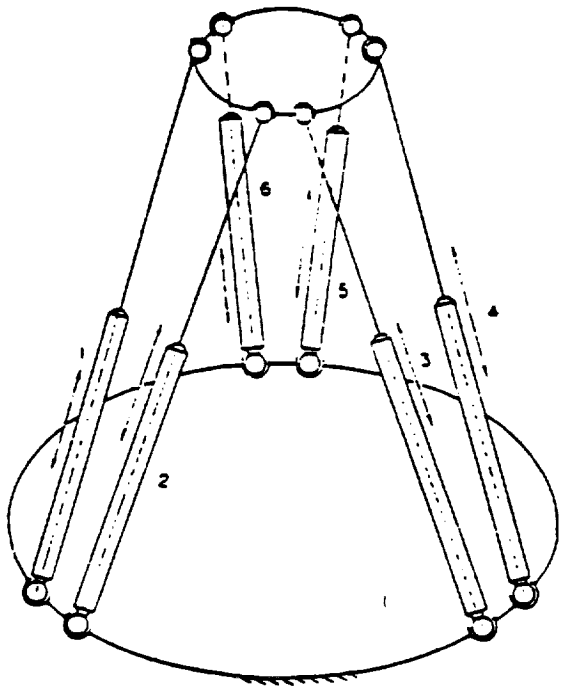

Figure 1.3: Stewart Platform Generic Kinematic Layout

The program plan provided for the design, construction and test of the Stewart Platform based force reflecting hand controller as an isolated subsystem in a bilateral teleoperator system. The program further provided that the system be integrated through a universal interface developed under the program with a slave robot manipulator for system level testing.

The research initiatives were introduced to realize the following objectives characteristic to space teleoperation:

- A force reflecting hand controller of small volume to function effectively in the restricted confines of a space vehicle,
- A force reflecting hand controller which could be "broken down" when not in use and stowed conveniently,
- A force reflecting hand controller with minimum mass therefore being a more worthy candidate for space flight,

Additionally as pure research objectives not directly related to space development, the following were put forward:

- A force reflecting hand controller having extremely high dynamic bandwidth and force feedback fidelity,

- A robotic mechanism having extremely high load generating capability to mass content ratio,
- Design methodologies for Stewart Platform mechanism realizations,
- Analysis of and empirical findings for the performance limitations of Stewart Platform mechanism,

The Stewart Platform mechanism and the control architecture are discussed in great detail in following report chapters. In general, the Stewart Platform is associated with the objectives pertaining to a smaller, lighter hand controller mechanism. By contrast with the JPL and Kraft devices, the Stewart Platform distributes loads across all actuators as opposed to the former mechanisms which isolate and sum loads into actuators through the cantilevered architecture. The force sensing cell in the handgrip is generally associated with the higher dynamic bandwidth.

1.3 Theoretical Considerations, Performance Requirements and Design Philosophy

This program represented the first attempt to realize a Stewart Platform based force reflecting hand controller. No previous system existed upon which to develop a rigorous set of performance requirements. However previous research in the general field delineates a clear set of theoretical considerations, and suggests a general set of performance requirements. Given the unconventional nature of the work, it became necessary to supplement rigorous performance standards with an intuitive design philosophy.

The following theoretical considerations are cited with respect to the force reflecting hand controller and bilateral teleoperation:

Mobility: Mobility is defined as the number of DOF of the hand controller handgrip.

Update Rate: The update rate represents the frequency with which the controlling computer can communicate the data and write new commands to the servo motors on both master and slave. This has a significant effect on system stability and force feedback fidelity.

Time Delay: The time delay is closely related to the update rate. It represents the amount of time associated with the unilateral transmission of information from either hand controller to slave manipulator or from slave manipulator to the hand controller. Significant time delays can cause operator disorientation.

Force Feedback Fidelity: This refers to the accuracy and amount of distortion with which the hand controller represents the force information to the operator. The frequency content of the force feedback is thought to be a significant parameter.

Translational Volume	300 mm (12 in.) cube
Incremental Translation	0.5 mm (.02 in)
Orientational Range	See Figure 1.4 [K1]
Force Feedback Range	0.5-15 N (1-30 lbf)
Incremental Force	5% of Applied Force
Torque Feedback Range	0.013-0.69 Nm (0.1-5 foot pounds)
Incremental Torque	5% of Applied Torque
Force Feedback Frequency Content	Less Than 0.64 Hz
Time Delay	Less Than 0.1 sec.
Mechanism Friction	Minimum; Less Than 0.25 N (0.5 lbf)
Update Rate	Greater Than 50 Hz.

Table 1.2: System Design Parameters

Cross Coupling: In the context of teleoperation, cross coupling refers to the inability of the human to exactly discriminate between rotations and translations or correspondingly between forces and torques. It arises primarily from the human inability to exactly perceive the center of the hand controller mechanism. For example, if the operator grasps the handgrip such that the center of the operator's hand and that of the hand controller do not coincide, then a pure force generated by the hand controller through its center will require the operator to generate a balancing force and torque which will lead the operator to believe that the slave manipulator is experiencing a torque loading. The common approach to alleviating this difficulty is to partition the system through software into a translational and rotational operational modes.

Given the above definition of some of the theoretical considerations, we now wish to assign quantitative design parameters to them and the other general design parameters. The design parameters are displayed in Table 1.2.

The translational volume specification is very subjective and varies largely with the space constraints imposed upon the mechanism. The orientational range of motion is taken from the human wrist capability. Almost all robot manipulators have a wrist rotational motion greater than that of the wrist requiring some rereferencing technique. The incremental motions relate to the human capability to create small motions and indicate the resolution required of the sensing system. The force and torque feedback ranges are also somewhat arbitrary depending upon the application. In space applications the magnitudes must be kept small due to the inability of the astronaut to generate counterbalancing forces. The frequency content limitation stems from a fundamental human limitation to track and respond to high frequencies [M2,M3]. The notion here is that if the hand controller can adequately reproduce high frequencies, the human would not be able to balance them so that they should not be passed on to the human.

Given some of the uncertainties in the above, the design philosophy became one of vastly

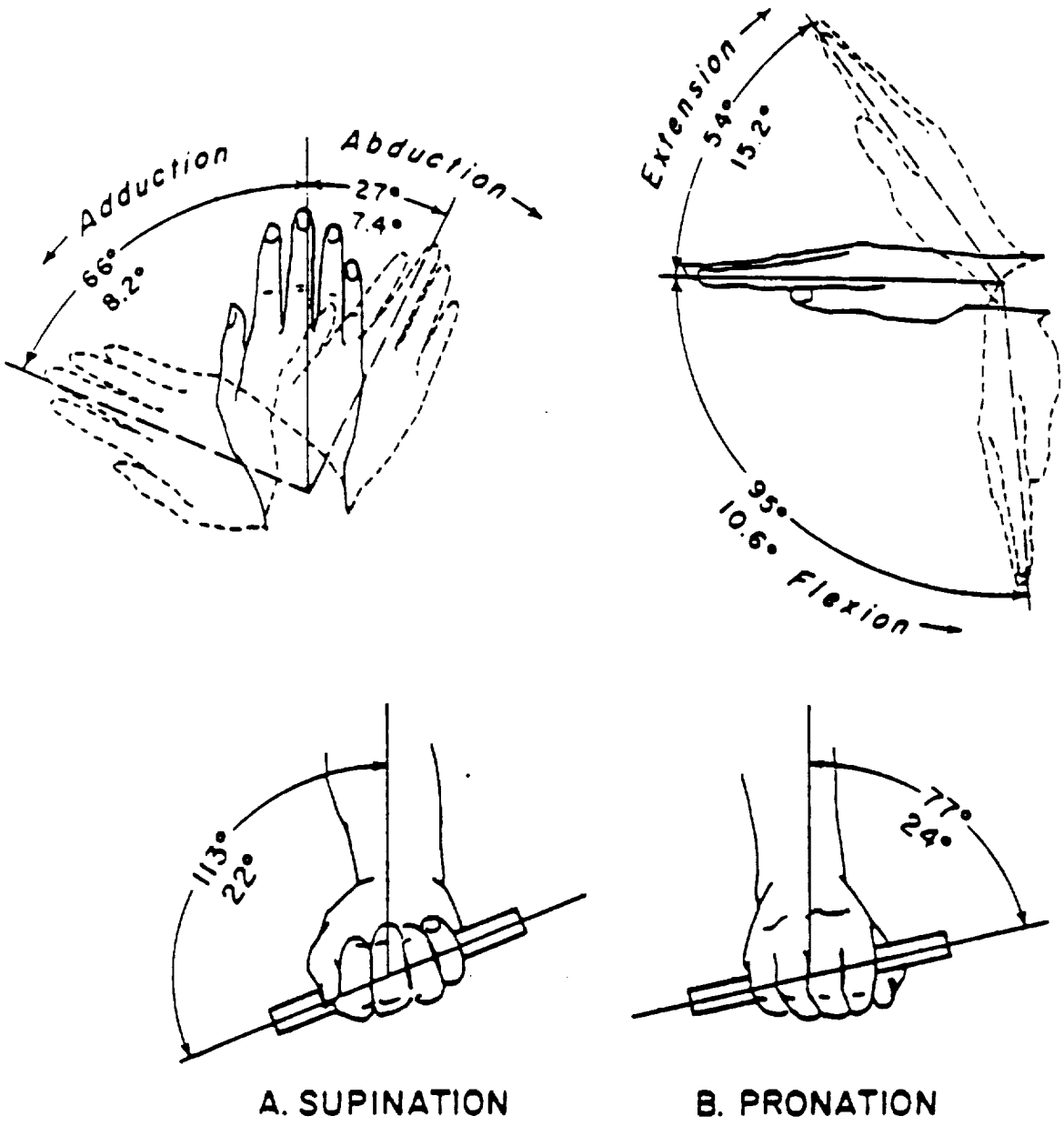

Figure 1.4: Human Hand Orientational Range of Motion

overdesigning the system with the notion that it would be easier to scale down the system, perhaps with only software changes then to create greater capability which would surely necessitate very expensive hardware changes. To that end, the translational volume of 300 mm was adopted. Additionally, the force generating capability was taken as roughly 18.18 N (40 lbf). Experience designing Stewart Platforms teaches that larger volume mechanisms are generally capable of generating larger loads. By having large initial actuators, when the system is scaled down assuming that the same actuators are used, there will be enough residual capability to develop a smaller load, say 9 N. Additionally, the construction and proof of a large system with greater mass and inertia content relative to a smaller system, tends to prove the capability of the smaller system. Finally selecting an apparently large static load capability, assures that there will be enough residual power in the actuators to absorb the dynamic loads of the mechanism thereby exerting a reasonable static force reflecting load against the operator.

1.4 Program History

This program began with the submission of a Phase I SBIR proposal in June of 1987. Phase I was awarded and ran from February, 1989 to August 1989, when the Phase II proposal was submitted. The Phase I effort: 1) established that a mechanism of reasonable size and load generating capability could be built, and 2) developed kinematic algorithms and tested their execution speed.

Phase II began in July of 1989 with the intent of continuing the research with the specific goals of constructing a mechanism, developing and constructing a universal controller and interface, integrating the system with a General Electric P60 robot equipped with a six DOF force sensing cell, and testing both the hand controller subsystem and the integrated master/slave teleoperation system.

1.5 Research Approach and Report Organization

The research approach dictated independent development of the mechanism and mechanism controller and universal interface. This decision followed from the early establishment in Phase I of the kinematic and control algorithms. Accordingly, the report documents the mechanism and controller development separately. Chapter 2 describes the mechanism design, Chapter 3 details the controller design while Chapter 4 documents the testing. The balance of the report discusses the results and suggests future research opportunities.

Chapter 2

Hand Controller Mechanism Development

This chapter details the development of the hand controller mechanism. It begins with a defense of the mechanism type, followed by a theoretical description of the mechanism, kinematic synthesis, mechanism detailed mechanical design, and actuator selection and design.

2.1 Type Synthesis

Chapter 1 made the argument for the development of a six DOF mechanical linkage mechanism as part of the man machine interface for force reflecting teleoperation. We now consider the task of realizing such a mechanism. Mechanism development classically proceeds along a three part sequence, type synthesis, kinematic synthesis and analysis, and detailed mechanical design. This section is devoted to type synthesis. Type synthesis as its name implies embodies the selection of the type of mechanism, that is the selection of the overall mobility, the number of links, and their general relative geometric relationship. Kinematic synthesis comprises the selection of the actual dimensions and proportions of the mechanism. Kinematic analysis determines the loads in the various links while the detailed mechanical design provides for bearings, material selection and descriptive drawings.

This research effort investigated the implementation of the Stewart Platform as the optimum type of mechanism for the force reflecting hand controller. Comparison of Figure 1.3 with Figures 1.2 and 1.1 reveals two disparate kinematic structures between these three six DOF mechanisms. The first mechanism features the "parallel" structure while the latter two have the "serial" structure. Differences in performance capabilities are discernable by inspection:

Actuator Size: The parallel mechanism can develop more payload capability for each unit of actuator motive capability due to the distribution of loads across the actuators as opposed to the serial mechanisms which feature a mechanically disadvantageous cantilevered structure and concentration of loads into individual actuators.

Power Consumption: By sharing the loads across the actuators, the parallel mechanism requires less power than the serial. The serial mechanisms can in certain configurations have the same load distributed through each actuator.

Range of Motion: The serial mechanisms in general will enjoy a greater translational and rotational range of motion relative to the parallel mechanism.

Mechanical Stiffness: The closed chain structure of the parallel mechanism has a decided advantage in mechanical stiffness over the open chain cantilevered serial mechanism.

Mechanical Mass and Inertia: In general, the parallel mechanism will have less mass and mechanical inertia, principally because the actuators can be made smaller and more easily located at the base of the joints in a relatively stationary position.

Mechanical Friction: An advantage in mechanical friction is not apparent by inspection. The parallel mechanism has twice the number of joints contributing to the system friction as does the serial mechanism. However the loading in parallel mechanism joints should be considerably less than that of the serial mechanisms thereby developing lower friction per joint.

Given the six DOF mobility requirement, the type synthesis reduced to the selection between the serial and parallel linkages. Given the advantages, ascribed above to the parallel mechanism, and the as yet undeveloped and unexploited nature of the Stewart Platform mechanism, the hand controller development based upon the Stewart Platform comprised a worthy research goal.

2.2 Stewart Platform Theory and Design Methodology

Mechanism theory and design routinely evolves from considerations of kinematics or from conceptualizing devices from the viewpoint of linkage positions and orientations, and constraint. Force and torque transfer relations then follow from Newtonian statics or Lagrangian mechanics. This viewpoint is natural for simple linkages such as the four bar planar mechanism. Typically design equations are couched exclusively in terms of kinematic parameters.

The Stewart Platform resists conceptualization from the kinematic viewpoint. It was found exceedingly convenient to take advantage of the duality in nature between position and orientation and force and torque, and to approach the Stewart Platform from the later viewpoint. This yielded insight into the mechanism behavior and allowed the development of a reasonably straightforward design methodology.

A Stewart Platform comprises a base platform usually taken to be fixed in inertial space, six sublinkages termed legs, and a moving payload platform. The legs are connected as shown in Figure 2.1. One joint connection is a three DOF rotational ball and socket or spherical joint. The other joint connection is a two DOF rotational universal or Hooke joint. The leg itself is a pure slider joint. Notwithstanding friction in the joints, this connection yields stress resultants of pure force aligned parallel to the major axis of the leg. The sequence of the joints, has no kinematic significance except that the slider must be between the two rotational terminations.

Consider the method of sections applied to the sublinkage of Figure 2.1. A plane is taken through the leg normal to its major axis. We assume that the joints are frictionless. If a torque resultant is developed in the section plane, we see that neither rotational joint can resist this load and the system will be dynamically unstable. If a torque resultant occurs normal to the plane, the leg section with the three DOF joint will not be stable since its joint termination cannot resist this component. Since an equal and opposite torque would be required on the leg section with the two DOF joint, and since the section with the three DOF joint can bear no axial torques, the former section must also have no axial torque. If force resultants exist in the section plane, these will generate torques about both rotary joints which neither joint can resist. Hence the only load component which can exist in the sublinkage is pure axial force. This analysis did not stipulate the sequence of the joints. The orientation of the section plane did not compromise the generality of the analysis.

Now consider the motion and dynamic balance of the payload platform. The payload platform represents a rigid body free to undergo general six DOF motion. In order to develop arbitrary motion, a corresponding system of dynamically balancing forces and torques each spanning R^3 must be brought to bear upon the payload platform. The succinct minimum design problem then reduces to arranging the six legs which each generates pure force along its axis, such that the resultant equipolent system of leg forces spans R^3 for force and torque. If this condition is satisfied, then we say that the system is nonsingular. Table 2.1 summarizes the complete set of theoretical design requirements. From the previous arguments it is obvious that a minimum of six legs is required, but more can be added if desired.

Given the theoretical design requirements of Table 2.1 a design methodology can be developed. The design methodology flows from adopting the force and torque viewpoint towards the mechanism. An optimum configuration from the dual viewpoint of singularity avoidance and actuator efficiency is asserted to be that depicted in Figure 2.2. In this figure, the legs lie pairwise in the three faces and face extensions of a right tetrahedron. The leg axes parallel to and equally spaced from the tetrahedron edges. The payload platform center coincides with that of the tetrahedron vertex. Each pair can generate a pure force along the tetrahedron edge if the individual leg forces have equal magnitude. If the forces are equal and opposite, a pure torque normal to the tetrahedron face results. Since the edges and planes are all mutually orthogonal, this configuration spans R^3 for both force and torque. This configuration is referred to as the decoupled configuration. The design methodology proceeds from attempts to maintain this configuration while satisfying the other theoretical design requirements.

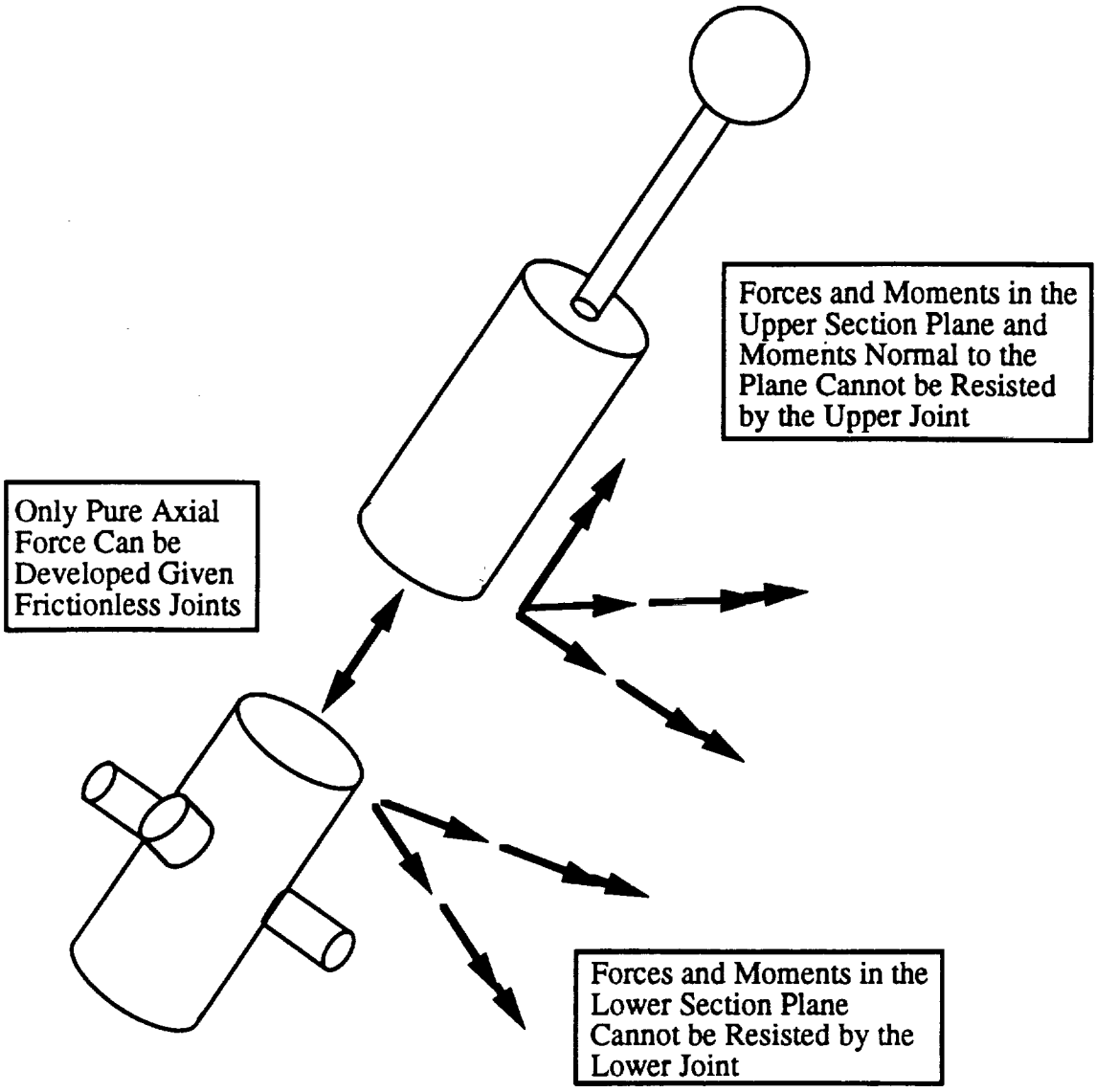

Figure 2.1: Stewart Platform Leg Connection

Mechanism Singularity	The legs must be arranged such that the force system is nonsingular for all required payload platform poses.
Leg Stroke	The legs must be arranged and designed such that for the required range of payload platform translational and rotational motion, the mechanical limitations for the stroke of the legs is not exceeded.
Leg/Actuator Loadings	The legs must be arranged in conjunction with actuator selection such that the required forces can be developed against the payload platform.
Inter Leg Interference	The legs must be arranged such that no mechanical interference exists between the legs during the payload platform motion.
Leg/Payload Platform Interference	The legs and payload platform must be arranged such that the legs and payload platform do not interfere mechanically during payload platform motion.
Leg/Base Platform Interference	The legs and base platform must be arranged such that the legs and base platform do not interfere mechanically during payload platform motion.
Joint Range of Motion	The joints must be designed such that they have a mechanical range of motion appropriate for the required motion of the payload platform.
Joint Singularity	The joints must be designed such that no mathematical singularity is encountered within the joint during payload platform motion.

Table 2.1: Mechanism Theoretical Design Requirements

Before proceeding with the development of the design methodology, let us examine the optimum or decoupled configuration more closely. This arrangement has several virtues other than meeting the minimum requirement for nonsingularity. First, it is asserted that this configuration is as "unsingular" as possible, since the leg resultant forces and torques are mutually orthogonal and span R^3, they constitute an orthogonal basis for the system. As the system moves, the resultants will no longer maintain the orthogonal configuration. However by starting from this configuration, orthogonality or near ogthogonality can be preserved as long as possible.

The second advantage of the decoupled configuration is minimum actuator force requirement for a given load to be exerted against the payload platform. Referring to Figure 2.3, the legs pairs have parallel axes equally spaced from the tetrahedron edge. The parallel alignment allows no component of force acting in opposition and cancelling between the legs. The fact that the legs are equally spaced from the edge also contributes to minimum actuator force requirement. Consider the situation where a pure force is required against the payload platform. If the legs were not equally spaced about the center then equal leg forces would develop an unwanted torque. With the legs equally spaced, they share loads equally resulting in minimum required actuator forces.

The decoupled configuration is felt to yield ease of control and control system design. In the hand controller application, each leg will be driven to produce a force corresponding to the required force and torque state at the handgrip. By having the legs orthogonal, the complication of the controller is reduced. With coupling, any inaccuracy in the force in one leg will show up as a noise disturbance in the other legs.

The decoupled configuration has one disadvantage pertaining to leg skewness and undesirable disturbance torques associated with rotational displacements of the payload platform. Figure 2.4 depicts two legs which were initially parallel and later subject to a rotation of the payload platform. The resulting skewness of the legs develops force components both parallel to and normal to the mutual orthogonal between the two legs. The normal force components generate an unwanted couple about the centerline of the two legs. This couple must be counteracted by some moment generated by another pair of legs. This situation can be counteracted by having the legs intersect at a point such that they never become skew. The price paid for this is less efficiency in developing force for the reasons cited in the previous paragraph.

Given that the decoupled configuration is best, the design methodology follows by attempting to arrange the legs such that the decoupled configuration is maximally preserved while satisfying the other theoretical design requirements. The general way to do this is simply to preserve the leg directions in absolute space. This can be done by making the legs as long as possible such that a given payload translation results in a small change in leg angle over the long leg length. A second method is to arrange the legs to be as parallel as possible to the desired direction of translational motion. This can only be done in one of the three orthogonal directions and results in the worst case situation in the other two directions. This later method does not suit the force reflecting hand controller application. The direction of the forces and torques are random such that the mechanism behavior should

be homogeneous over R^3.

A method of maximizing leg stroke is displayed in Figure 2.5. This arrangement relies on the fact that minimal leg extension occurs when the translational motion occurs in a direction normal to the leg axis. If the workspace is to be cubic as in the force reflecting hand controller, then each leg pair should be orthogonal to one of the faces of the cube when the mechanism is centered in its workspace. This is easily accomplished with the decoupled configuration by simply aligning the tetrahedron edges to be parallel to the faces of the workspace cube.

Experience has shown that mechanism rotation as opposed to translation contributes most significantly to mechanism singularity. Consider Figure 2.6 which displays a view normal to a leg pair for several different platform orientations. The key factor to consider is the leg pair's ability to generate torque with the changing orientation. As the rotation approaches 90 degrees from center, the moment arm of the leg about center vanishes leaving no torque generating capability and hence a mechanism singularity. By this line of reasoning, a 90 degree rotation represents an absolute maximum for a Stewart Platform. This capability will be diminished as the mechanism translates from center due to the changing leg angles with pure translation. To set up the legs for maximum rotational capability, they should terminate at a point in the payload platform on a line normal to the line containing the payload platform center point and the leg base joint.

The leg mechanical interference issue is not easily described in prose. The interference between the leg and upper and lower terminating bodies is most easily managed by arranging the mechanical hardware to lie opposite the leg side of a plane which intersects joints and is normal to the leg axis when the mechanism is centered. The inter leg interference is more complicated and is best managed with solid modelling computer graphic systems. A configuration particularly resistant to inter leg interference is shown in Figure 2.7. Speaking in terms of the decoupled configuration, the lower leg of each pair is given zero offset from the tetrahedron axis and these legs all terminate at the tetrahedron vertex. These three legs could never interfere due to a mechanism rotational change and could only interfere at extreme translational limits when the legs become nearly parallel. The three remaining legs are offset an arbitrary amount from the tetrahedron edges and share a common base joint termination point with their pair counterpart. Interference can occur at extreme rotations when one upper leg strikes the lower leg from a different pair. This configuration suffers from low actuator efficiency due to the unequal leg offsets from the tetrahedron edge.

The actual kinematic design proceeds on an iterative basis using the above described intuitive methods and the analytic procedures described in the next section pertaining to actuator loads and leg lengths. Table 2.2 reiterates a number of design insights to be used during the iterative design process and also introduces a reduced set of design parameters relative to the decoupled configuration. The complete kinematic specification of a Stewart Platform requires the placement in R^3 of 12 joints for a total of 36 parameters selections. This large number is not amenable to computer parametric study. The reduced set of six parameters described in Table 2.2 and depicted in Figure 2.8 greatly simplifies the design task.

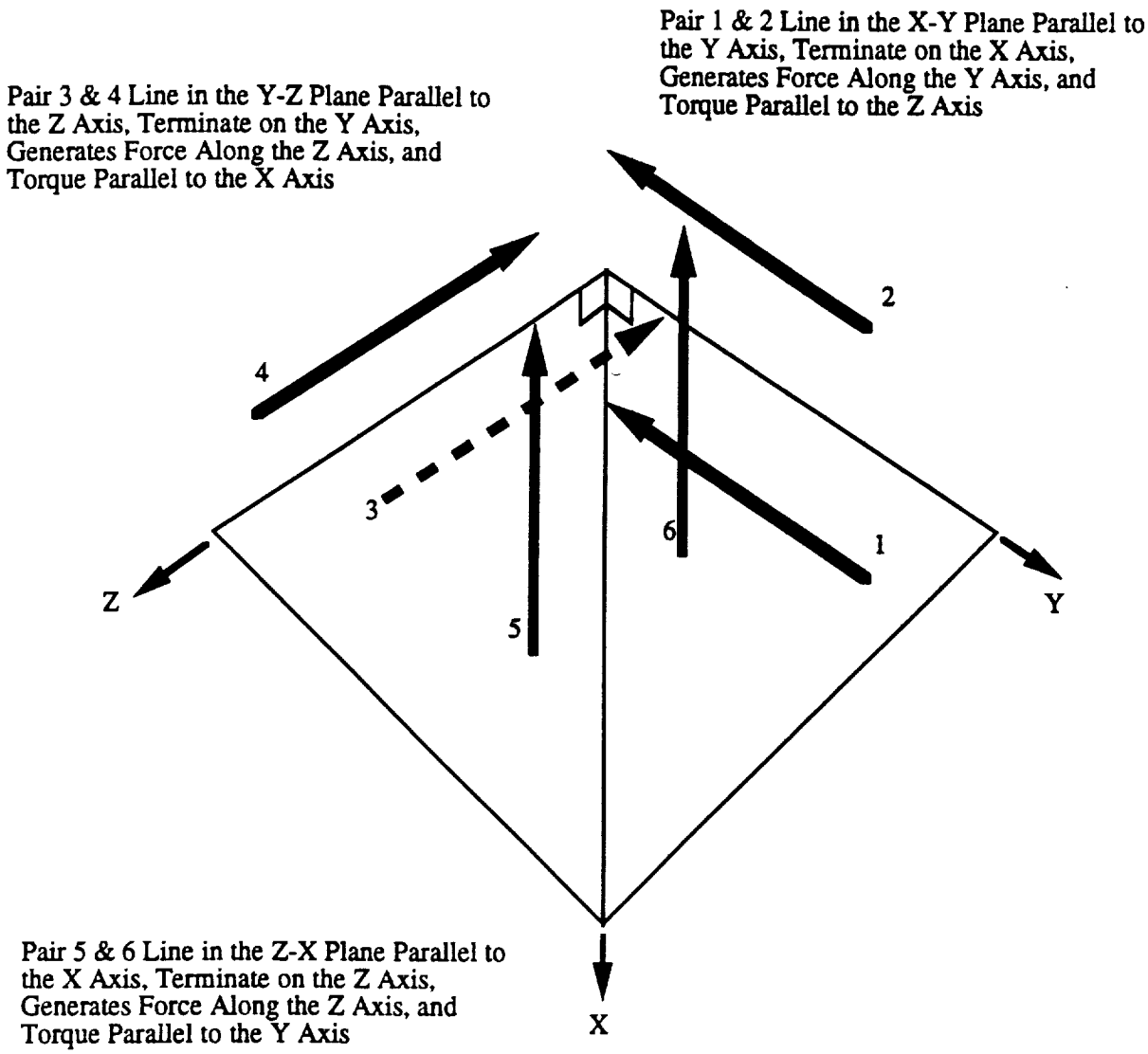

Figure 2.2: Optimum Stewart Platform Configuration

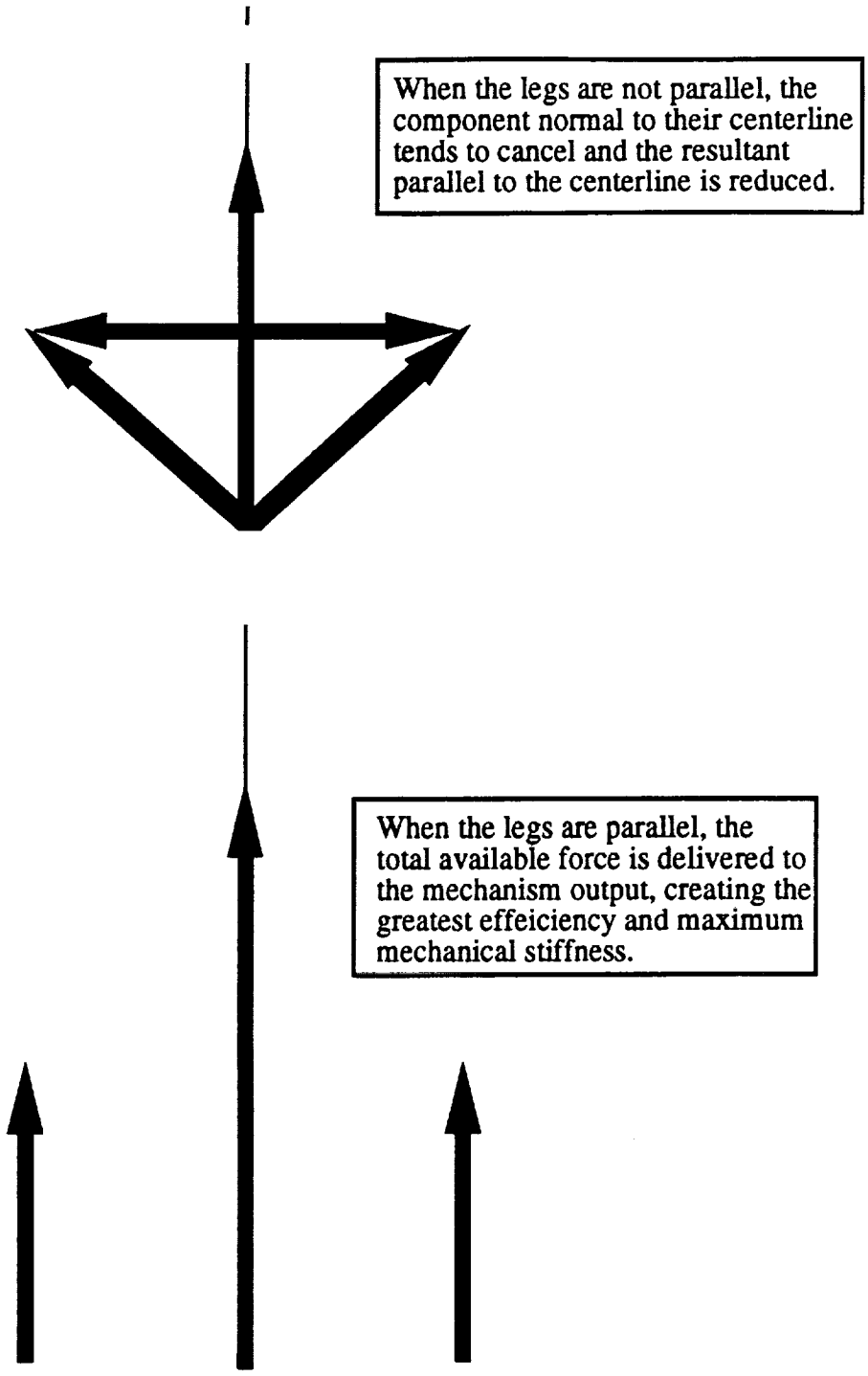

Figure 2.3: Actuator and Mechanical Stiffness Force Maximization

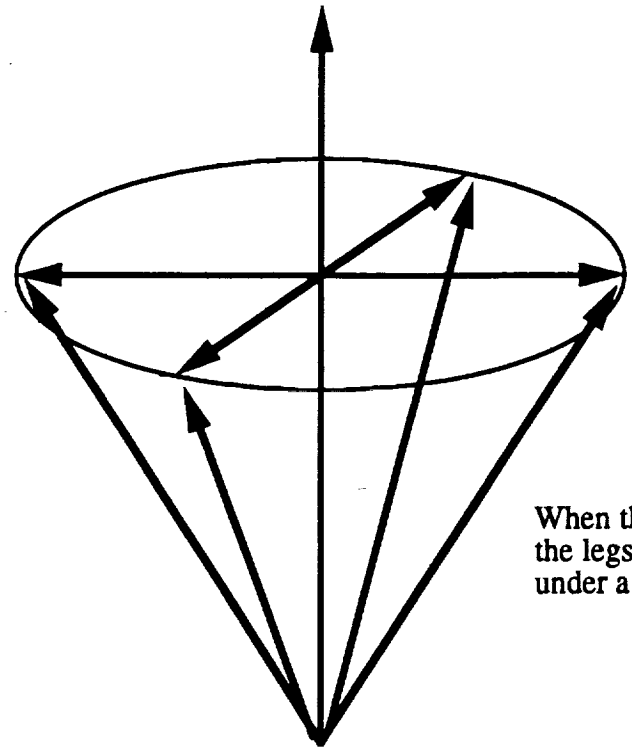

When the base joints coincide, the legs always remain planar under a platform rotation.

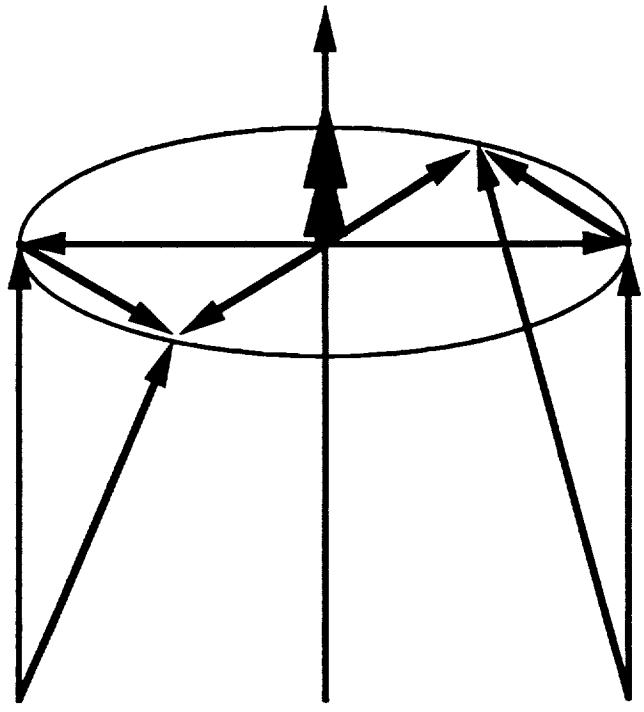

When the base joints do not coincide, the legs become skewed under a platform rotation, thereby developing an unwanted, disturbance torque.

Figure 2.4: Actuator Pair Skewness Torque

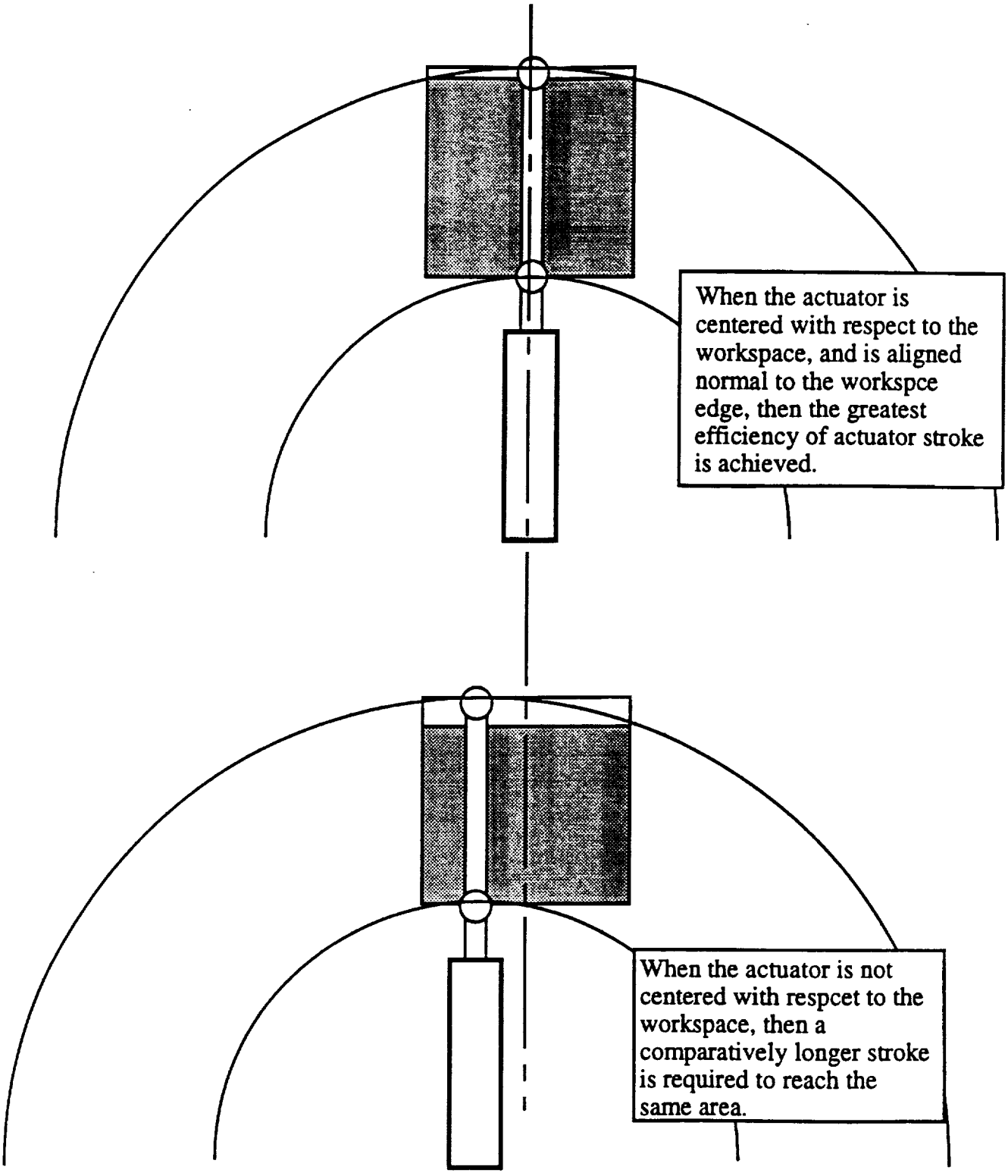

Figure 2.5: Leg Stroke Optimization

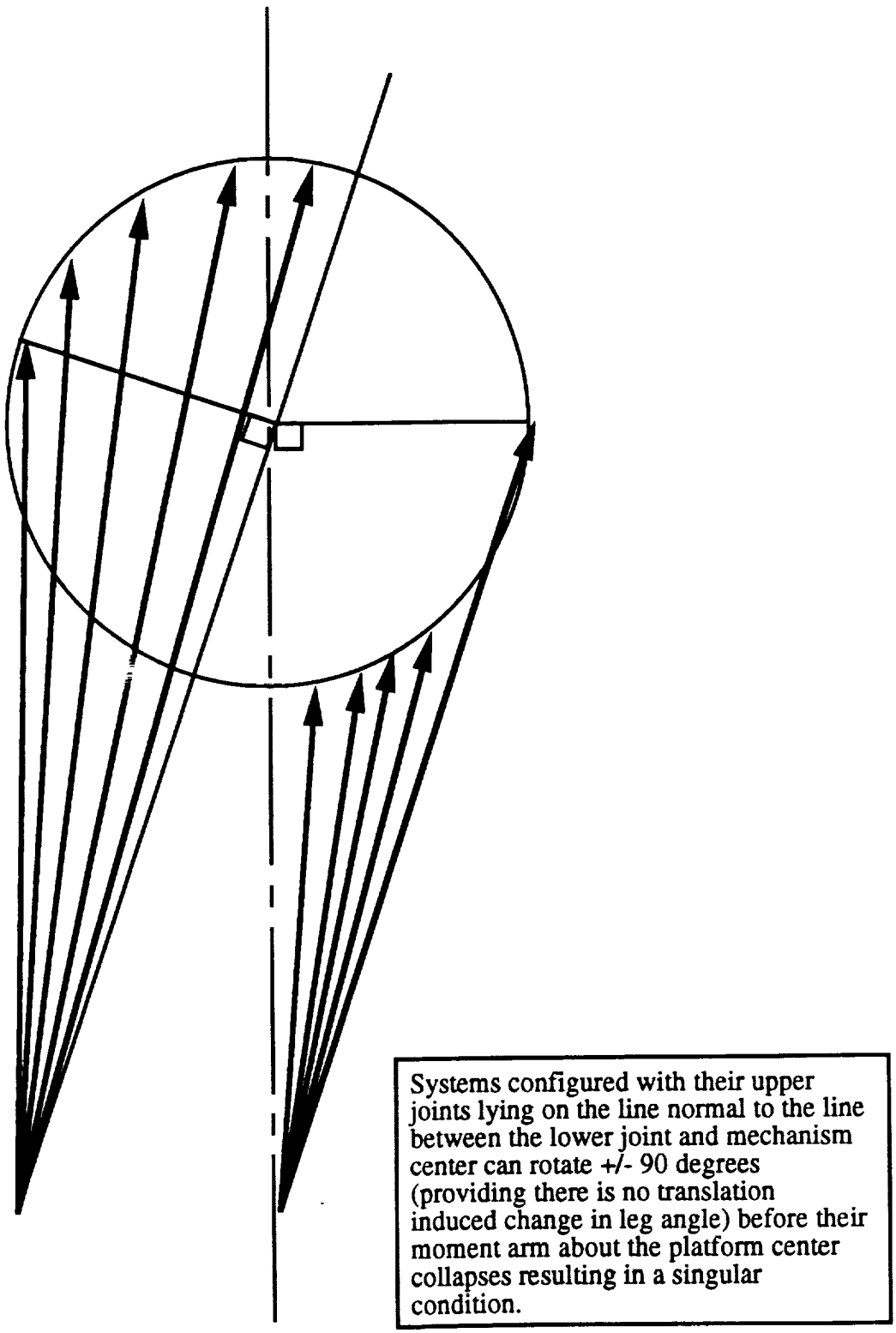

Figure 2.6: Theoretical Maximum Payload Platform Rotation from Center

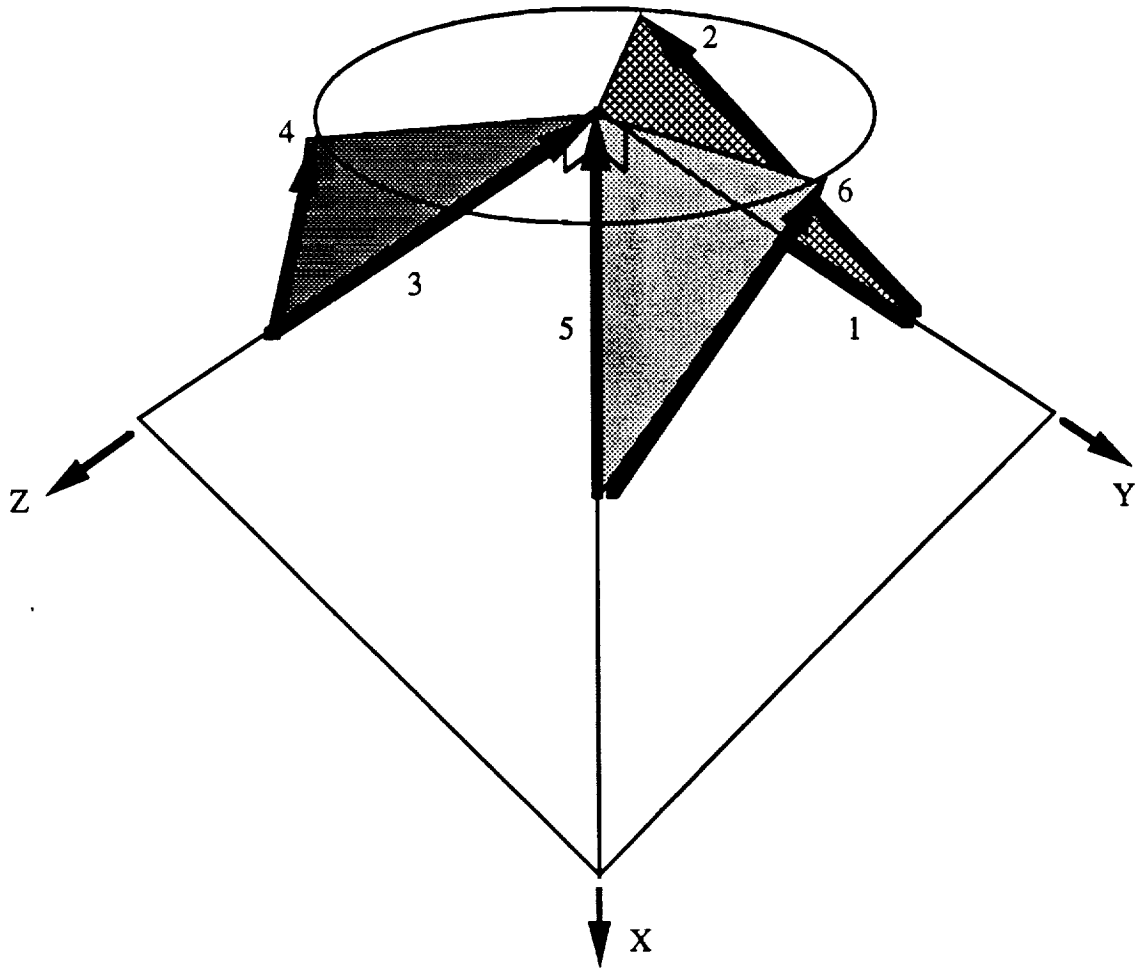

In this configuration, the odd numbered, lower legs on the tetrahedron edges can never hit each other. Similarly, the even numbered, upper legs can never contact each other. Only under extreme rotations can the legs within the pairs contact when they become close to parallel. The greatest possibility for interference is between adjacent upper and lower legs (e.g. 2 & 3). Because these legs lie in mutually orthogonal planes, they can only contact with a 90 degree rotation, at the mechanism theoretical maximum rotational limit.

Figure 2.7: Configuration with Minimum Inter Leg Interference

$\mathcal{L}$ Pair Twist Angle	This parameter represents the twist of the pair plane about the tetrahedron edge. It is best kept as zero. Changing the angle results in the coupling of torques across the pairs. It is sometimes convenient to change this parameter to avoid inter leg interference.
$\mathcal{M}$ Upper Leg Lateral Offset	This parameter represents the lateral offset of the upper leg within the pair from the tetrahedron edge. Large values yield huge torque generating capability at the expense of large leg stroke requirements. Actuator loads are optimized by making its value equal to that of the lower leg offset.
$\mathcal{N}$ Lower Leg Lateral Offset	This parameter represents the lateral offset of the lower leg within the pair from the tetrahedron edge. Large values yield huge torque generating capability at the expense of large leg stroke requirements. Actuator loads are optimized by making its value equal to that of the upper leg offset.
$\mathcal{O}$ Upper Joint Axial Offset	This parameter refers to the distance along the leg axis of the upper leg joint from the plane normal to the tetrahedron edge containing the tetrahedron vertex. The value should be selected such that the upper joint lies on the line normal to the line containing the base joint and the tetrahedron vertex.
$\mathcal{P}$ Lower Joint Axial Offset	This parameter refers to the distance along the leg axis of the lower leg joint from the plane normal to the tetrahedron edge containing the tetrahedron vertex. Large values yield long legs and increased mechanism stability since the change in leg angle with payload platform translation is decreased with longer legs.
$\mathcal{Q}$ Lateral Rotation	This parameter represents the change in leg axes direction from the parallel to the tetrahedron edge in the plane containing the two legs.

Table 2.2: Reduced Design Parameter Set and Insights

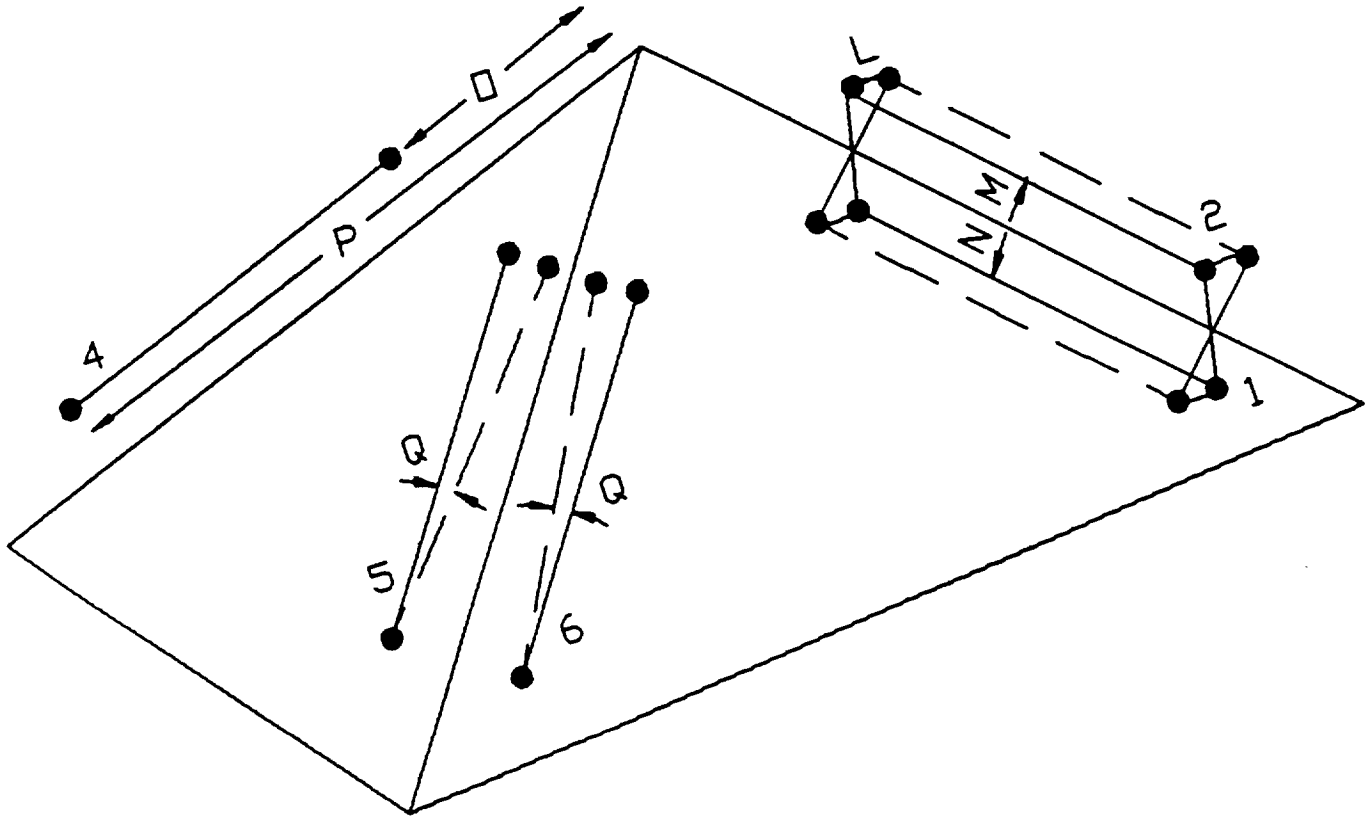

Figure 2.8: Reduced Design Parameter Set

2.3 Stewart Platform Analytics

This section develops the analytic descriptions of the Stewart Platform, namely the kinematics and force transfer relations. In mechanism analysis we describe the zeroth, first, and second order kinematics, implying the mechanism pose, rate of change of pose or speed, and acceleration respectively. We also speak of the forward and inverse kinematics. The forward kinematics implies the determination of the pose of the mechanism as a function of some generalized coordinate set. The inverse kinematics implies the determination of the generalized coordinate values when the pose is known.

2.3.1 Vector Description and Generalized Coordinates Selection

Figure 2.9 depicts a general vector configuration useful for describing the Stewart Platform. The global coordinate frame, {B}, is shown fixed in the base platform. The vectors, $\bar{b}_i$, describe the position of the attachment points of the proximal leg joints in the base platform. The payload platform is shown with a coordinate frame {P} fixed at the centroid. The rotation matrix expressing in the global frame will be denoted as $\Re$. The vectors, $\bar{p}_i$, describe the position of the attachment points of the distal joints in the payload platform relative to the payload platform coordinate origin. The vectors, $\bar{\ell}_i$, describe the position of the $\bar{p}_i$ relative to the $\bar{b}_i$. The vector $\bar{d}$ describes the position of the coordinate origin of the payload platform relative to the coordinate origin of the base. All these vectors are expressed in the global coordinate frame.

Many selections of generalized coordinates are possible for the Stewart Platform. The most convenient set is the length between terminal joints for each leg, denoted herein as the scalar θ_i. This selection is made primarily on the basis of ease transducer placement. A closed form expression of the payload platform pose as a function of the $\bar{\theta}$ does not yet exist. Researchers have postulated that if it does exist, that it would be at least a 32 degree polynomial. A numerical method described in the following subsection converges quickly and accurately.

2.3.2 Zeroth Order Kinematics

The zeroth order inverse kinematics express the generalized coordinates as a function of the payload platform pose which is known and expressed by $\bar{d}$ and $\Re$. From simple vector algebra we have:

$$\theta_i = \left([[\bar{d} + \bar{p}_i] - \bar{b}_i]^T \; [[\bar{d} + \bar{p}_i] - \bar{b}_i] \right)^{\frac{1}{2}} \tag{2.1}$$

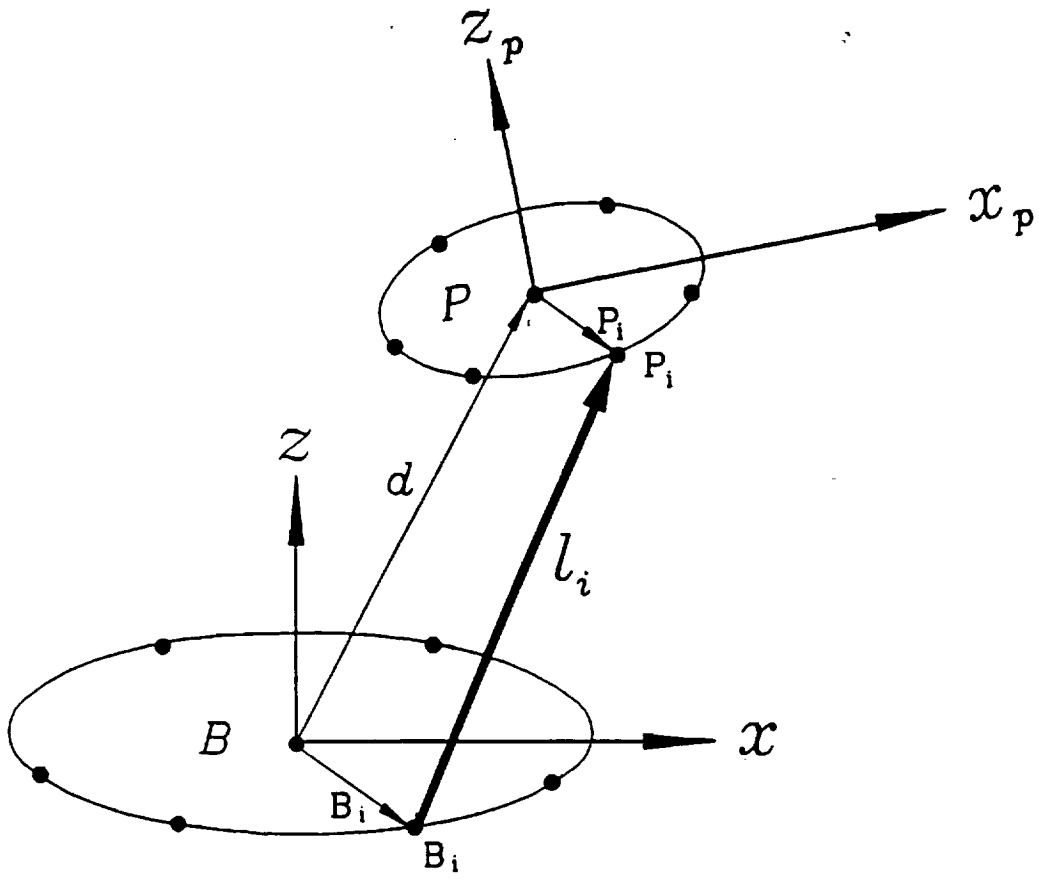

Figure 2.9: Stewart Platform Vector Description

The forward kinematics express $\Re$ and $\bar{d}$ as a function of the $\bar{\theta}$. The forward kinematics proceed by an iterative method starting from a guess of the initial pose, usually taken as the center of the workspace with neutral orientation. First we calculate:

$$\Delta\bar{\theta} = \bar{\theta}_{act} - \bar{\theta}_{old} \tag{2.2}$$

$$\epsilon = \| \Delta\bar{\theta} \| \tag{2.3}$$

$$\epsilon < \eta \tag{2.4}$$

where:

$\bar{\theta}_{act}$ = the vector in R^6 of actual or measured leg lengths,

$\bar{\theta}_{old}$ = the vector in R^6 of leg lengths corresponding to the initial or previous mechanism pose,

η = a small convergence test constant.

If the method converges immediately implying that Equation 2.4 is satisfied, the pose corresponding to the initial guess is assumed to be correct.

If the convergence criteria is not satisfied, then we proceed by adjusting the mechanism pose. The Stewart Platform has several theoretical assembly configurations. In order to force convergence into the proper configuration, the amount of motion allowed in a single step must be restricted. This is done by scaling the vector of leg length changes as follows:

$$\delta\bar{\theta} = \left(\frac{\Delta\bar{\theta}}{\| \Delta\bar{\theta} \|}\right) (\| \Delta\bar{\theta} \| \lfloor \nu) \tag{2.5}$$

where:

$\lfloor$ = the mathematical "floor" symbol implying the smaller of the left and right hand terms,

ν = a small limiting constant.

We then proceed to calculate a change in the platform pose using the differential properties of the first order forward kinematics (See the following section):

$$\begin{bmatrix} \delta x \\ \delta y \\ \delta z \\ \delta\Omega_x \\ \delta\Omega_y \\ \delta\Omega_z \end{bmatrix} = \begin{bmatrix} \quad \mathcal{J} \quad \end{bmatrix} \delta\bar{\theta} \tag{2.6}$$

where:

$\{\delta x, \delta y, \delta z\}$ = the incremental translational change of the payload platform position along the x, y, and z axes respectively,

$\{\delta\Omega_x, \delta\Omega_y, \delta\Omega_z\}$ = the incremental orientational change of the payload platform orientation about the x, y, and z axes respectively.

We then update the translational portion of the pose:

$$\bar{d}_{new} = \bar{d}_{old} + \begin{bmatrix} \delta x \\ \delta y \\ \delta z \end{bmatrix} \tag{2.7}$$

To update the orientational portion of the pose we form the cross product of the orientational change vector with the orientation matrix, add the change to the old matrix, and orthonormalize the result:

$$\Delta\Re = \begin{bmatrix} 0 & -\delta\Omega_z & \delta\Omega_y \\ \delta\Omega_z & 0 & -\delta\Omega_x \\ -\delta\Omega_y & \delta\Omega_x & 0 \end{bmatrix} \begin{bmatrix} \\ \Re_{old} \\ \\ \end{bmatrix} \tag{2.8}$$

$$\Re' = \begin{bmatrix} \\ \bar{i}' \quad \bar{j}' \quad \bar{k}' \\ \\ \end{bmatrix} = \Delta\Re + \Re_{old} \tag{2.9}$$

$$\bar{i}_{new} = \frac{\bar{i}'}{\|\bar{i}'\|} \tag{2.10}$$

$$\bar{k}_{new} = \frac{\bar{i}_{new} \times \bar{j}'}{\|\bar{i}_{new} \times \bar{j}'\|} \tag{2.11}$$

$$\bar{j}_{new} = \frac{\bar{k}_{new} \times \bar{i}_{new}}{\|\bar{k}_{new} \times \bar{i}_{new}\|} \tag{2.12}$$

$$\Re_{new} = \begin{bmatrix} \\ \bar{i}_{new} \quad \bar{j}_{new} \quad \bar{k}_{new} \\ \\ \end{bmatrix} \tag{2.13}$$

Given $\bar{d}_{new}$ and $\Re_{new}$ we return to the inverse kinematics and perform the calculations prescribed in Equation 2.1 through Equation 2.4 to determine if the tolerance ϵ, has become sufficiently small.

2.3.3 First Order Kinematics

Mathematicians refer to a Jacobian matrix as a linear mapping between differential quantities. The robotics community embraces a tighter definition of the Jacobian matrix, $\mathcal{J}$, implying the linear mapping from the vector of generalized coordinates or actuator speeds to the translational and angular velocity vectors of the mechanism output. We write:

$$\begin{bmatrix} \bar{v} \\ \bar{\omega} \end{bmatrix} = \begin{bmatrix} \quad \mathcal{J} \quad \end{bmatrix} \dot{\bar{\theta}} \tag{2.14}$$

where:

$\bar{v}$ = translational velocity vector in R^3 of the payload platform expressed in global coordinates,

$\bar{\omega}$ = angular velocity vector in R^3 of the payload platform expressed in global coordinates,

$\dot{\bar{\theta}}$ = vector in R^6 of the leg speeds.

We now need to derive $\mathcal{J}$ assuming that it exists. We proceed by writing the inverse of the relation whereby:

$$\dot{\bar{\theta}} = \begin{bmatrix} \quad \mathcal{J}^{-1} \quad \end{bmatrix} \begin{bmatrix} \bar{v} \\ \bar{\omega} \end{bmatrix} \tag{2.15}$$

We observe that for each leg, the leg linear speed vector is the projection of the total translational velocity of the upper joint onto the leg axis vector. The total translational velocity of each joint is taken as the sum of the platform translational velocity plus the amount induced by the angular velocity. We write:

$$\dot{\theta}_i \, \bar{s}_i = \left[\bar{v} + \bar{\omega} \times [\Re] \, \bar{p}_i^{\,\{P\}} \right]^T \bar{s}_i = \left[\bar{v} + \bar{\omega} \times \bar{p}_i \right]^T \bar{s}_i \tag{2.16}$$

where:

$\Re$ = the orientation matrix expressing the coordinate axes of $\{\mathbf{P}\}$ in $\{\mathbf{B}\}$,

$\bar{p}_i^{\,\{P\}}$ = the expression of the $\bar{p}_i$ in $\{\mathbf{P}\}$,

$\bar{s}_i = \bar{\ell}_i \, / \, \| \bar{\ell}_i \|$, the unit vector describing the leg direction.

The $\bar{\ell}_i$ are found from simple vector algebra by:

$$\bar{\ell}_i = [\bar{d} + \bar{p}_i] - \bar{b}_i \tag{2.17}$$

The inner product in Equation 2.16 can be distributed and the resulting equation factored to form:

$$\dot{\theta}_i \, \bar{s}_i = [\, \bar{s}_i{}^T \quad (\bar{p}_i \times \bar{s}_i)^T \,] \begin{bmatrix} \bar{v} \\ \\ \bar{\omega} \end{bmatrix} \bar{s}_i \tag{2.18}$$

Forming the inner product of both sides of the above vector equation with $\bar{s}_i$ yields the scalar relation:

$$\dot{\theta}_i = [\, \bar{s}_i{}^T \quad (\bar{p}_i \times \bar{s}_i)^T \,] \begin{bmatrix} \bar{v} \\ \\ \bar{\omega} \end{bmatrix} \tag{2.19}$$

Equation 2.19 can be written simultaneously for each of the six legs to yield the expression in vector matrix form:

$$\dot{\bar{\theta}} = \begin{bmatrix} \bar{s}_1{}^T & (\bar{p}_1 \times \bar{s}_1)^T \\ \bar{s}_2{}^T & (\bar{p}_2 \times \bar{s}_2)^T \\ \bar{s}_3{}^T & (\bar{p}_3 \times \bar{s}_3)^T \\ \bar{s}_4{}^T & (\bar{p}_4 \times \bar{s}_4)^T \\ \bar{s}_5{}^T & (\bar{p}_5 \times \bar{s}_5)^T \\ \bar{s}_6{}^T & (\bar{p}_6 \times \bar{s}_6)^T \end{bmatrix} \begin{bmatrix} \bar{v} \\ \\ \bar{\omega} \end{bmatrix} \tag{2.20}$$

Comparing with Equation 2.15 we have our results:

$$\mathcal{J}^{-1} = \begin{bmatrix} \bar{s}_1{}^T & (\bar{p}_1 \times \bar{s}_1)^T \\ \bar{s}_2{}^T & (\bar{p}_2 \times \bar{s}_2)^T \\ \bar{s}_3{}^T & (\bar{p}_3 \times \bar{s}_3)^T \\ \bar{s}_4{}^T & (\bar{p}_4 \times \bar{s}_4)^T \\ \bar{s}_5{}^T & (\bar{p}_5 \times \bar{s}_5)^T \\ \bar{s}_6{}^T & (\bar{p}_6 \times \bar{s}_6)^T \end{bmatrix} \tag{2.21}$$

and

$$\mathcal{J} = \begin{bmatrix} \bar{s}_1{}^T & (\bar{p}_1 \times \bar{s}_1)^T \\ \bar{s}_2{}^T & (\bar{p}_2 \times \bar{s}_2)^T \\ \bar{s}_3{}^T & (\bar{p}_3 \times \bar{s}_3)^T \\ \bar{s}_4{}^T & (\bar{p}_4 \times \bar{s}_4)^T \\ \bar{s}_5{}^T & (\bar{p}_5 \times \bar{s}_5)^T \\ \bar{s}_6{}^T & (\bar{p}_6 \times \bar{s}_6)^T \end{bmatrix}^{-1} \tag{2.22}$$

2.3.4 Static Force Transfer Relations

In order to properly size the actuators, we must be able to determine the magnitude of the forces in the legs as a function of the forces and torques associated with the payload platform. We now derive these relations from the principle of virtual work. This principle states that the work or energy input at one point of the mechanism must equal the work or energy output at some other point of the mechanism. We must necessarily account for all six DOF in the derivation. We write:

$$\bar{\mathcal{F}}_{act}^{T}\,\delta\bar{\theta} = [\,\bar{\mathcal{F}}_{env}^{T}\,\bar{\mathcal{T}}_{env}^{T}\,] \begin{bmatrix} \delta x \\ \delta y \\ \delta z \\ \delta\Omega_x \\ \delta\Omega_y \\ \delta\Omega_z \end{bmatrix} \tag{2.23}$$

where:

$\bar{\mathcal{F}}_{act}$ = the vector in R^6 of forces in the leg actuators,

$\bar{\mathcal{F}}_{env}$ = the vector in R^3 of forces exerted by the platform against the environment,

$\bar{\mathcal{T}}_{env}$ = the vector in R^3 of torques exerted by the platform against the environment.

Substituting Equation 2.6 into Equation 2.23 we have:

$$\bar{\mathcal{F}}_{act}^{T}\,\delta\bar{\theta} = [\,\bar{\mathcal{F}}_{env}^{T}\,\bar{\mathcal{T}}_{env}^{T}\,] \begin{bmatrix} \\ \mathcal{J} \\ \\ \end{bmatrix} \delta\bar{\theta} \tag{2.24}$$

Now recall that the $\bar{\theta}$ are independent of each other. This results from the observation that the actuators can be moved on an independent basis. Cancelling the $\bar{\theta}$ in the above and transposing we have:

$$\bar{\mathcal{F}}_{act} = \begin{bmatrix} \\ \mathcal{J}^{T} \\ \\ \end{bmatrix} \begin{bmatrix} \bar{\mathcal{F}}_{env} \\ \\ \bar{\mathcal{T}}_{env} \end{bmatrix} \tag{2.25}$$

2.4 Kinematic Synthesis

This section documents the results of the kinematic synthesis. A computer program was developed to calculate the leg lengths according to Equation 2.1 and forces according to Equation 2.25. According to the design methodology, a design was postulated according to the insights described and parameters of Table 2.2. For this design, the mechanism was analyzed by computer by stepping across an array in translational and orientational space with the values of maximum and minimum leg length and actuator loads being recorded. This process of kinematic design postulation and computer analysis was repeated until a suitable design was achieved.

2.4.1 Data Presentation Format

All analytic data are presented in the format of Tables 2.3, 2.4, 2.5, and 2.6. In each table the data represent a maximum or minimum of a performance parameter as a function of position in the $x - y$ plane. The individual entries bound the parameter for the particular position in the plane across a z translational range of $+/-$ 12.7 cm from center, with simultaneous handgrip orientational displacements of $+/-$ 45 degrees about axes spaced every 22.5 degrees in azimuth and elevation.

The Jacobian transpose matrix of Equation 2.25 is six by six. The individual entries vary with the position and orientation of the handgrip. Each represents a ratio of force or torque exerted by the handgrip along one of the coordinate axes against the operator to the force in one of the legs. The rows of the Jacobian transpose represent the six ratios for leg number one. Tables 2.3 and 2.4 represent the maximum and minimum values of the third entry of the first row which corresponds to force in the z direction. When the mechanism is centered in the $x - y$ plane, the algebraic maximum and minimum ratios across all vertical, and rotational displacements are seen to be 0.22 and -0.44 respectively. The entries are dimensionless being ratios of force to force. Hence for the mechanism to generate a force of $1N$ in the x direction would require a maximum $0.44N$ in leg one at the worst case pose. The magnitude of the force entries varies with displacement from center, eventually growing exponentially. Small variations are desirable for both actuator sizing and ease of control.

Tables 2.5 and 2.6 display the absolute values of joint to joint leg length or Θ for leg number one. Figure 2.10 depicts a bare bones schematic of the optimal configuration with coordinate axes and leg numbers labeled. Comparison of the tables and the figure confirms the computer modelling. A general symmetry is observed about the y axis with shorter lengths for large negative y values and large lengths for large positive y values. The minor asymmetry arises from the orientational changes of the handgrip.

Tables of the maximum values for force, torque and leg length across all legs, vertical positions and orientations are presented in Appendix A. The torque tables have dimensions of reciprocal centimeters, such that a torque exerted by the mechanism against the operator in units of $N \cdot cm$ will require a corresponding force in the legs in units of N.

Y (cm)	*Units – Dimensionless*										
12.7	0.06	0.04	0.02	0.01	0.03	0.06	0.09	0.14	0.19	0.26	0.32
10.16	0.10	0.07	0.04	0.03	0.05	0.07	0.09	0.14	0.20	0.26	0.32
7.62	0.13	0.10	0.06	0.04	0.06	0.08	0.10	0.15	0.20	0.26	0.32
5.08	0.16	0.15	0.13	0.11	0.09	0.10	0.12	0.16	0.21	0.27	0.33
2.54	0.26	0.24	0.21	0.19	0.16	0.14	0.13	0.17	0.22	0.27	0.33
0	0.37	0.34	0.30	0.27	0.25	0.22	0.19	0.18	0.23	0.28	0.34
-2.54	0.49	0.45	0.41	0.37	0.34	0.30	0.27	0.24	0.24	0.29	0.35
-5.08	0.63	0.58	0.53	0.49	0.44	0.40	0.36	0.32	0.29	0.30	0.36
-7.62	0.80	0.73	0.68	0.62	0.57	0.52	0.47	0.43	0.38	0.34	0.37
-10.16	0.99	0.92	0.84	0.78	0.72	0.66	0.60	0.55	0.49	0.44	0.39
-12.7	1.23	1.14	1.05	0.97	0.89	0.82	0.76	0.69	0.63	0.57	0.51
	-12.7	-10.16	-7.62	-5.08	-2.54	0	2.54	5.08	7.62	10.16	12.7
	$X\,(cm)$										

Table 2.3: Maximum of $\mathcal{F}_z$ for Leg 1 vs Position in X-Y

Y (cm)	*Units – Dimensionless*										
12.7	-1.34	-1.16	-1.01	-0.89	-0.79	-0.70	-0.62	-0.55	-0.49	-0.44	-0.43
10.16	-1.18	-1.01	-0.90	-0.79	-0.71	-0.63	-0.56	-0.50	-0.45	-0.43	-0.44
7.62	-1.04	-0.90	-0.79	-0.70	-0.63	-0.56	-0.51	-0.45	-0.43	-0.44	-0.45
5.08	-0.92	-0.80	-0.70	-0.62	-0.56	-0.50	-0.45	-0.43	-0.44	-0.45	-0.47
2.54	-0.81	-0.71	-0.63	-0.56	-0.49	-0.44	-0.43	-0.44	-0.45	-0.47	-0.48
0	-0.71	-0.63	-0.56	-0.49	-0.44	-0.44	-0.45	-0.46	-0.47	-0.48	-0.49
-2.54	-0.62	-0.55	-0.49	-0.45	-0.46	-0.46	-0.47	-0.48	-0.49	-0.50	-0.51
-5.08	-0.54	-0.48	-0.47	-0.47	-0.48	-0.48	-0.49	-0.50	-0.51	-0.52	-0.53
-7.62	-0.51	-0.49	-0.49	-0.49	-0.50	-0.51	-0.51	-0.52	-0.53	-0.54	-0.56
-10.16	-0.56	-0.54	-0.51	-0.52	-0.52	-0.53	-0.54	-0.55	-0.56	-0.57	-0.58
-12.7	-0.62	-0.59	-0.56	-0.54	-0.55	-0.55	-0.56	-0.57	-0.58	-0.60	-0.61
	-12.7	-10.16	-7.62	-5.08	-2.54	0	2.54	5.08	7.62	10.16	12.7
	$X\,(cm)$										

Table 2.4: Minimum of $\mathcal{F}_z$ for Leg 1 vs Position in X-Y

Y (cm)	*Units – Centimeter*										
12.7	96.2	95.7	95.3	95.0	94.8	94.6	94.5	94.4	94.5	94.5	94.7
10.16	93.7	93.3	92.9	92.5	92.3	92.1	92.0	91.9	91.9	92.0	92.2
7.62	91.3	90.8	90.4	90.0	89.8	89.6	89.5	89.4	89.4	89.5	89.7
5.08	88.8	88.3	87.9	87.5	87.3	87.1	87.0	86.9	86.9	87.0	87.2
2.54	86.3	85.8	85.4	85.1	84.8	84.6	84.4	84.4	84.4	84.5	84.7
0	83.9	83.4	82.9	82.6	82.3	82.1	81.9	81.9	81.9	82.0	82.2
-2.54	81.5	80.9	80.5	80.1	79.8	79.6	79.4	79.4	79.4	79.5	79.7
-5.08	79.0	78.5	78.0	77.6	77.3	77.1	76.9	76.9	76.9	77.0	77.2
-7.62	76.6	76.0	75.5	75.1	74.8	74.6	74.4	74.4	74.4	74.5	74.7
-10.16	74.2	73.6	73.1	72.7	72.3	72.1	72.0	71.9	71.9	72.1	72.3
-12.7	71.8	71.2	70.6	70.2	69.9	69.6	69.5	69.4	69.5	69.6	69.8
	-12.7	-10.16	-7.62	-5.08	-2.54	0	2.54	5.08	7.62	10.16	12.7
	$X\,(cm)$										

Table 2.5: Maximum of Θ for Leg 1 vs Position in X-Y

Y (cm)	*Units – Centimeter*										
12.7	85.8	85.6	85.4	85.3	85.3	85.4	85.5	85.7	86.0	86.4	86.8
10.16	83.3	83.1	82.9	82.8	82.8	82.9	83.0	83.2	83.5	83.9	84.3
7.62	80.8	80.6	80.4	80.3	80.3	80.4	80.5	80.7	81.0	81.4	81.8
5.08	78.3	78.1	77.9	77.8	77.8	77.9	78.0	78.2	78.5	78.9	79.3
2.54	75.9	75.6	75.4	75.3	75.3	75.4	75.5	75.7	76.0	76.4	76.9
0	73.4	73.1	72.9	72.8	72.8	72.8	73.0	73.2	73.6	74.0	74.4
-2.54	70.9	70.6	70.4	70.3	70.3	70.3	70.5	70.7	71.1	71.5	71.9
-5.08	68.4	68.1	67.9	67.8	67.8	67.8	68.0	68.3	68.6	69.0	69.5
-7.62	65.9	65.6	65.4	65.3	65.3	65.3	65.5	65.8	66.1	66.5	67.0
-10.16	63.5	63.1	62.9	62.8	62.8	62.8	63.0	63.3	63.6	64.1	64.6
-12.7	61.0	60.6	60.4	60.3	60.3	60.3	60.5	60.8	61.2	61.6	62.1
	-12.7	-10.16	-7.62	-5.08	-2.54	0	2.54	5.08	7.62	10.16	12.7
	$X\,(cm)$										

Table 2.6: Minimum of Θ for Leg 1 vs Position in X-Y

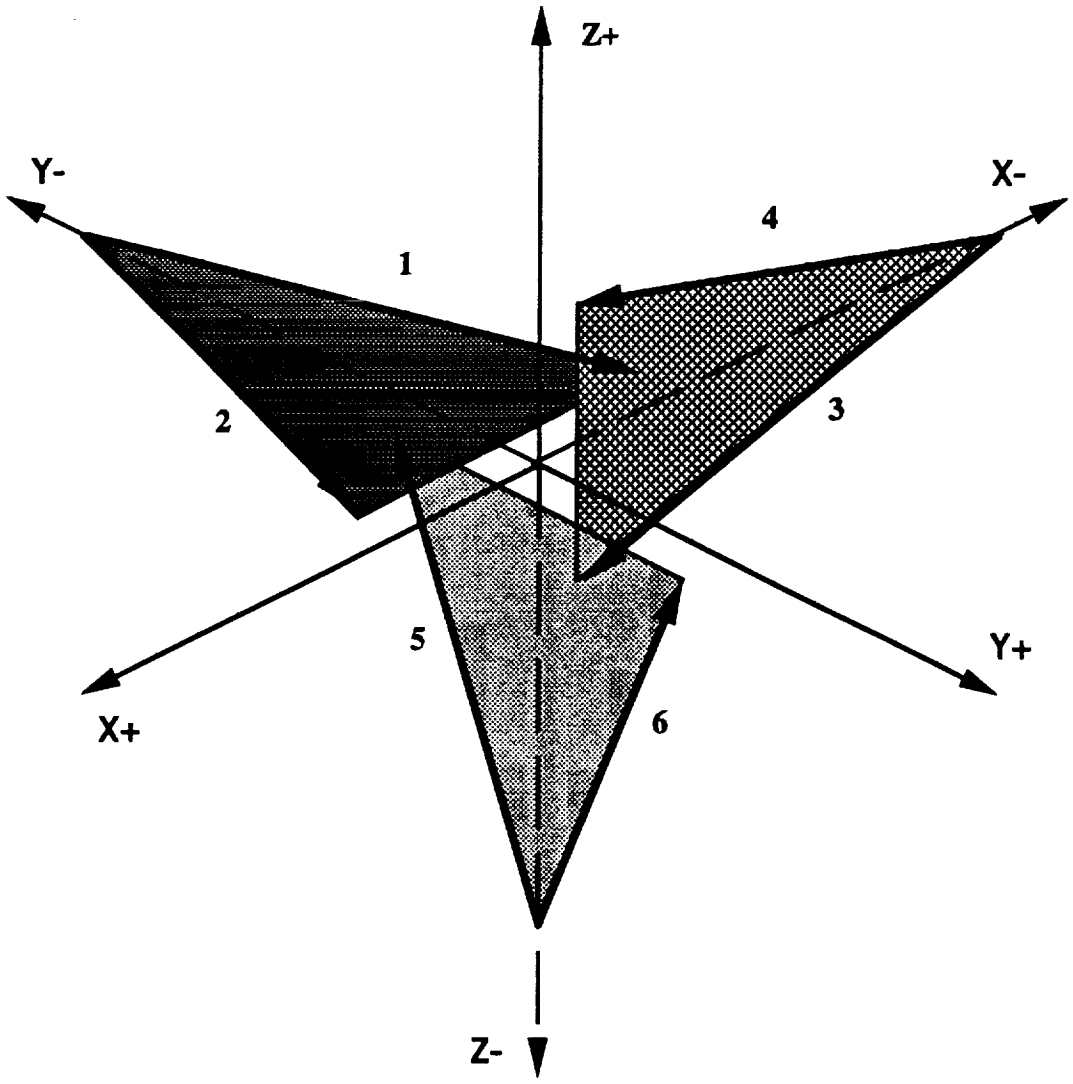

The optimum configuration is based upon the decoupled configuration. The handgrip joint terminations had to be slightly withdrawn from the coordinate axes (tetrahedron edges) to allw room for the operator's hand. The operator reaches in with his forearm parallel to the Y axis. The cubic workspace is aligned with edges parallel to and centered about the coordinate axes. When the handgrip is centered, the hangrip and base frames share the same coordinate system.

Figure 2.10: Optimal Hand Controller Schematic

2.4.2 Optimal Kinematic Design

Over 20 different designs were analyzed before the design depicted in Figure 2.10 was developed. Unlike Figure 2.9 which depicts a generic Stewart Platform with noncoincident Cartesian coordinate systems for the base platform and payload platform or handgrip, the optimal configuration has coincident Cartesian references when the handgrip is centered in its workspace. The vectors, $\bar{p}$ and $\bar{b}$, describing the position of the handgrip and base joint terminations respectively in their own coordinate frames are given in Tables 2.7 and 2.8. The units of displacement in the tables are centimeters.

Some observations are in order relating to the geometry of the optimal design. This particular hand controller is intended to be used by a right handed operator standing and facing the $-y$ direction, with his right arm parallel to the $-y$ direction. The arrangement could easily be inverted for a left handed operator. The translational cube has axes parallel to the global reference axes to maximize the translational range for the given leg stroke. The design adheres very closely to the decoupled configuration. The handgrip joints are withdrawn slightly towards the base from the ideal point where they would intersect the normal to the line from the base joint to the handgrip center. The base joints within the leg pairs were placed as close together as the mechanical design constraints would allow. The handgrip is designed for an average sized hand. The geometric center of the mechanism was taken to be coincident with what would appear to be the center of a loosely clenched fist.

The design suffers from several ergonomic drawbacks. First, when large rotations about the $+x$ direction are required, joint six tends to contact the operator's wrist. This was tolerated to maximize the leg stroke as discussed in the previous paragraph. Second, the mechanism itself is very large, certainly too large for consideration for space flight. The large size was chosen so that smaller working volumes could be tested with the same hardware to find a region of comfort for the operator. A careful study should be performed to determine an optimal hand controller range of motion such that the mechanism size could be reduced accordingly.

The ergonomic difficulties could be attenuated by rearranging the system by passing a plane through the base joints, rotating this plane to the vertical, and having the operator carry his forearm normal to the plane. The upper joints were extended away from the handgrip to allow more space around the hand which enters the handgrip from the side. With the alternative arrangement, the upper joints could probably be extended upwards towards their optimal position to realize minimum force variations with rotation and to realize maximum rotational capability.

Table 2.9 displays the system level results of the kinematic synthesis to include the maximum and minimum actuator ratios for force, $\mathcal{F}$, and torque, $\mathcal{T}$, joint to joint leg length, Θ, and leg stroke. These values represent the worst case numbers for the optimal kinematic arrangement for hand controller positions within a 25.4 cm cube centered about the origin, and with rotations of +/- 45 degrees taken about any axis passing anywhere through the cube in arbitrary directions.

	$\bar{p}_1$ {P}	$\bar{p}_2$ {P}	$\bar{p}_3$ {P}	$\bar{p}_4$ {P}	$\bar{p}_5$ {P}	$\bar{p}_6$ {P}
x	-6.58	6.58	-6.59	-6.59	0.00	0.00
y	-6.59	-6.59	0.00	0.00	-6.58	6.58
z	0.00	0.00	-6.58	6.58	-6.59	-6.59

Table 2.7: Handgrip Joint Coordinates *cm*

	$\bar{b}_1$	$\bar{b}_2$	$\bar{b}_3$	$\bar{b}_4$	$\bar{b}_5$	$\bar{b}_6$
x	-3.70	3.70	-81.08	-81.08	0.00	0.00
y	-81.08	-81.08	0.00	0.00	-3.70	3.70
z	0.00	0.00	-3.70	3.70	-81.08	-81.08

Table 2.8: Base Platform Joint Coordinates *cm*

Hand Controller Kinematic Synthesis Results	
$\mathcal{F}_{max}$	2.13
$\mathcal{F}_{min}$	-1.34
$\mathcal{T}_{max}$	0.22 *(1/cm)*
$\mathcal{T}_{min}$	-0.22 *(1/cm)*
Θ_{max}	96.38 *(cm)*
Θ_{min}	59.08 *(cm)*
$\Theta_{max} - \Theta_{min}$	37.31 *(cm)*
Translational Volume	25.4 *(cm cube)*
Rotational Capability	+/- 45 *Degrees About Any Axis Intersecting the Translational Cube*

Table 2.9: Hand Controller Kinematic Synthesis Results

2.5 Actuator and Drive Selection and Design

This section discusses the actuation and drive selection. It covers the type synthesis, analysis and detailed mechanical design. The actuation and drive selection was of such importance that it was performed first and allowed to steer the rest of the mechanical design. The optimum kinematic design of the last section was not rendered without iterative input from a conceptual actuation and drive selection process.

In the development of the actuation and drive, the following tenets were taken as guiding principals to achieving a successful prototype:

Actuation Force The actuation had to provide not only the motive force to satisfy the static loading requirements of generating force and torque against the operator according to Equation 2.25, but also to accelerate the system inertia. To repeat an earlier theme, the hand controller was intended to have transparency from the operator's viewpoint, or equivalently very high force feedback fidelity. The design philosophy therefore was to provide a superabundance of actuation capability.

Actuator Inertia Actuation generally contributes significantly to system inertia. In developing actuation the actuator inertia had to be kept small both from the viewpoint of the internal actuator moving parts but also from the gross moving mass of the entire actuator assembly.

Actuation Transmission One method to achieve high actuation force is to implement transmissions to achieve mechanical advantage. Transmissions universally add to friction, inertia, and backlash. Transmissions were never seriously considered and a direct drive philosophy was adopted from the beginning.

Mechanical Backlash Mechanical backlash sharply attenuates force feedback fidelity and also introduces destabilizing influences into the control system. Backlash was viewed as a fatal entity and treated accordingly.

Mechanical Friction Mechanical friction attenuates the force feedback fidelity. All reasonable measures were taken to reduce friction.

Actuator Mechanical Interference The actuator had to be placed such that it would suffer no mechanical interference during system motion.

Drive Internalization The system drive coupling the actuator to the moving sliders in the legs should be internalized to reduce the danger of the entanglement with the operator's person or other equipment.

Drive Mass The mass of the drive attenuates the force feedback fidelity by virtue of its contribution to the system inertia. Efforts were made to minimize this.

Drive Friction The drive itself can contribute to the system friction by the bending of cables or other sliding contact mechanisms. Efforts were made to minimize this.

Drive Compliance The drive itself has some compliance and can effectively introduce backlash or mechanical vibration modes. Stiffness of the drive was held to be very valuable.

Flexibility The nature of mechanical hardware allows very little opportunity for flexibility once a design is executed. The actuator and drive design process emphasized creating opportunities for simple alterations after the final design was developed.

Capability Risk Exposure All design activities introduce the notion that the final implementation may not be the best way of realizing a particular function. A philosophy of implementing difficult, new concepts which could prove beneficial was adopted providing these concepts had a well known backup mechanism which could be interchanged quickly and economically.

Three actuation methods, electric, hydraulic and pneumatic, were considered. For space applications, only electric was deemed to be appropriate. Also, severe control problems were anticipated with hydraulic and pneumatic due to compliance.

The following electric actuator embodiments were considered:

Direct Current Brush Type Motors A wide variety of these motors is commercially available at low cost. Brushes have the disadvantage of wearing out, creating airborne dust in a space environment, and being susceptible to dust created elsewhere in a space environment.

Direct Current Frameless Brush Type Motors These motors are identical to the previous motor, except that the user must provide the housing and bearings.

Direct Current Brushless Motors These motors operate without brushes by implementing electronic commutation. Electronic commutation has a distinct advantage in overcoming torque ripple, a phenomena where the torque output of a motor varies with rotor angular position for constant current. The concept is very well developed but the motors and controllers are very expensive. Increasingly, more models are becoming available and the price is dropping. Due to their advanced nature, one must procure a motor and controller from the same vendor.

Linear Electric Motors Linear electric motors provide linear force and motion directly as opposed to the previous motors which are all rotary. Linear motors are attractive because the hand controller requires linear motion in the legs and the potential for realizing a leg with a linear motor is realistic. However, these motors require an array of magnets or electromagnets along their length and are therefore very massive and consume large amounts of power.

The brush type DC motors were selected for the hand controller application. The opportunity of creating a very compact package was felt to be very valuable. Additionally, research

suggested that friction and inertia could be reduced with their application. Under the prototype and proof of principle nature of the effort, the advantages of the brushless motors were not deemed to be worth the cost. For the ultimate space application, brushless motors should be given very serious consideration.

The specific motor selected was the QT-1401-D manufactured by Inland Motors, Radford, Virginia. This motor features high magnetic flux, rare earth, samarium cobalt magnets. The pertinent motor performance data are given in Table 2.10. The motors were configured into an actuator subsystem as shown in Figure 2.11. Two motors were placed on the outer ends of a single drive shaft with their poles angularly spaced to be completely out of phase with each other. This was done for the following reasons:

Maximum Actuation Capability With two motors on a single shaft and a cable pickoff of 0.5 cm radius, the actuator package can generate a maximum of 15.87 N (34.92 lbf) linear force.

Minimum Torque Ripple With the rotors phased on the shaft, the averaged torque ripple is cut in half.

Minimum Cogging Torque With the rotors phased on the shaft, the magnitude of the cogging torque is cut in half.

Minimum Bearing Friction Prepackaged motors have a bearing on each end of the rotor with a cantilevered power pickoff on the motor shaft. The cantilevered loading produces huge loads and friction in the bearings. By using two motors on the ends of a shaft and taking the power off between the rotors and bearings, the bearing friction is greatly reduced.

Minimum Motor Motion With a prepackaged motor, the motor would have to be mounted to the side of the lower joint, requiring that it undergo significantly more motion than with the motor effectively centered about the joint. This also reduces the mechanical interference of the motors.

At the worst case handgrip pose the force scaling factor is 2.13. With this actuator configuration, the system can generate 7.45 N (16.39 lbf) along any one of the coordinates axes with no torque about any axis. At the mechanism center pose, the worst case force scaling factor is 0.5004 implying that the mechanism can generate 31.75 N (69.85 lbf) along any one of the coordinate axes with no torque. The force generating capability is suitably excessive. When the mechanism is eventually scaled down, the force scaling factors will become larger such that the actuator package will be merely adequate. The calculation of simultaneous force and torque generating capability is straightforward mathematically through Equation 2.25, but is highly dependent upon the specific loading and mechanism pose. A very crude estimation is to simply use the worst case force and torque scaling factors in the following equation based upon generating the maximum possible leg force:

$$(2.13 \times \mathcal{F}_{desired}) + (0.22\ (1/cm) \times \mathcal{T}_{desired}) = 15.875\,N. \tag{2.26}$$

Inland QT-1401-D Performance Data	
Peak Torque	3.96 $N \cdot cm$
Motor Constant	0.269 $\frac{N \cdot cm}{\sqrt{W}}$
Torque Sensitivity	0.325 $\frac{N \cdot cm}{Amp}$
Static Friction	0.130 $N \cdot cm$
Maximum Winding Temperature	155 ° C
Temperature Rise	15 $\frac{C^\bullet}{W}$
Average Ripple Torque	7 %
Poles	8

Table 2.10: Inland Motor QT-1401-D Performance Data

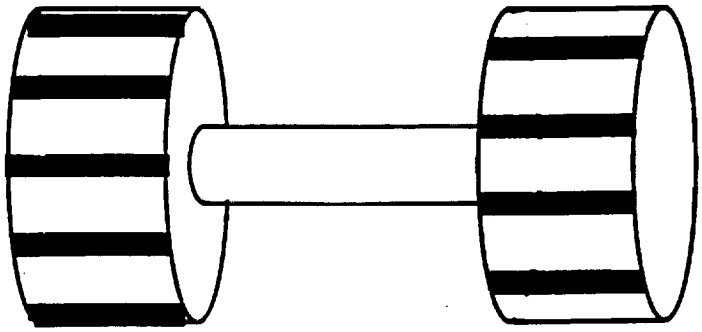

Two brush type motor rotors were press fit onto each motor shaft. The rotor poles were carefully set completely out of phase to reduce torque ripple and cogging.

Figure 2.11: Actuator Configuration

Thermal considerations of the motor package were a concern. A crude thermal analysis was performed to evaluate the situation. Simple conduction calculations indicated large temperature rises. Fin stock was added to the ends of the motor shaft to aid in cooling. Under continuous operation conditions, a temperature rise of 107 C° was calculated. The actual duty cycle of the hand controller is not known however a good guess should be around 25% for each actuator. No heating was noticed during system testing.

As previously indicated a cable drive system was selected in conjunction with the rotary DC motors. The drive consisted of a cable wrapping 4.5 times around the grooved motor shaft with the one cable end terminating directly on the bottom or retracting end of the leg slider, while the other passed up the leg and over a turning shaft to terminate on the extending end of the leg. The cable tension could be altered by a threaded adjustment and nut on the top end of the cable. The cable displayed some noticeable stretch under load and slippage on the motor shaft when violent load changes occurred. This is discussed further in the chapter devoted to system testing.

The following other drive configurations were considered in making the selection:

Cable with Rack and Pinion In this configuration, a continuous cable made a single pass around the motor shaft to drive an idler shaft on the upper end of the nonextensible outer leg. The idler in turn drove a pinion which engaged a rack mounted on the sliding portion of the leg. This approach was rejected due to the additional moving mass of the rack, the difficulty in removing the backlash from the gearing, and the friction associated with the gearing.

Cable with Friction Drive This approach is identical to the previous one except that a friction wheel drive was used against the sliding leg instead of the rack and pinion. It was abandoned due to the anticipated difficulty in making the friction adjustment.

Timing Belt with Direct Termination on Leg In this approach, a timing belt is used to make a single pass about the motor and upper turning shaft to a single termination on the sliding leg. The approach has the advantage of positive traction on the motor shaft. It is more difficult to provide a tension adjustment for the timing belt because it is continuous. The best method is to move the upper turning shaft. This inevitably compromises the position transducer calibration. A second method involves pressing a idler against the belt from the side at the expense of system friction. It is recommended that experimentation be performed with the timing belt. The mechanical hardware can be easily adapted.

Torque Tube with Nut and Lead Screw This concept involved a turning nut at the upper end of the nonextensible portion of the leg mechanism. A torque tube extending from the motor and surrounding a lead screw would drive the system. The concept was rejected due to the mass of the torque tube and lead screw, mechanical packaging difficulties associated with the transducer, nonbackdriveability, and high friction associated with an anti backlash nut.

2.6 Transducer Selection

As previously mentioned, the leg length was selected as the generalized coordinate set. The direct measurement of this parameter was desirable to avoid the computational burden associated with rotary to linear conversion, loss of origin associated with rotational transducers, and space constraints on the motor shaft. A penalty was paid in placing moving mass on the leg.

The type of transducer selected was the Induced Voltage Position Sensor (IVPS) Model # D1051-0001-IVPS-400, Manufactured by Lucas Schaevitz of Pennsauken, New Jersey. The device comprises a female coil into which a male, soft iron, spoiler rod is introduced. An audio frequency range voltage sinusoid is impressed upon the coil. The extent to which the spoiler is immersed into the coil influences the coil inductance and hence the voltage observed across the coil. The voltage varies linearly with the position.

The transducer type selection was influenced by the technical background of the design team, previous favorable experience with devices based upon the same operational principal, and previous favorable experience with the manufacturer. The second leading candidate was a conductive plastic potentiometer manufactured by Vernitech, of Deer Park, New York. This device is light but consumed a large volume. The manufacturer was hesitant to support a custom design for the application. The IVPS functions very well but adds mass and volume to the legs. It is seriously recommended on a redesign effort that internal acoustic or laser ranging devices be thoroughly investigated.

The IVPS model featured a 40 cm stroke as an "off the shelf" product. This particular stroke influenced the ultimate kinematic configuration. The accuracy of the product +/- 0.3 % of full scale stroke as a worst case, with 0.2 % typical. Since the hand controller is fundamentally a relative versus absolute positioning device, extreme accuracy was not felt to be a requirement. The device features an external electronics module separated by a one meter cable.

The spoiler portion of the device was mounted with a male thread on a tapped hole in the extending portion of the leg. The coil was mounted on a custom nylon flange pressed onto the coil body. The nylon flange featured a lateral position adjustment on four screws to allow alignment of the coil and spoiler. The spoiler is sleeved in a slippery plastic and is expected to contact the coil. The device was found to be very forgiving of lateral and angular misalignment.

2.7 Mechanical Design

This section closes Chapter 2. The major components of the mechanical design are discussed in this section under separate subsections. Comments on the performance of each component and suggestions for improvement are presented here as opposed to the system performance

section. The majority of components were fabricated from 7000 series aluminum. The components were finished with a hard coat with teflon impregnation for appearance and bearing function.

2.7.1 Base Joint

The base joint comprised a two DOF Hooke or universal joint. The Hooke joint was placed on the base as opposed to the handgrip because the opposite arrangement would require the rotation of the entire leg about its major axis contributing undesirably to the system inertia. The base side of the joint was realized with male pins on the motor housing engaging holes on an open yoke mounted to the base plate. The pins were formed on a detachable flange. The joint is assembled by placing the flanges into the yoke, sliding the housing into the flanges, and screwing the flanges into the housing. The teflon hardcoat did not provide an especially good bearing. Precision machining was attempted but some backlash remained. It is recommended that the flange be drilled larger and fitted with a solid teflon bushing.

The leg side of the joint was formed with a yoke on the base of the leg. The yoke was fitted with ball bearings which engaged the heat sink pins. The heat sinks are on long aluminum pins which screw into the motor shaft. The system is assembled by aligning the yoke on the motor shaft and screwing the heat sinks through the yoke bearings. No difficulties were found in this arrangement. The ball bearings were used as opposed to the bushings on the base side of the joint because friction in this joint would impede the rotation of the motor shaft, a critical function.

2.7.2 Lower Leg

The lower leg and yoke were machined out of a solid slab of aluminum. The leg was counter bored to allow space for the sliding upper leg. The top of the lower leg was precisely bored to a larger diameter to allow for a linear bearing package for the sliding upper leg. The leg can be easily shortened by cutting a portion off the top and counter boring a new bearing seat. This component functioned perfectly. It did require a significant amount of machining which was felt to be unavoidable.

2.7.3 Slider Bearing

The slider bearing interfaced the lower leg to the upper leg. The bearing comprised a prismatic joint in the sense that it allowed sliding of the upper leg, but prevented the rotation of the upper leg about its major axis. The internalization of the cable drive and position transducer prohibited the rotation of the upper leg. The upper turning shaft of the cable drive engaged a slot the length of the upper leg to prevent the shaft rotation. The upper turning shaft engaged the bearing seat in ball bearings since the shaft had to

rotate freely. The upper shaft was under considerable stress due to its small diameter and accordingly was fabricated from tool steel.

Initially the sliding bearing relied only on the teflon hardcoat. The system felt smooth but was very noisy. The bearing housing was relieved for a thin teflon annulus. The modification resulted in dramatic reduction of friction and noise. The antirotation bearing relied on the upper turning shaft literally rolling on the slot in the upper leg. The system was kinematically designed such that the peripheral speed of the turning shaft exactly matched the liner speed of the upper leg. To allow for machining error the shaft was turned down slightly and fitted with teflon collars which actually engaged the upper leg. This was a fortunate design precaution since the slot in the upper leg proved to be difficult to machine to specification.

2.7.4 Upper Leg

The upper leg was formed from aluminum tube with the outer diameter reduced on a lathe to decrease mass and the antirotation slot cut with an end mill. The reduced wall thickness prohibited accurate machining of the slot. Additionally the wall deflected under load to allow a small amount of lateral play in the leg. To accommodate the variation in the slot, the outer diameter of the teflon on the turning shaft was reduced. End plugs were machined and bonded into the tube. The cable tension provided a natural additional mechanism to retain the plugs.

2.7.5 Upper Joint

The Stewart Platform kinematics require a spherical joint on one leg end. Given that the Hooke joint was placed on the base, the upper joint had to be spherical. The upper joint posed a difficult design problem. Calculations of the joint rotational range of motion based upon the handgrip angular excursion superimposed upon the deviation due to the translation of the handgrip indicated a 60 degree from center displacement. The mechanical limitation of the spherical joint comprises the significant limitation on the angular excursion of the Stewart Platform.

Commercially available ball and sockets typically allow only 30 degrees from center. A special ball and socket could conceivably be designed to allow a greater range of motion by implementing a very thin constraining web. Such a joint could potentially suffer from high friction due to large stresses. Keeping with the philosophy of risking novel approaches when reasonable backups exist, an alternative realization was sought.

A joint having three rotations intersecting at a point comprises a kinematic equivalent to a spherical joint. This arrangement suffers from a mathematical singularity at large displacements when two of the axes become nearly aligned. In this application, a very conservative approach was taken by developing a joint with four rotational axes. The

fourth axis was arranged to rotate into the region vacated by the delinquent axis at the large angular displacements. Figure 2.12 depicts the singularity condition of the three DOF joint. Figure 2.13 shows the layout of the four DOF joint.

The joint was formed using bearing bronze pins. Great care was taken in machining but a significant amount of residual backlash exists. A great deal of this is due to the cap arrangement of the base rotation which has a radial split to allow the standoff to pass during assembly. The split allows the cap to deform and bind against the internal moving part such that the cap cannot be fitted securely. It is recommended that new caps be fabricated with a large hole in top replacing the radial split to allow the standoff to pass axially during assembly. The gimbal rings should be bored slightly larger and tight fitting solid teflon bushings installed. Finally, a ball and socket arrangement should be attempted for the sake of completeness in the research.

2.7.6 Handgrip Frame

The handgrip frame was fabricated from four thin webs welded into an assembly. The current frame is functional but massive and awkward. The hardware does not reflect the massive design effort required to achieve the current arrangement. Time and resources did not allow for the optimization of the structure to remove more mass while maintaining structural integrity. This approach should be considered but only after a decision is made on the net system range of motion and the approach of rotating the entire mechanism relative to the operator.

2.7.7 Force/Torque Sensing Cell

A six DOF force torque measuring cell was mounted in the handgrip. The specific model was the 50 lbf version offered by JR3, Inc of Woodland, California. A commercially available model was contemplated as opposed to developing a six DOF sensing bridge within the handgrip. The cell was mounted such that its center coincided with that of the handgrip with the intention that the operator wrap his hand about the cell. This was done because the cell has a very low torque limit. If the cell was offset to a distance such that the operator could close his hand about a separate handgrip without his fingers contacting the cell, then the cell would reach torque saturation with only moderate handgrip forces.

The current arrangement is not ergonomic. It served the purpose well for the system tests with the handgrip mechanically linked to a test stand. The cell should be offset if lower force limitations are adopted, or a custom sensing bridge should be developed. The current cell cost $7,160.00 as an off the shelf item. A custom arrangement would be proportionately more expensive.

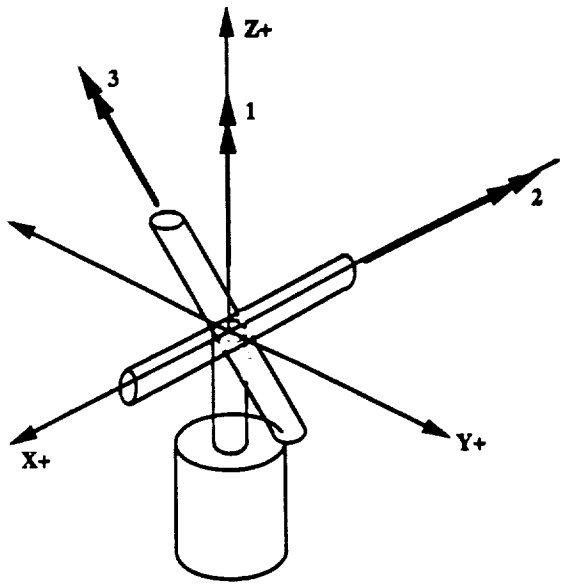

With Joint 1 and Joint 3 nearly aligned, the mechanism looses the capability to rotate about the Y axis.

Figure 2.12: Three DOF Joint in Singularity Position

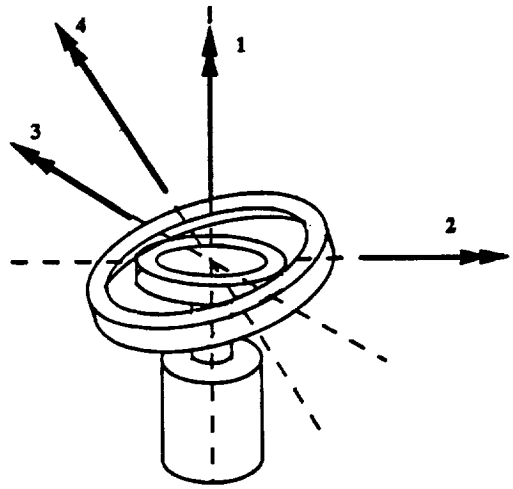

Joint 1 provides a permanent rotation about the vertical. The inner gimbal ring is pinned through the Joint 1 standoff to provide rotational Axis 2. The outer gimbal ring is pinned through the inner gimbal ring to provide rotational Axis 3. The outer gimbal ring is held in a retaining cup to allow the ring to rotate about its major axis to provide rotational Axis 4. Axis 3 & 4 are always normal to each other. Similarly, Axis 1 & 2 are always mutually orthogonal. As Axis 2 rotates, Axis 3 & 4 always have a sufficient projection normal to the plane of Axis 1 & 2 to allow rotation about the the axis normal to that plane.

Figure 2.13: Four DOF Joint Structure

Chapter 3

Computation, System Electronics, and Controller

This chapter discusses the computer processor arrangement forming the computational base, the interfacing and communication electronics, and the control architecture for regulating the forces and torques within the hand controller mechanism. The computational hardware and control architecture are highly interrelated. For organizational purposes, the computational electronics are discussed followed by the control approach.

3.1 Hand Controller Electronics

The force reflecting hand controller is controlled by using the following hardware components:

- One 80386 33MHz. Personal Computer.
- Three Alicron i860 boards.
- Two parallel I/O boards.
- One analog to digital board.
- One digital to analog board.

The following sections will describe the operation of each of the above components and finally an overview of the operation of the entire system will be presented. Figure 3.1 presents the electronic layout graphically.

3.1.1 The Personal Computer

The Personal Computer (PC) used for this project is a 80386 33Mhz PC with a 2 megabyte memory and a 80387 math co-processor chip. The PC had an extended industry standard architecture bus which included 8, 16 and 32 bit card slots. In addition to the PC, an extension card cage was utilized to support the large amount of cards used for the project. The extension card cage has a 220 watt power supply and ten 16 bit card slots. The PC and card cage acted as a host machine to house the cards and was used to control the various boards used.

3.1.2 Alacron i860 Boards

The Al860 is a board-level co-computer for the PC-AT designed to perform high speed arithmetic computations using the Intel i860. A single Al860 is capable of performing at 40 MIPS or 80 MFLOPS in single precision, and multiple Al860 boards can be linked for even greater performance.

The Al860 is built around the 64-bit 160 MByte per second bus of the i860 MPU. Connected to this bus are the i860 processor chip, local memory, the host (AT) interface, and the expansion board interface. The i860 is a single-chip RISC-technology microprocessor unit. The highly-parallel, highly-integrated MPU operates at either 33 or 40 Mhz, depending on the model of Al860. The chip has the capability to complete an integer operation, an integer and floating point operation, or an integer and floating point multiply and add operation within a single clock cycle. The i860 operation is pipelined so that a floating point result for vector-data sets can be produced on every clock cycle.

In the Slave Processor Mode,the Alacron numerical library for he Al860 is pre-compiled and loaded into the Al860 memory and is accessible from the host application. Additional functions are provided to dynamically allocated data storage and load and retrieve data from the Al860. Programs benefit from the performance of the i860 without the need to write and debug i860 specific code. Slave Processor Mode may also be used to call individual functions of the user written C or Fortran application. A control program loads the user provided i860 program, whose functions may be individually invoked.

3.1.3 Parallel I/O Boards

The MetraByte parallel digital I/O card, PIO-12, provides 24 TTL/DTL compatible digital I/O lines, interrupt input and enable lines and external connections to the IBM PC's bus power supplies. It is a flexible interface for parallel input/output devices such as instruments and displays, and user constructed systems and equipment.

The 24 digital I/O lines are provided through an 8255-5 programmable peripheral in-

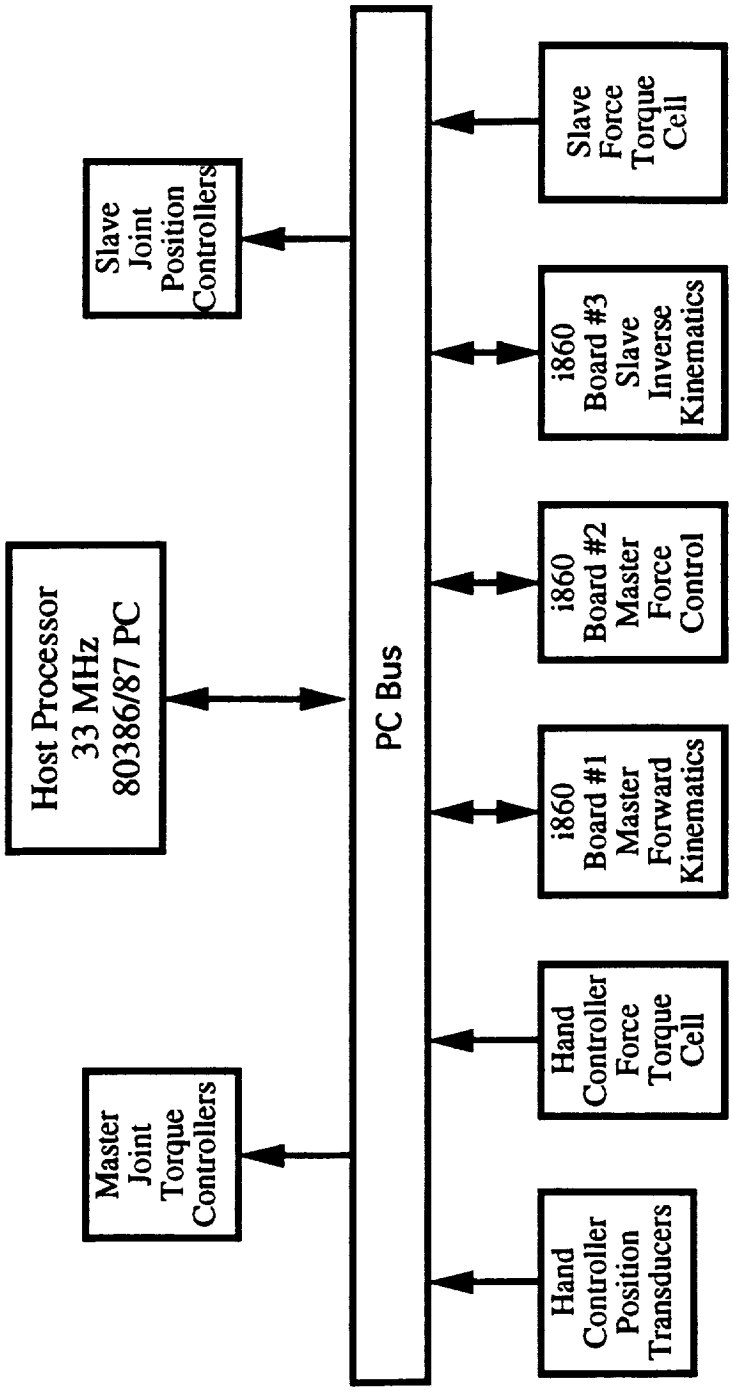

Figure 3.1: Electronics Schematic

terface (P.P.I) I.C. and consist of three ports, an 8 bit PA, an 8 bit PB port, and an 8 bit PC port. The PC port may also be used as two half ports of 4 bits, PC upper (PC4-7) and PC lower (PC0-3). Each of the ports and half ports may be configured as an input or an output by software control according to the contents of a write only control register in the P.P.I. The PA, PB and PC ports may be read as well as written to. In addition, certain other configurations are possible for unidirectional and bidirectional strobed I/O where the PC ports are used for control of data transfer and interrupt generation etc. Users are referred to the Intel 8255-5 data sheet for complete technical description and summary of the various operating modes of the P.P.I.

3.1.4 Analog to Digital Board

The DT2841 series board is a high performance analog and digital I/O board designed to be used with the IBM Personal Computer AT or compatible computer systems. The DT2841 contains the following subsystems:

- A/D conversion.
- D/A conversion.
- Digital I/O.

The board is plugged into one of the six fully bussed system expansion slots on the Personal Computer AT backplane.

The DT2841 series board is designed to operate with the DT7020 Array Processor for maximum throughput. The DT2841 series board use neither the DMA channels of the system nor the system bus for data transfers. All digital data transfers from the A/D conversions or D/A conversions take place between the DT2841 series board and the DT7020 Array Processor over dedicated ports and without the intervention of the host processor. This arrangement not only provides enhanced performance to the DT2841, but also greatly reduces overhead on the AT bus.

The DT2841 board is a 12-bit high level board which uses the DT5713-PGH A/D converter. It is equipped with a programmable gain amplifier which provides gains of 1, 2, 4, 8. It accepts both unipolar and bipolar inputs. Unipolar inputs range from 0 to 1.25V to 0 +10V, and bipolar inputs from +/-1.25V to +/-10V. The DT2841 is configurable for 16 single-ended or 8 differential inputs. It operates at a maximum throughput of 40Khz.

3.1.5 Digital to Analog Board

The DT2815 digital-to-analog converter (DAC) subsystem is a half-size board developed by Data Translation for use with the IBM PC/XT/AT and compatible microcomputer systems.

The board converts a 12-bit binary data word from the host processor into an analog output voltage or current.

The DT2815 provides eight analog output channels. Each channel can be set for voltage or current output. The board can function at a rate of up to 3300 conversions per second. However, the actual throughput depends on a number of factors including the settling time of the DACs (300 microseconds), the operating firmware program, the number of channels enabled, and the software running it.

The board can be configured for unipolar or bipolar outputs. The unipolar output range in 0 to +5V for voltage outputs and 4 to 20mA for current output. The bipolar output range is +/-5V. The DT2815 can provide voltage output channels and current output channels at the same time.

All data transfers in and out of the DT2815 are controlled by the program stored in the host microcomputer. The DT2815 contains two registers: the Data Register and the Status Register. The Data Register receives the digital code to be converted into an analog signal. The Status Register conveys information about the state of the on-board RAM and ROM, and the progress of D/A conversions.

The DT2815 requires +5V, +12V and -12V power which it receives from the microcomputer backplane. If operating in the current loop output mode, the loop supply can be taken from the host computer's +12V line or can be supplied internally.

3.1.6 System Operation

The personal computer acted as the host machine for the entire system in which all the additional boards reside. The three i860 boards are used to run independent processes in parallel, while the remaining boards are used as I/O boards to communicate and control the hand controller and the slave robot.

The system is configured in such a way to support the following software architecture. Because of its comparatively slow speed and its critical path role in information routing, the personal computer was intended to run only the main program which distributes information to the Alacron boards and controls the I/O boards and AT bus. The personal computer was intended to perform a minimal amount of computation. The Alacron boards run the following processes respectively: **Board 1** - the forward kinematics of the hand controller, **Board 2** - the force control algorithm for the hand controller, and **Board 3** - the inverse kinematics of the slave robot.

The main program starts by reading the leg lengths of the hand controller and downloading this information to Board 1. While this board is running, the host processor acquires data from the force/torque cells in the hand controller and slave robot. When finished the forward kinematic computation, Board 1 sends an interrupt on the AT bus. The host

processor then reads the forward kinematic output, the measured forces and torques from the force cells in the hand controller and the slave robot, downloads all this information to Board 2, and also downloads the forward kinematic result to Board 3. Board 2 and Board 3 can then begin their computational cycle. During this cycle, the host processor reads the leg lengths of the hand controller, downloads that information to Board 1, and then awaits the termination of the computation on Board 2. Upon the completion of the Board 2 process, the host reads the control command result from Board 2 and sends it out the motors driving the hand controller. The host machine then reads Board 3 and transmits the slave inverse kinematic command to the slave robot to complete the cycle. The advantage of this architecture is the parallel processing which takes place by distributing the computational requirements across the four processors.

3.2 Control of the Force Feedback

This section discusses the approach to the control of the feedback forces within the hand controller mechanism. It begins with a brief section on control philosophy followed by the actual control law development.

3.2.1 Force Feedback Philosophy

The design philosophy of this program has been that the proper goal of force feedback teleoperation system research is to make the entire teleoperation system transparent to the operator - to make the operator feel as if he were actually on site and an integral part of the slave robot. Certainly, the operator should not be cognizant of any dynamics in the hand controller mechanism. In all likelihood, the operator should be made cognizant of the dynamics of the slave robot. Simply stated, the slave and human arm have dramatically different dynamics, and it is the slave which performs the work and not the human.

The human has limitations which no amount of "software massaging" can overcome. In particular, the human has a very limited bandwidth in tracking oscillations by either providing counterbalancing forces through his arm or by position tracking. This is intuitive and has been shown experimentally [M2,M3] . Certainly the actuation force of human muscle has limitations. It is coupled to a mechanical link with mass, the bone. Such a system has bandwidth limitations. In direct interaction with a vibrating member, the human is usually thrown back. In a force feedback system, if the human is thrown back, a new position command is generated to the slave robot which will usually set up a limit cycle oscillation. It is completely fitting to low pass filter the force information throughout the system to remove frequencies beyond the human bandwidth. Beyond that, the human should experience the force as realistically as possible.

Computational hardware will eventually and probably very soon have the capability to compute the complete dynamics of a slave manipulator to account for the entire mass content

of the manipulator and its grasped object at rates which are suitable for teleoperation. If a very dynamically sound hand controller mechanism exists, then it will surely be useful to provide the dynamics of the slave to the operator through the mechanism. Success will depend upon the integrity of the hand controller.

3.2.2 Control Law Development

The control law for the hand controller relied upon an inner and outer control loop. The inner loop comprised a current control loop around each of the actuators. This loop was introduced basically to compensate for electrical dynamics of the actuators. The outer attempted to compensate for the friction and mass content of the hand controller system. The control schematic is shown in Figure 3.2.

The inner control loop was particularly easy to implement. A theoretical current was calculated based upon Equation 2.25 and the electric motor characteristics. This current command was fed as a voltage signal to a local current controller and amplifier package supplied by Inland Motor. The controller implemented a proportional, plus derivative, plus integral (PID) control law on the current. The bandwidth of the controller and motor combination is in the kilohertz range. The control module provides a port for an externally mounted current limiting resistor. This can be used in addition to software clamps to provide a measure of safety against the high force generating capability.

The outer control loop was based initially upon a proportional plus derivative (PD) control action acting upon the error in force and torque measured at the handgrip. This approach was adopted from a "seat of the pants" viewpoint as opposed to rigorous mathematical analysis, fundamentally because of the large amount of labor involved in the analysis and the questionable worth in this highly nonlinear system. The proportional action was included for basic accuracy, while the derivative action was included to encourage high dynamic response. A menu was set up on the host computer to allow individual gains to be easily downloaded during system test for what was to be an empirical search for suitable gains.

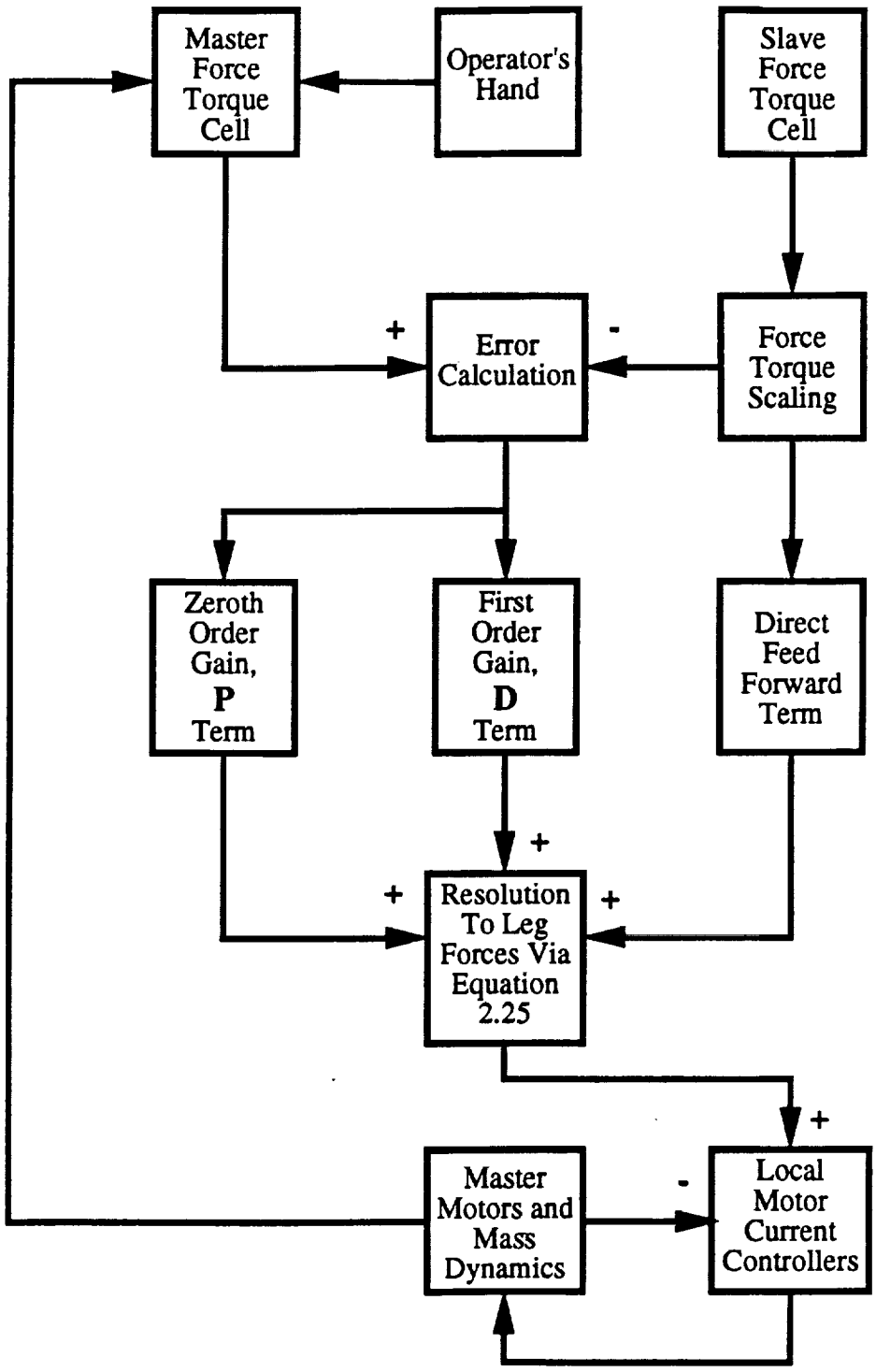

Figure 3.2: System Control Law Schematic

Chapter 4

System Testing

This chapter documents the system testing. System testing basically proceeded in two phases. The first phase included tests of the hand controller as an isolated system element. The second phase comprised an integrated test of the hand controller with a slave robot equipped with a force cell in the end effector as a full up, man in the loop demonstration. The test phases are discussed separately in the following.

4.1 Hand Controller Subsystem Testing

The subsystem testing comprised assembly and testing of the individual components, qualitative or empirical testing of the hand controller subsystem against simulated slave loads with a human in the loop, and more rigorous testing of the subsystem with a test fixture to obtain quantitative data on system performance. Much of the mechanical testing was described in the previous chapter.

4.1.1 Actuator Testing

The electric motors were assembled into their housings and bench tested as a subsystem. Two great concerns exist with the assembly: axial alignment and axial preload. The axial alignment was checked with a set of specially fabricated alignment and torquing tools. The fundamental alignment was set with the tool. Extreme care and intuition then had to be used in the subsequent preloading of the motor bearings. Several brushes were destroyed during the assembly phase before the assembly technique was well developed.

The bearing preloading proceeded by starting from the initial alignment provided with the jig. The bearings were then loosened on their retaining collars by alternately backing the screws by identical amounts on each end of the motor housing. This proceeded until

the motor "felt" good. Individual screws were sometimes found loose on the retaining ring. Subsequently all screws were set with flexible gasket cement to retain their position.

All motor assemblies were bench tested for starting current. The individual motors were tested at the factory and found to have a staring current of approximately 0.23 Amp. All six actuator assemblies were capable of being tuned down to this level of starting current. A higher starting current was expected reflecting the bearing friction.

After actuator testing, the complete leg subsystems were assembled and tested. Testing involved cycling the legs under sinusoidal position control. It was during this testing that the interference between the upper turning shaft and the upper leg antirotation slot was noticed. The system generated large amplitude vibrations as the turning shaft passed over high spots on the upper leg and the upper leg wall deflected under the load. As previously mentioned, the correction involved reducing the diameter of the turning shaft at the price of some upper leg rotation. A better correction would be to locally stiffen the tube wall before machining to allow for a better machining operation and to provide a stiffer final product. Some warming of the motors was noticed in the high duty cycle oscillatory tests.

The leg assemblies display some undesirable lateral wobble at near full extension. This wobble arises primarily from the deflection of the upper leg wall with side loads. When held horizontally, gravity generates a significant side load against the leg assembly. The wobble also comes from the intentionally loose running fit of the upper leg in the teflon bushing. This condition can best be corrected by a stiffer wall section of the upper leg. Honeycomb may be worth investigating for this condition.

The friction of the individual legs was measured with a hand held force gage. High friction forces naturally are noticed with higher preload tension in the drive wire since the radial forces in the motor shaft and upper turning bearing increase with the preload. The leg friction forces measured with the manual force gage with the cable preload as adjusted for the final system testing are presented in Table 4.1. The forces are given for three positions, at approximately full extension, center, and full retraction. The forces were also measured in both directions, labeled "Out" and "In," for extension and retraction respectively.

The friction levels are disappointingly high. Extrapolation of the starting current of the isolated actuators, with the DC torque constant and the working radius of the cable take off, shows a friction force associated with the actuator only of:

$$\mathcal{F}_{friction} = \frac{2\ (motors) \times 0.23\ (Amp) \times 0.325\ \frac{N \cdot cm}{Amp \cdot motor}}{0.5\,cm} = 0.30\,N = 0.66\,lbf \qquad (4.1)$$

Comparison with the measured force data with the manual force gage suggests that the contribution of the magnetic friction of the motor assembly to the entire leg friction is 40% to 50%. Starting current measurements of the leg assembly would provide a better base of comparison to identify the source of the system friction.

Leg - Position	Friction Force In *(N)*	Friction Force Out *(N)*	Average Force *(N)*	Average Force *(lbf)*
Leg 1 - Extended	0.59	0.64	0.53	1.17
Leg 1 - Center	0.36	0.59		
Leg 1 - Retracted	0.50	0.50		
Leg 2 - Extended	0.61	0.66	0.57	1.25
Leg 2 - Center	0.48	0.50		
Leg 2 - Retracted	0.57	0.59		
Leg 3 - Extended	0.55	0.59	0.57	1.26
Leg 3 - Center	0.61	0.45		
Leg 3 - Retracted	0.61	0.61		
Leg 4 - Extended	0.57	0.55	0.58	1.28
Leg 4 - Center	0.52	0.61		
Leg 4 - Retracted	0.61	0.64		
Leg 5 - Extended	0.70	0.61	0.61	1.33
Leg 5 - Center	0.45	0.57		
Leg 5 - Retracted	0.68	0.61		
Leg 6 - Extended	0.59	0.64	0.55	1.22
Leg 6 - Center	0.45	0.52		
Leg 6 - Retracted	0.55	0.67		

Table 4.1: Leg Friction by Direct Measurement

4.1.2 Empirical Subsystem Testing

After the individual leg tests, the hand controller subsystem was assembled for preliminary integrated testing. The outer loop gains were gradually increased from zero to develop a sense for the system behavior. Often instability was encountered. The system clearly demonstrated excessive load generating capabilities. In some instances, the upper joint standoffs were bent under large torque loads.

The cable drive system displayed significant defects during the subsystem testing. In particular, the cable would slip on the motor shaft in conjunction with large magnitude, unstable oscillations. The slippage would occur when the motor would drive very hard in one direction leading to slack in the unloaded side of the cable. When the motor would suddenly change directions, the shaft would slip due to the slack in the cable. This mechanism was attenuated with higher cable preload at the expense of friction. The motor shafts originally had a circular groove. The motor assemblies were disassembled and the shafts remachined for a "V" groove in an attempt to bite into the cable to prevent slippage. This allowed a significant reduction in preload, and a corresponding reduction of roughly 30

The current shaft is fabricated from hard tool steel. This choice was made for strength and the need to press fit the motor rotors on the shaft. Visual inspection of the shaft shows a "shiny" surface, perhaps as a result of slippage and subsequent polishing by the cable. The cable is made from stainless steel. Steel on steel has a relatively high coefficient of friction of 0.8, while solids on rubber have a value ranging from 1 to 4 [O1, pg.545- 546]. Some improvement might be made by impregnating the wire with rubber. However, this must be done with caution due to the possibility of contaminating the brushes and the likelihood that the solution lacks permanence.

Testing with a timing belt drive is highly recommended. The motor shafts could likely be modified for a timing belt by bolting two split belt pulleys onto the current motor shaft. An interface method for the timing belt with the leg would have to be designed. This could most easily be done by developing a new bottom cap. The caps are set with a mild epoxy which releases at elevated temperatures. The upper shaft would require a simple modification to provide a centering groove for the belt. The system could be tensioned by moving the turning shaft bearing collar axially on the lower leg.

4.1.3 Quantitative Subsystem Testing

Quantitative evaluation of the hand controller system was desired to verify the performance of the Stewart Platform in the hand controller application, measure the system friction, evaluate the effectiveness of the outer feedback control loop in enhancing the force feedback fidelity, and measure the system execution time.

Force Feedback Fidelity

In addition to providing the feedback transducer, the force and torque sensing cell was used to measure the forces and torques at the handgrip during the system testing. The test fixture featured as external frame with a linear slider bearing. The slider was aligned with the y axis. The normal handgrip was removed from the force torque cell, and the slider bearing was bolted in its place. This allowed the measurement of static forces in five DOF and dynamic forces in one DOF. The test arrangement is shown in Figure 4.1.

The test procedures universally featured a finite step input command of force or torque along one of the DOF with the command for all other freedoms held at zero. With the force or torque command held constant at the step output level, the hand controller was then driven by hand in the negative y direction, allowed to be stationary for a brief time, then drawn outward in the positive y direction. Two outer loop gain values, **P** and **D** had to be specified. The first value multiplied the error in force or torque in each of the six DOF. The second value multiplied the first difference in force or torque error. Additionally, a general force or torque scaling value had to be specified. As a backup stabilization method, the capability to employ velocity damping based upon differentiation of the leg lengths was also implemented. The testing proceeded by simply varying the gains and observing the behavior until an optimum was discovered.

One of the first tests to be performed was to remove the feedforward term from the control calculation. This term exactly implements Equation 2.25. The system was then driven completely by the error sensed through the handgrip. The results were too poor to justify recording. **The system cannot be completely error driven.** The feedforward term must be implemented.

The optimum gain values were found to be **P=0.5** and **D=0.5**. The system essentially went unstable for any value of **P** above 0.5. Surprisingly, the **D** value contributed only slightly to the speed of the response. In an attempt to generate very fast response, the sign of the **D** term was changed to act as a damping agent to allow proportionately high **P** values. This proved of little benefit. The position based damping also proved of little benefit. The system apparently has a fundamental limit of **P=0.5**.

A reasonable course of investigation in explaining the stability limitation is that the control law was requesting forces which the actuators simply could not produce. Separate monitoring of the actuator commands indicated that the actuator torque limit was never approached. To support this point, Figure 4.2 displays the voltage command to Leg 5 for a step command of $10\,lbf$ in the positive z direction. The ordinate represents coded numbers which range from 0 to 4000, corresponding to $-20\,V$ and $20\,V$ respectively. As can be seen, the control law never requested a voltage anywhere near the system maximum or saturation value.

Proceeding in a different vein the stability limit could possibly result from the speed of the processing. The **D** term should help to increase stability and enhance performance

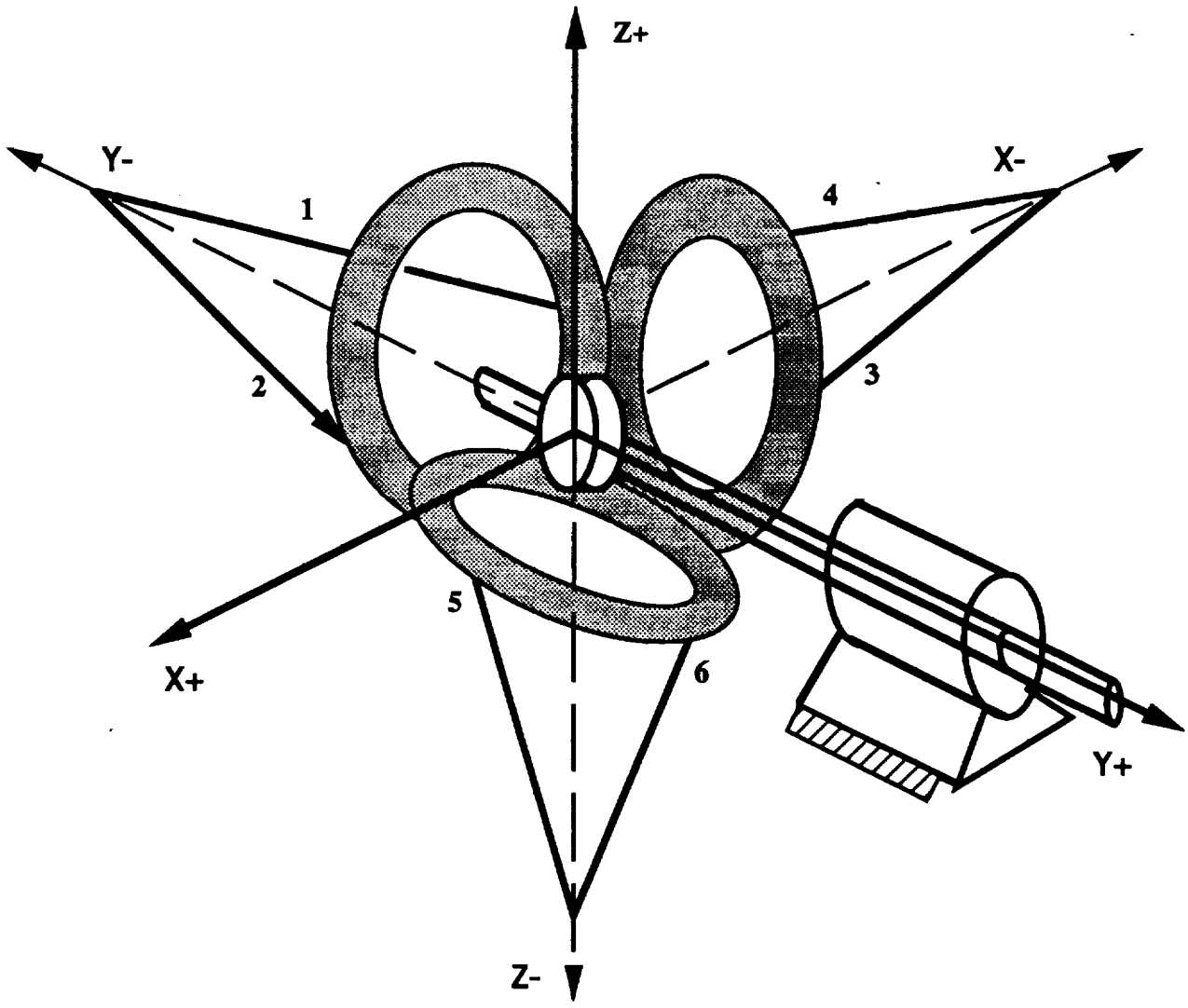

A linear bearing was mounted on a frame external to the hand controller mechanism. The axis of the bearing was parallel to, but offset from the Y axis. The bearing shaft tied into the face plate of the force cell at an offset in the -X direction from the force cell center.

Figure 4.1: Quantitative Force Measuring Apparatus

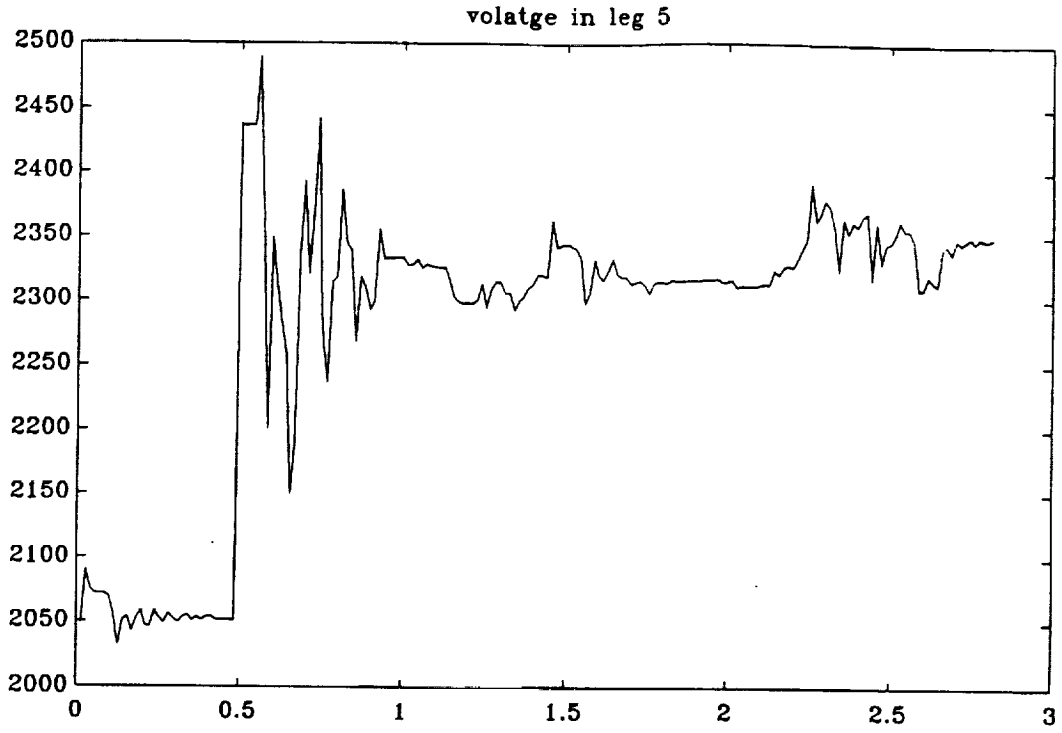

Figure 4.2: Coded Command History in Leg 5 for 10 lbf in z

and is probably being rendered ineffective by the computational limits. Classical control thought warns against numerical differentiation to produce stabilizing feedback, primarily because of noise. In this case the data input and output time may also be a limiting factor.

The data from four tests are included in toto for reference in Appendix B. The results include data for the force/torque in all six DOF as well as the corresponding force history in the legs. Test A featured no feedback and a force command of 10 lbf in the positive z direction. Test B, featured the optimum gains previously cited and the same step command. Comparison of these results was intended in indicate the overall worth of the outer loop. For additional comparison, Tests C and D both featured the optimum gains, but had step inputs of 10 lbf in the positive x direction and 5 $in \cdot lbf$ about the positive y axis respectively.

Figures 4.3 and 4.4 which are repeated in this chapter show the system response along the z axis for Test A and Test B respectively. The solid line indicates the command, while the broken line indicates the response. Both tests feature a time delay of approximately 0.1 sec. before the response occurs. The actual delay will be less due to the fact that the command is recorded at the instant it is given, whereas time is required to read the response and record the information after the response has actually occurred. The performance of the Test A, the zero gain case, is superior having little overshoot and better steady state error. Figures 4.5 and 4.6, also repeated in this chapter indicate the response in force along the x axis for Tests A and B respectively. For these graphs, the solid lines show the force in x while the broken lines show the relative mechanism position in y, the ordinate for y not

being provided in the graph. The y position is plotted to provide a sense of the mechanism dynamics at each instant of time. In this instance, Test B with the outer feedback loop compensation is superior having less average steady state error and less peak to peak error.

Execution Timing

The computation cycle is described in Section 3.1.6. The cycle start corresponds to the reading of the leg lengths. The test program read the system clock in the host PC at the time the first set of leg lengths was read. The system then executed continuously without interruption. In conjunction with the 4,000th reading of the leg lengths, the system clock was again read. The elapsed time divided by the number of cycles yielded the execution rate. The system achieved a complete cycle frequency of 83 Hz.

4.2 Integrated System Test

The program plan called for integrating the system with a slave robot to demonstrate complete system capability. To this end, the hand controller was integrated with a General Electric P60 robot equipped with a Lord force/torque measuring cell in its handgrip. The integration took place at the Center for Intelligent Machines and Robotics at the University of Florida. Program resources did not allow for any quantitative testing with the integrated system. Successful demonstration of position feedforward and force feedback was demonstrated in six DOF. Additionally, the system was integrated with a real time solid model computer display of the slave robot to include force histograms and a vector display of the force and torque developed at the slave end effector.

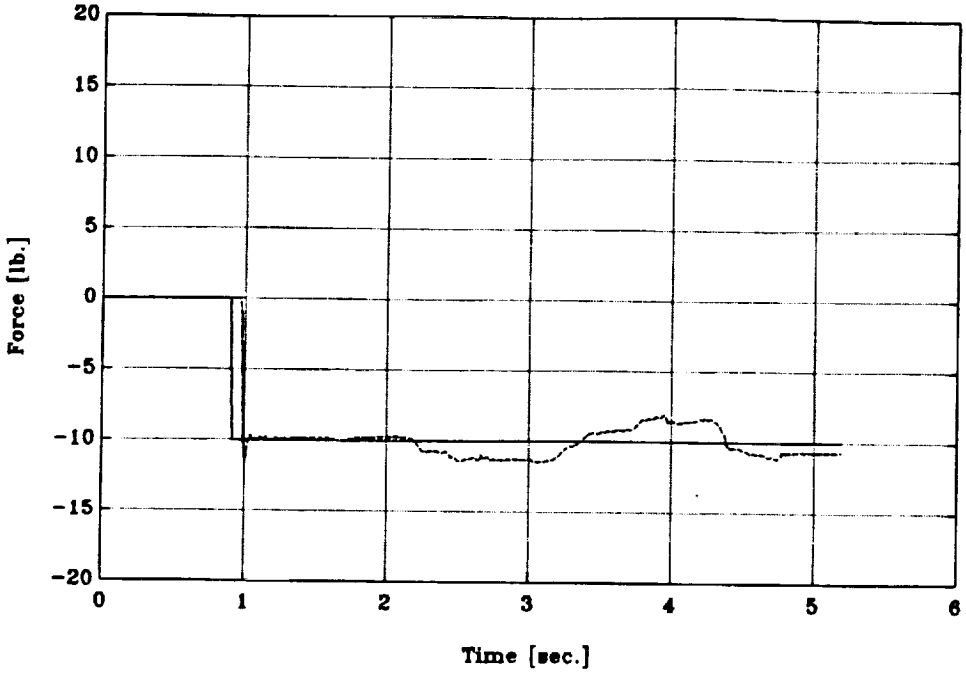

Figure 4.3: Test A - Force Response in z

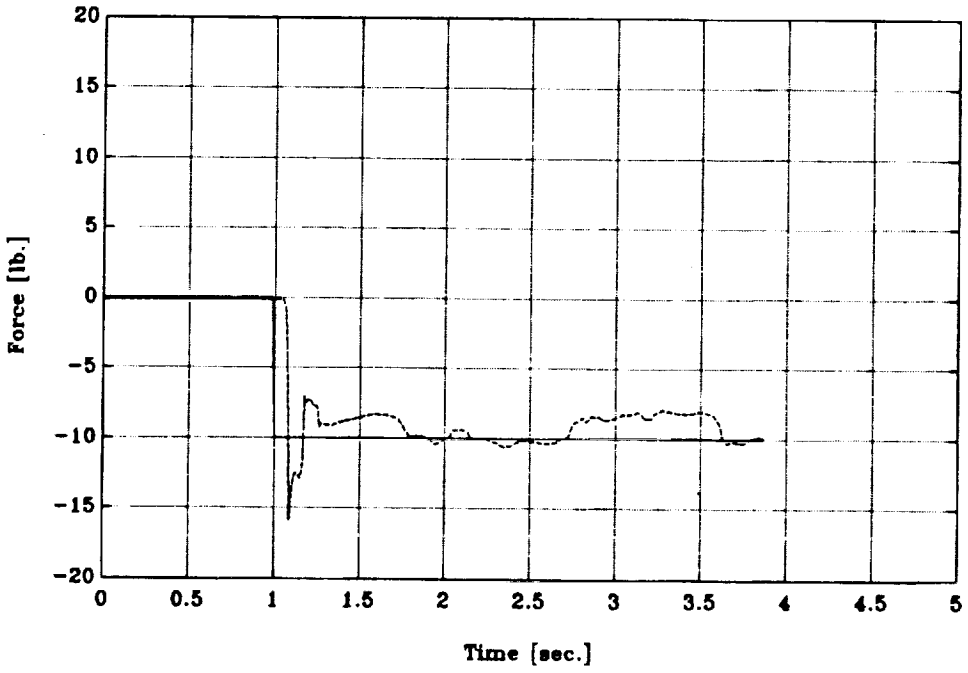

Figure 4.4: Test B - Force Response in z

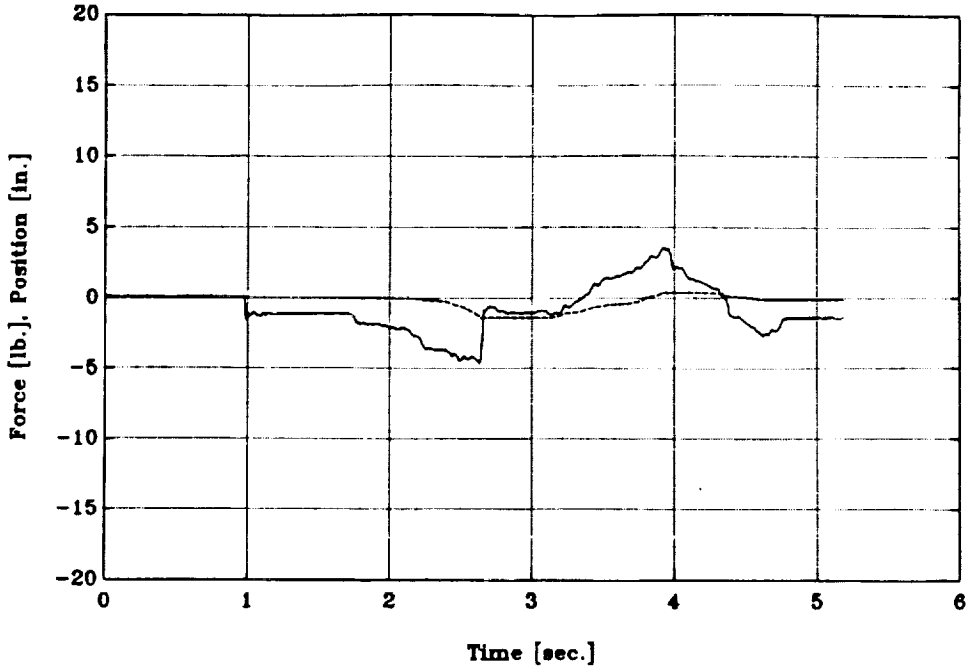

Figure 4.5: Test A - Force Response in x

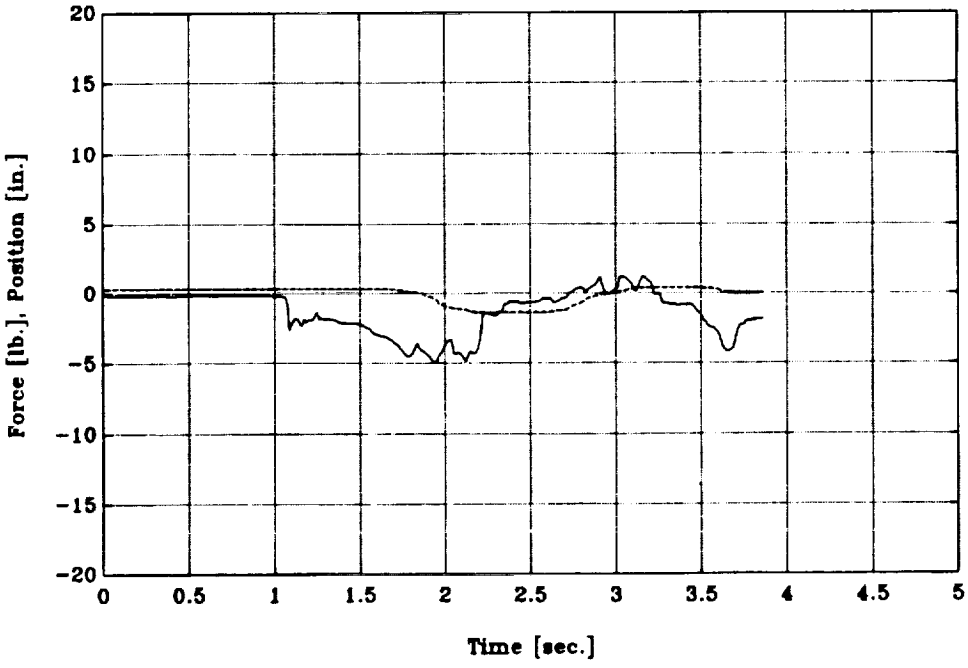

Figure 4.6: Test B - Force Response in x

Chapter 5

Conclusions and Recommendations

This research program embraced the thesis that a superior force reflecting hand controller could be constructed from the Stewart Platform mechanism. The program provided a means to perform basic research on the Stewart Platform and also to investigate advanced concepts in the development of force reflecting hand controllers, namely the implementation of a friction and inertia cancelling control loop about the entire mechanism based upon force and torque sensing in the mechanism handgrip.

5.1 Conclusions

During this research program, the following results and conclusions were developed:

Mechanisms Design Rules A set of design rules for the Stewart Platform mechanism were developed and documented.

Mechanism Performance Capabilities Theoretical limitations on the range of motion of the Stewart Platform mechanism were established. In particular a mathematical limitation of 90 degrees pure rotation from center was established. Because of mechanical limitations, realistic systems can expect perhaps 60 degrees rotation from center.

Hand Controller Kinematic Design A force reflecting hand controller kinematic design was developed based upon the Stewart Platform mechanism. The design featured the capability to move within a 25 *cm* cube, and rotate +/- 45 degrees about any axis intersecting that cube.

Mechanical Design A detailed mechanical design of the concept based upon the kinematic design was developed and executed. The system had a theoretical capability to generate 7.45 N (16 lbf) of force anywhere in the workspace at the worst case orientation, with a maximum of 31.75 N (70 lbf) in the most favorable position and orientation.

Controller A computer and control architecture for the system was developed and executed. The architecture was based upon distributed parallel processing using three i860 processors. The system featured a bilateral control update rate of 83Hz.

Hand Controller Testing The hand controller subsystem was tested with the following salient results:

- The hand controller subsystem is basically functional. It can produce large forces and torques against the human operator while the operator executes positioning motions.
- The cable drive system needs improvement due to cable slippage on the motor shaft.
- The usefulness of the force and torque cell in the handgrip is not conclusive. In some instances it improves accuracy and force feedback fidelity while in others it introduces instability.

Integrated System Testing The hand controller system was integrated with a GE P60 slave robot equipped with a force and torque sensing cell in its handgrip. Bilateral control of the integrated system was demonstrated.

5.2 Recommendations

Based upon the above, the following research recommendations are set forward:

Timing Belt Drive The mechanical system can be readily reconfigured with a timing belt drive in anticipation of relieving the cable slippage problem and potentially reducing friction with associated drop in preload. This change and subsequent testing is highly recommended.

Active Friction Attenuation The friction of the mechanism was dissapointingly high. It may be possible to feed forward a compensating current of roughly 0.2 Amp to aid in breaking the friction. The direction of the current would have to be based upon force feedback from the force cell in anticipation of the operator's intended motion.

Alternative Force Sensing The current force cell is massive, expensive and awkward. It should be possible to mount force sensing devices (strain gages or piezo-electric) elements between the upper joints and the handgrip to sense directly the force output of each leg upon the handgrip.

Outer Feedback Loop More development is required before definitive conclusions can be reached regarding usefulness of the outer feedback loop. Some insights into the stability limitations were mentioned. More careful analysis and testing is recommended.

Bibliography

[B1] Bejczy, A.K., Salisbury, J.K., "Controlling Remote Manipulators Through Kinesthetic Coupling," *Computers in Mechanical Engineering*, Vol. 2, No. 1, July 1983. pp. 48-60.

[H1] Hirzinger, G. Heindl, J. and Landzettel, K, "Predictive and Knowledge Based Telerobotic Control Concepts," Transactions 1989 IEEE Robotics and Automation Conference, pp 1768-1777.

[K1] Kilpatrick, P.J., "The Use of a Kinesthetic Supplement in an Interactive Graphics System," Ph.D. Dissertation, Univ. of North Carolina at Chapel Hill, 1976.

[M1] Martin, H.L. and Hammel, W.R., "Joining Teleoperationwith Robotics for Remote Manipulation in Hostie Environments," Conference Proceedings Robots 8, Robotics International of Society of Manufacturing Engineers, Vol. 1, Dearborn, Michigan, June 1984.

[M2] McRuer, D.T. and Krendel, E.S., "The Human Operator as a Servo System Element, Part1," Journal of the Franklin Institute, Vol 267, May 1959, pp. 381-404.

[M3] McRuer, D.T. and Krendel, E.S., "The Human Operator as a Servo System Element, Part2," Journal of the Franklin Institute, Vol 267, June 1959, pp. 511-536.

[O1] Oberg, E., Jones, F., and Horton, H., *Machinery's Handbook*, Industrial Press Inc., New York, N.Y.; Revised 21st Edition, 1980.

[S1] Stewart, D., "A Platform with Six Degrees of Freedom," *Proc. Institute of Mechanical Engineering*, Vol. 180, Part 1, No. 5, pp. 371- 386, 1965-1966.

Appendix A

Tabular Mechanism Performance Parameters

Y (cm)	*Units – Dimensionless*										
12.7	1.57	1.53	1.50	1.47	1.45	1.42	1.39	1.37	1.34	1.32	1.29
10.16	1.58	1.54	1.50	1.47	1.43	1.41	1.38	1.35	1.33	1.30	1.28
7.62	1.59	1.55	1.51	1.48	1.45	1.42	1.39	1.36	1.34	1.31	1.29
5.08	1.62	1.57	1.53	1.49	1.46	1.43	1.40	1.38	1.35	1.33	1.33
2.54	1.64	1.59	1.55	1.51	1.48	1.45	1.42	1.39	1.37	1.37	1.39
0	1.68	1.62	1.58	1.54	1.50	1.47	1.44	1.42	1.42	1.44	1.46
-2.54	1.72	1.66	1.61	1.57	1.53	1.50	1.47	1.47	1.49	1.52	1.54
-5.08	1.76	1.70	1.65	1.60	1.56	1.52	1.54	1.57	1.59	1.61	1.64
-7.62	1.82	1.75	1.69	1.64	1.60	1.62	1.65	1.68	1.71	1.74	1.76
-10.16	1.89	1.81	1.74	1.69	1.73	1.76	1.79	1.82	1.85	1.89	1.92
-12.7	1.97	1.88	1.81	1.85	1.89	1.93	1.96	2.00	2.04	2.08	2.13
	-12.7	-10.16	-7.62	-5.08	-2.54	0	2.54	5.08	7.62	10.16	12.7
	$X\,(cm)$										

Table A.1: Maximum of $\mathcal{F}_x$ vs. Position in X-Y

Y (cm)	*Units – Dimensionless*										
12.7	-0.83	-0.82	-0.82	-0.82	-0.83	-0.83	-0.83	-0.84	-0.84	-0.85	-0.86
10.16	-0.79	-0.79	-0.79	-0.79	-0.79	-0.79	-0.79	-0.80	-0.80	-0.81	-0.88
7.62	-0.78	-0.78	-0.78	-0.78	-0.77	-0.77	-0.77	-0.77	-0.78	-0.85	-0.93
5.08	-0.77	-0.77	-0.76	-0.76	-0.76	-0.75	-0.75	-0.75	-0.82	-0.89	-0.98
2.54	-0.77	-0.76	-0.76	-0.75	-0.75	-0.74	-0.74	-0.78	-0.85	-0.93	-1.03
0	-0.77	-0.76	-0.75	-0.75	-0.74	-0.73	-0.74	-0.80	-0.88	-0.97	-1.08
-2.54	-0.79	-0.78	-0.77	-0.76	-0.76	-0.75	-0.75	-0.82	-0.91	-1.01	-1.13
-5.08	-0.89	-0.88	-0.87	-0.87	-0.86	-0.85	-0.85	-0.85	-0.93	-1.04	-1.17
-7.62	-1.01	-1.00	-0.99	-0.99	-0.98	-0.98	-0.97	-0.97	-0.97	-1.07	-1.22
-10.16	-1.16	-1.15	-1.14	-1.14	-1.13	-1.13	-1.12	-1.12	-1.13	-1.13	-1.26
-12.7	-1.34	-1.33	-1.33	-1.32	-1.32	-1.32	-1.32	-1.32	-1.32	-1.33	-1.33
	-12.7	-10.16	-7.62	-5.08	-2.54	0	2.54	5.08	7.62	10.16	12.7
	$X\,(cm)$										

Table A.2: Minimum of $\mathcal{F}_x$ vs Position in X-Y

Y (cm)	*Units – Dimensionless*										
12.7	1.71	1.48	1.29	1.18	1.25	1.35	1.47	1.60	1.75	1.92	2.13
10.16	1.59	1.40	1.24	1.19	1.23	1.32	1.44	1.56	1.71	1.88	2.08
7.62	1.51	1.34	1.24	1.20	1.20	1.30	1.40	1.53	1.67	1.84	2.04
5.08	1.43	1.31	1.26	1.21	1.18	1.27	1.37	1.49	1.64	1.80	2.00
2.54	1.39	1.33	1.28	1.23	1.18	1.24	1.34	1.46	1.60	1.77	1.96
0	1.42	1.35	1.30	1.24	1.19	1.22	1.32	1.43	1.57	1.73	1.93
-2.54	1.48	1.39	1.32	1.26	1.20	1.19	1.29	1.40	1.53	1.69	1.89
-5.08	1.53	1.43	1.34	1.27	1.21	1.17	1.26	1.37	1.50	1.66	1.85
-7.62	1.60	1.48	1.38	1.29	1.22	1.16	1.24	1.34	1.47	1.62	1.81
-10.16	1.67	1.54	1.43	1.33	1.24	1.17	1.21	1.31	1.43	1.59	1.78
-12.7	1.75	1.61	1.48	1.37	1.27	1.18	1.19	1.28	1.40	1.55	1.74
	-12.7	-10.16	-7.62	-5.08	-2.54	0	2.54	5.08	7.62	10.16	12.7
	$X\,(cm)$										

Table A.3: Maximum of $\mathcal{F}_y$ vs Position in X-Y

Y (cm)	*Units – Dimensionless*										
12.7	-1.30	-1.13	-0.99	-0.93	-0.96	-1.00	-1.04	-1.08	-1.13	-1.19	-1.33
10.16	-1.13	-1.00	-0.89	-0.89	-0.92	-0.96	-1.00	-1.04	-1.09	-1.17	-1.33
7.62	-1.00	-0.90	-0.83	-0.85	-0.88	-0.92	-0.96	-1.00	-1.06	-1.16	-1.32
5.08	-0.88	-0.85	-0.83	-0.82	-0.85	-0.88	-0.93	-0.97	-1.02	-1.15	-1.32
2.54	-0.87	-0.85	-0.82	-0.80	-0.82	-0.85	-0.89	-0.94	-1.01	-1.15	-1.32
0	-0.87	-0.84	-0.82	-0.79	-0.79	-0.83	-0.87	-0.92	-1.00	-1.15	-1.32
-2.54	-0.86	-0.84	-0.81	-0.79	-0.78	-0.81	-0.85	-0.90	-1.00	-1.15	-1.32
-5.08	-0.86	-0.83	-0.81	-0.78	-0.76	-0.80	-0.84	-0.89	-1.00	-1.14	-1.32
-7.62	-0.86	-0.83	-0.81	-0.78	-0.76	-0.79	-0.83	-0.88	-0.99	-1.15	-1.33
-10.16	-0.85	-0.83	-0.80	-0.78	-0.76	-0.78	-0.82	-0.87	-0.99	-1.15	-1.33
-12.7	-0.85	-0.83	-0.80	-0.78	-0.76	-0.77	-0.81	-0.86	-1.00	-1.15	-1.34
	-12.7	-10.16	-7.62	-5.08	-2.54	0	2.54	5.08	7.62	10.16	12.7
	$X\,(cm)$										

Table A.4: Minimum of $\mathcal{F}_y$ vs Position in X-Y

Y (cm)	*Units – Dimensionless*										
12.7	2.13	1.92	1.76	1.64	1.54	1.46	1.39	1.33	1.28	1.24	1.27
10.16	1.92	1.76	1.63	1.53	1.44	1.37	1.31	1.26	1.22	1.20	1.23
7.62	1.75	1.62	1.51	1.43	1.36	1.30	1.25	1.20	1.17	1.18	1.21
5.08	1.60	1.49	1.41	1.34	1.28	1.23	1.18	1.15	1.13	1.15	1.18
2.54	1.47	1.38	1.31	1.26	1.21	1.16	1.13	1.10	1.11	1.13	1.16
0	1.35	1.29	1.23	1.18	1.15	1.15	1.15	1.15	1.16	1.17	1.18
-2.54	1.29	1.26	1.24	1.22	1.22	1.21	1.21	1.22	1.22	1.23	1.24
-5.08	1.42	1.38	1.35	1.33	1.30	1.29	1.28	1.29	1.29	1.30	1.31
-7.62	1.57	1.53	1.48	1.45	1.42	1.40	1.38	1.37	1.37	1.37	1.39
-10.16	1.75	1.69	1.64	1.59	1.56	1.53	1.50	1.48	1.47	1.46	1.47
-12.7	1.97	1.89	1.82	1.76	1.72	1.68	1.64	1.62	1.59	1.58	1.57
	-12.7	-10.16	-7.62	-5.08	-2.54	0	2.54	5.08	7.62	10.16	12.7
	$X\,(cm)$										

Table A.5: Maximum of $\mathcal{F}_z$ vs Position in X-Y

Y (cm)	*Units – Dimensionless*										
12.7	-1.34	-1.16	-1.01	-0.90	-0.82	-0.75	-0.69	-0.67	-0.68	-0.69	-0.70
10.16	-1.19	-1.06	-0.96	-0.87	-0.80	-0.73	-0.68	-0.67	-0.68	-0.69	-0.72
7.62	-1.13	-1.02	-0.93	-0.85	-0.78	-0.72	-0.67	-0.68	-0.68	-0.70	-0.73
5.08	-1.08	-0.98	-0.90	-0.82	-0.76	-0.71	-0.67	-0.68	-0.69	-0.72	-0.74
2.54	-1.04	-0.95	-0.87	-0.81	-0.75	-0.70	-0.68	-0.68	-0.71	-0.73	-0.76
0	-1.00	-0.92	-0.85	-0.79	-0.74	-0.71	-0.68	-0.70	-0.72	-0.75	-0.77
-2.54	-0.96	-0.89	-0.83	-0.80	-0.77	-0.74	-0.71	-0.72	-0.74	-0.76	-0.79
-5.08	-0.93	-0.90	-0.87	-0.84	-0.82	-0.79	-0.76	-0.74	-0.76	-0.78	-0.81
-7.62	-0.99	-0.96	-0.92	-0.90	-0.87	-0.84	-0.81	-0.78	-0.78	-0.80	-0.82
-10.16	-1.13	-1.09	-1.05	-1.01	-0.97	-0.93	-0.89	-0.84	-0.80	-0.81	-0.84
-12.7	-1.30	-1.26	-1.22	-1.17	-1.13	-1.08	-1.03	-0.98	-0.93	-0.88	-0.86
	-12.7	-10.16	-7.62	-5.08	-2.54	0	2.54	5.08	7.62	10.16	12.7
	$X\,(cm)$										

Table A.6: Minimum of $\mathcal{F}_z$ vs Position in X-Y

Y (cm)	*Units – Reciprocal Centimeter*										
12.7	0.20	0.18	0.17	0.17	0.17	0.17	0.18	0.19	0.20	0.21	0.22
10.16	0.18	0.16	0.16	0.16	0.16	0.17	0.18	0.18	0.19	0.20	0.22
7.62	0.16	0.15	0.15	0.16	0.16	0.17	0.17	0.18	0.19	0.20	0.21
5.08	0.15	0.14	0.15	0.15	0.16	0.16	0.17	0.17	0.18	0.19	0.21
2.54	0.14	0.14	0.14	0.15	0.15	0.16	0.16	0.17	0.18	0.19	0.20
0	0.14	0.14	0.14	0.14	0.15	0.15	0.16	0.17	0.18	0.19	0.20
-2.54	0.15	0.14	0.14	0.14	0.15	0.15	0.16	0.16	0.17	0.18	0.20
-5.08	0.16	0.16	0.15	0.15	0.14	0.15	0.15	0.16	0.17	0.18	0.19
-7.62	0.18	0.17	0.17	0.16	0.16	0.15	0.15	0.16	0.17	0.18	0.19
-10.16	0.20	0.19	0.18	0.18	0.17	0.17	0.16	0.16	0.16	0.18	0.19
-12.7	0.22	0.21	0.21	0.20	0.19	0.19	0.18	0.17	0.17	0.17	0.19
	-12.7	-10.16	-7.62	-5.08	-2.54	0	2.54	5.08	7.62	10.16	12.7
	X (cm)										

Table A.7: Maximum of $\mathcal{T}_x$ vs Position in X-Y

Y (cm)	*Units – Reciprocal Centimeter*										
12.7	-0.22	-0.19	-0.18	-0.16	-0.17	-0.17	-0.18	-0.19	-0.20	-0.21	-0.22
10.16	-0.19	-0.18	-0.16	-0.16	-0.16	-0.17	-0.17	-0.18	-0.19	-0.20	-0.22
7.62	-0.17	-0.16	-0.15	-0.15	-0.16	-0.16	-0.17	-0.18	-0.19	-0.20	-0.21
5.08	-0.16	-0.15	-0.14	-0.15	-0.15	-0.16	-0.16	-0.17	-0.18	-0.19	-0.21
2.54	-0.15	-0.14	-0.14	-0.14	-0.15	-0.15	-0.16	-0.17	-0.18	-0.19	-0.21
0	-0.14	-0.13	-0.14	-0.14	-0.14	-0.15	-0.16	-0.17	-0.18	-0.19	-0.20
-2.54	-0.14	-0.14	-0.14	-0.14	-0.14	-0.15	-0.15	-0.16	-0.17	-0.18	-0.20
-5.08	-0.16	-0.15	-0.15	-0.15	-0.14	-0.14	-0.15	-0.16	-0.17	-0.18	-0.20
-7.62	-0.17	-0.17	-0.16	-0.16	-0.16	-0.15	-0.15	-0.16	-0.17	-0.18	-0.20
-10.16	-0.20	-0.19	-0.18	-0.18	-0.17	-0.17	-0.16	-0.16	-0.17	-0.18	-0.19
-12.7	-0.22	-0.22	-0.21	-0.20	-0.19	-0.19	-0.18	-0.18	-0.17	-0.18	-0.19
	-12.7	-10.16	-7.62	-5.08	-2.54	0	2.54	5.08	7.62	10.16	12.7
	X (cm)										

Table A.8: Minimum of $\mathcal{T}_x$ vs Position in X-Y

Y (cm)	*Units – Reciprocal Centimeter*										
12.7	0.20	0.18	0.17	0.17	0.17	0.17	0.18	0.19	0.20	0.21	0.22
10.16	0.18	0.16	0.16	0.16	0.16	0.17	0.18	0.18	0.19	0.20	0.22
7.62	0.16	0.15	0.15	0.16	0.16	0.17	0.17	0.18	0.19	0.20	0.21
5.08	0.15	0.14	0.15	0.15	0.16	0.16	0.17	0.17	0.18	0.19	0.21
2.54	0.14	0.14	0.14	0.15	0.15	0.16	0.16	0.17	0.18	0.19	0.20
0	0.14	0.14	0.14	0.14	0.15	0.15	0.16	0.17	0.18	0.19	0.20
-2.54	0.15	0.14	0.14	0.14	0.15	0.15	0.16	0.16	0.17	0.18	0.20
-5.08	0.16	0.16	0.15	0.15	0.14	0.15	0.15	0.16	0.17	0.18	0.19
-7.62	0.18	0.17	0.17	0.16	0.16	0.15	0.15	0.16	0.17	0.18	0.19
-10.16	0.20	0.19	0.18	0.18	0.17	0.17	0.16	0.16	0.16	0.18	0.19
-12.7	0.22	0.21	0.21	0.20	0.19	0.19	0.18	0.17	0.17	0.17	0.19
	-12.7	-10.16	-7.62	-5.08	-2.54	0	2.54	5.08	7.62	10.16	12.7
	$X\,(cm)$										

Table A.9: Maximum of $\mathcal{T}_y$ vs Position in X-Y

Y (cm)	*Units – Reciprocal Centimeter*										
12.7	-0.22	-0.19	-0.18	-0.16	-0.17	-0.17	-0.18	-0.19	-0.20	-0.21	-0.22
10.16	-0.19	-0.18	-0.16	-0.16	-0.16	-0.17	-0.17	-0.18	-0.19	-0.20	-0.22
7.62	-0.17	-0.16	-0.15	-0.15	-0.16	-0.16	-0.17	-0.18	-0.19	-0.20	-0.21
5.08	-0.16	-0.15	-0.14	-0.15	-0.15	-0.16	-0.16	-0.17	-0.18	-0.19	-0.21
2.54	-0.15	-0.14	-0.14	-0.14	-0.15	-0.15	-0.16	-0.17	-0.18	-0.19	-0.21
0	-0.14	-0.13	-0.14	-0.14	-0.14	-0.15	-0.16	-0.17	-0.18	-0.19	-0.20
-2.54	-0.14	-0.14	-0.14	-0.14	-0.14	-0.15	-0.15	-0.16	-0.17	-0.18	-0.20
-5.08	-0.16	-0.15	-0.15	-0.15	-0.14	-0.14	-0.15	-0.16	-0.17	-0.18	-0.20
-7.62	-0.17	-0.17	-0.16	-0.16	-0.16	-0.15	-0.15	-0.16	-0.17	-0.18	-0.20
-10.16	-0.20	-0.19	-0.18	-0.18	-0.17	-0.17	-0.16	-0.16	-0.17	-0.18	-0.19
-12.7	-0.22	-0.22	-0.21	-0.20	-0.19	-0.19	-0.18	-0.18	-0.17	-0.18	-0.19
	-12.7	-10.16	-7.62	-5.08	-2.54	0	2.54	5.08	7.62	10.16	12.7
	$X\,(cm)$										

Table A.10: Minimum of $\mathcal{T}_y$ vs Position in X-Y

Y (cm)	*Units – Reciprocal Centimeter*										
12.7	0.20	0.18	0.17	0.17	0.17	0.17	0.18	0.19	0.20	0.21	0.22
10.16	0.18	0.16	0.16	0.16	0.16	0.17	0.18	0.18	0.19	0.20	0.22
7.62	0.16	0.15	0.15	0.16	0.16	0.17	0.17	0.18	0.19	0.20	0.21
5.08	0.15	0.14	0.15	0.15	0.16	0.16	0.17	0.17	0.18	0.19	0.21
2.54	0.14	0.14	0.14	0.15	0.15	0.16	0.16	0.17	0.18	0.19	0.20
0	0.14	0.14	0.14	0.14	0.15	0.15	0.16	0.17	0.18	0.19	0.20
-2.54	0.15	0.14	0.14	0.14	0.15	0.15	0.16	0.16	0.17	0.18	0.20
-5.08	0.16	0.16	0.15	0.15	0.14	0.15	0.15	0.16	0.17	0.18	0.19
-7.62	0.18	0.17	0.17	0.16	0.16	0.15	0.15	0.16	0.17	0.18	0.19
-10.16	0.20	0.19	0.18	0.18	0.17	0.17	0.16	0.16	0.16	0.18	0.19
-12.7	0.22	0.21	0.21	0.20	0.19	0.19	0.18	0.17	0.17	0.17	0.19
	-12.7	-10.16	-7.62	-5.08	-2.54	0	2.54	5.08	7.62	10.16	12.7
	X (cm)										

Table A.11: Maximum of T_z vs Position in X-Y

Y (cm)	*Units – Reciprocal Centimeter*										
12.7	-0.22	-0.19	-0.18	-0.16	-0.17	-0.17	-0.18	-0.19	-0.20	-0.21	-0.22
10.16	-0.19	-0.18	-0.16	-0.16	-0.16	-0.17	-0.17	-0.18	-0.19	-0.20	-0.22
7.62	-0.17	-0.16	-0.15	-0.15	-0.16	-0.16	-0.17	-0.18	-0.19	-0.20	-0.21
5.08	-0.16	-0.15	-0.14	-0.15	-0.15	-0.16	-0.16	-0.17	-0.18	-0.19	-0.21
2.54	-0.15	-0.14	-0.14	-0.14	-0.15	-0.15	-0.16	-0.17	-0.18	-0.19	-0.21
0	-0.14	-0.13	-0.14	-0.14	-0.14	-0.15	-0.16	-0.17	-0.18	-0.19	-0.20
-2.54	-0.14	-0.14	-0.14	-0.14	-0.14	-0.15	-0.15	-0.16	-0.17	-0.18	-0.20
-5.08	-0.16	-0.15	-0.15	-0.15	-0.14	-0.14	-0.15	-0.16	-0.17	-0.18	-0.20
-7.62	-0.17	-0.17	-0.16	-0.16	-0.16	-0.15	-0.15	-0.16	-0.17	-0.18	-0.20
-10.16	-0.20	-0.19	-0.18	-0.18	-0.17	-0.17	-0.16	-0.16	-0.17	-0.18	-0.19
	-0.22	-0.22	-0.21	-0.20	-0.19	-0.19	-0.18	-0.18	-0.17	-0.18	-0.19
	-12.7	-10.16	-7.62	-5.08	-2.54	0	2.54	5.08	7.62	10.16	12.7
	X (cm)										

Table A.12: Minimum of T_z vs Position in X-Y

Y (cm)	*Units – Centimeter*										
12.7	96.4	96.1	95.8	95.7	95.6	95.5	95.6	95.7	95.8	96.1	96.4
10.16	95.9	95.6	95.4	95.2	95.1	95.1	95.1	95.2	95.4	95.6	96.1
7.62	95.5	95.2	95.0	94.8	94.7	94.7	94.7	94.8	95.0	95.2	95.8
5.08	95.2	94.9	94.7	94.5	94.4	94.4	94.4	94.5	94.7	94.9	95.7
2.54	95.0	94.7	94.4	94.3	94.2	94.1	94.2	94.3	94.4	94.7	95.6
0	94.8	94.5	94.2	94.1	94.0	93.9	94.0	94.1	94.2	94.5	95.5
-2.54	95.0	94.7	94.4	94.3	94.2	94.1	94.2	94.3	94.4	94.7	95.6
-5.08	95.2	94.9	94.7	94.5	94.4	94.4	94.4	94.5	94.7	94.9	95.7
-7.62	95.5	95.2	95.0	94.8	94.7	94.7	94.7	94.8	95.0	95.2	95.8
-10.16	95.9	95.6	95.4	95.2	95.1	95.1	95.1	95.2	95.4	95.6	96.1
-12.7	96.4	96.1	95.8	95.7	95.6	95.5	95.6	95.7	95.8	96.1	96.4
	-12.7	-10.16	-7.62	-5.08	-2.54	0	2.54	5.08	7.62	10.16	12.7
	$X\,(cm)$										

Table A.13: Maximum of Θ vs Position in X-Y

Y (cm)	*Units – Centimeter*										
12.7	61.0	60.6	60.2	60.0	59.8	59.7	59.8	60.0	60.2	60.6	61.1
10.16	60.6	60.2	59.9	59.6	59.5	59.4	59.5	59.6	59.9	60.3	60.8
7.62	60.2	60.0	59.6	59.4	59.2	59.2	59.2	59.4	59.7	60.1	60.5
5.08	60.0	59.9	59.5	59.3	59.1	59.1	59.1	59.3	59.6	59.9	60.4
2.54	59.8	59.8	59.5	59.3	59.1	59.1	59.1	59.3	59.6	59.9	60.4
0	59.7	59.9	59.6	59.4	59.2	59.2	59.2	59.4	59.6	59.9	60.4
-2.54	59.8	59.8	59.5	59.3	59.1	59.1	59.1	59.3	59.6	59.9	60.3
-5.08	60.0	59.9	59.5	59.3	59.1	59.1	59.1	59.3	59.6	59.9	60.3
-7.62	60.2	60.0	59.6	59.4	59.2	59.2	59.2	59.4	59.7	60.1	60.5
-10.16	60.6	60.2	59.9	59.6	59.5	59.4	59.5	59.6	59.9	60.3	60.7
-12.7	61.0	60.6	60.2	60.0	59.8	59.7	59.8	60.0	60.2	60.6	61.0
	-12.7	-10.16	-7.62	-5.08	-2.54	0	2.54	5.08	7.62	10.16	12.7
	$X\,(cm)$										

Table A.14: Minimum of Θ vs Position in X-Y

Appendix B

Quantitative Test Results

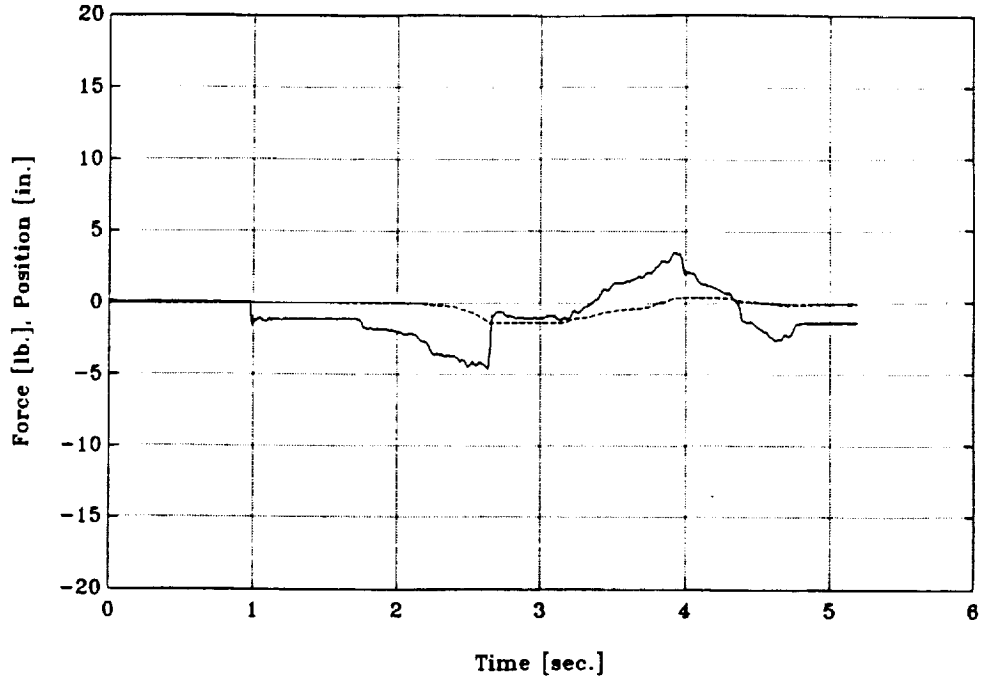

Figure B.1: Test A - Force Response in x

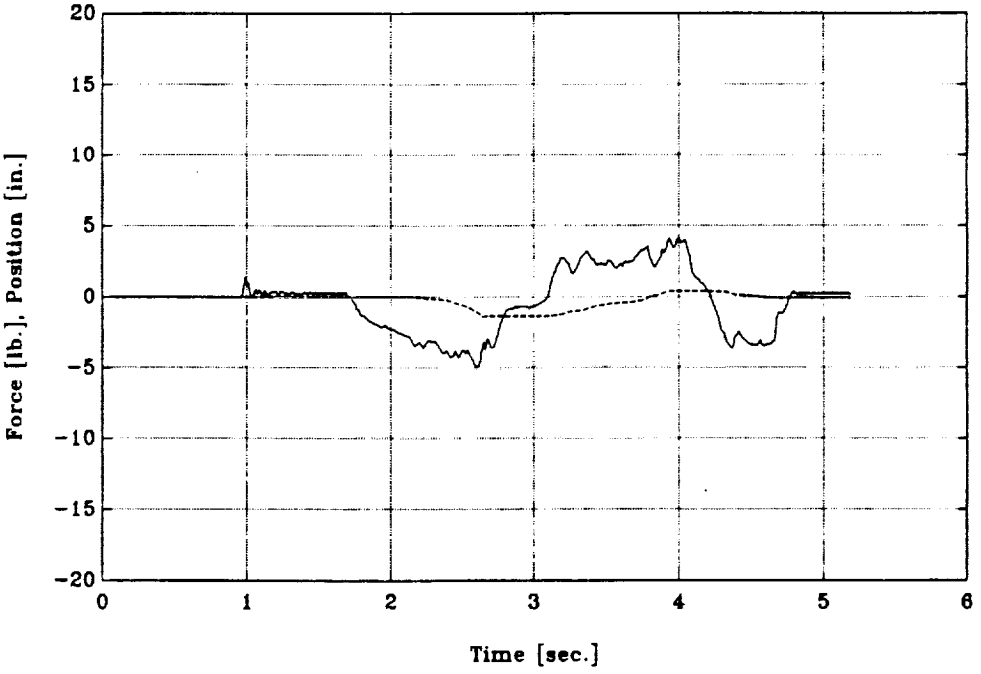

Figure B.2: Test A - Force Response in y

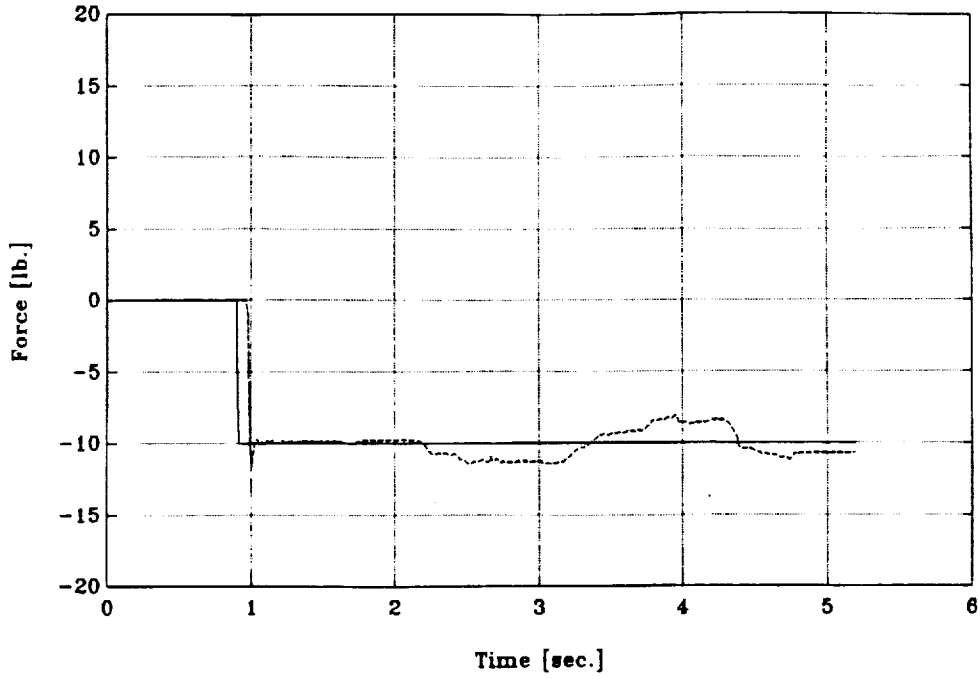

Figure B.3: Test A - Force Response in z

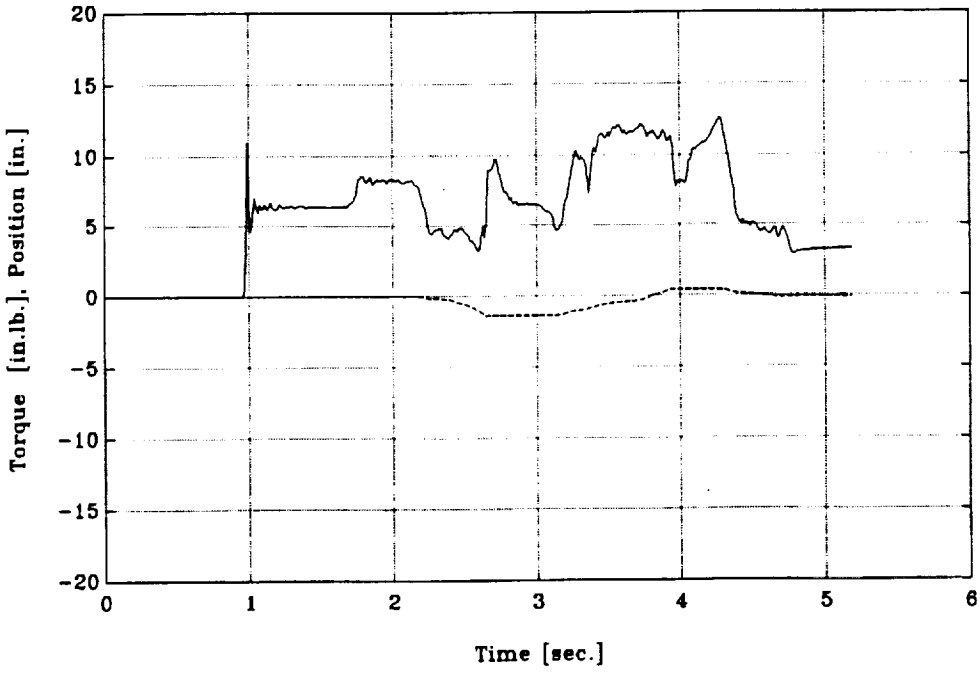

Figure B.4: Test A - Torque Response in x

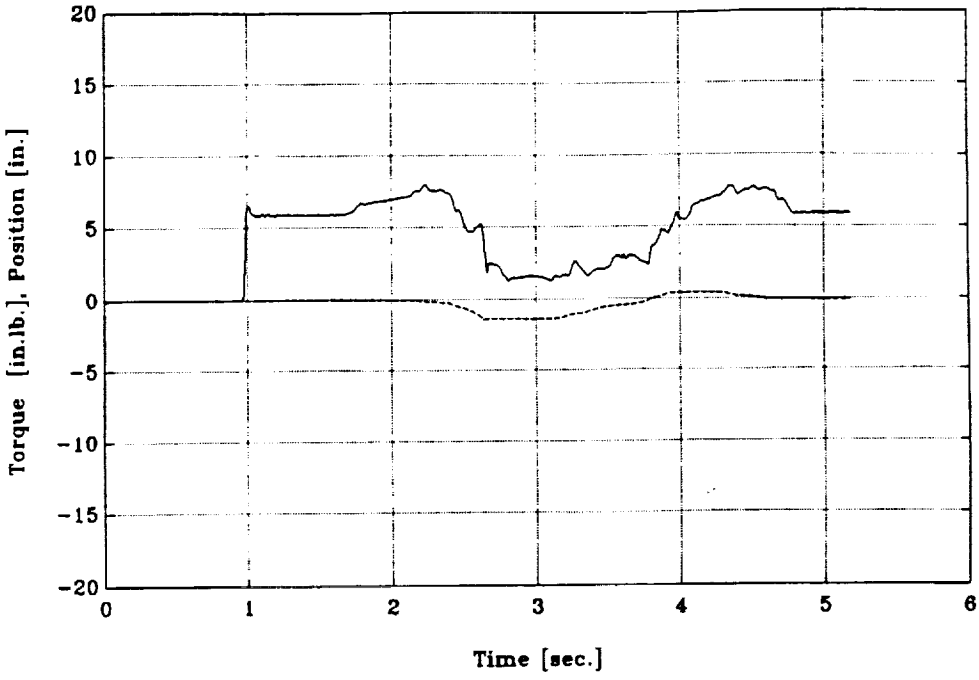

Figure B.5: Test A - Torque Response in y

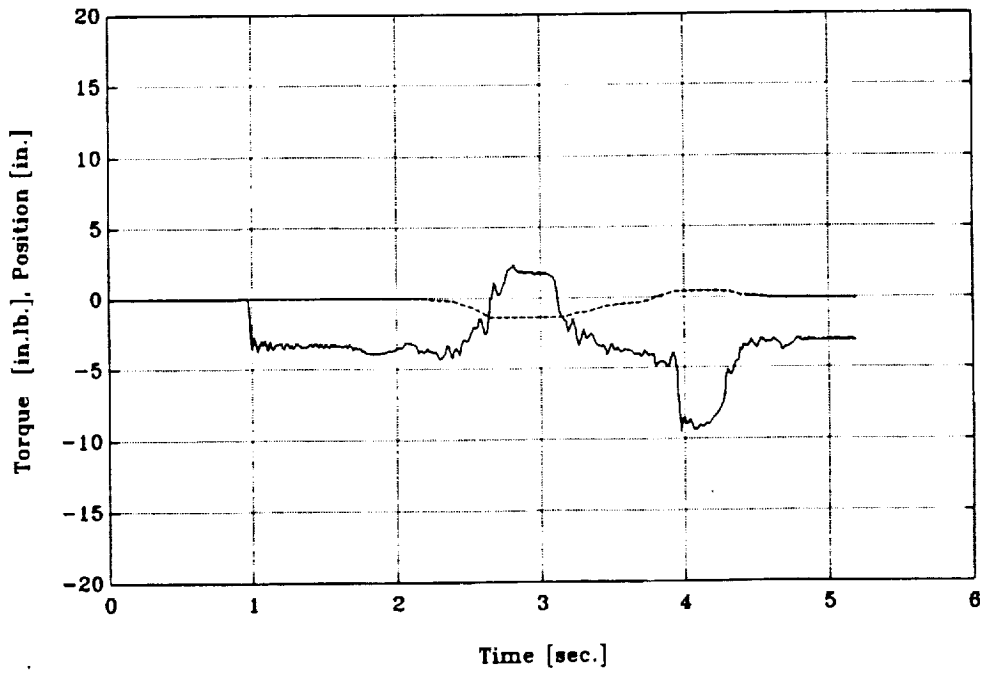

Figure B.6: Test A - Torque Response in z

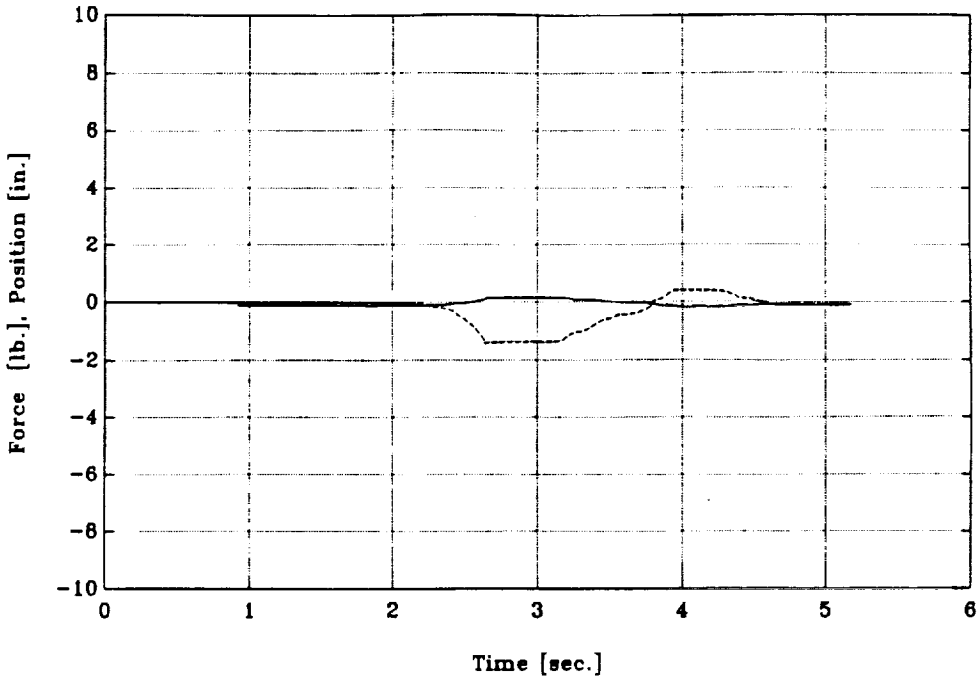

Figure B.7: Test A - Leg 1 Force History

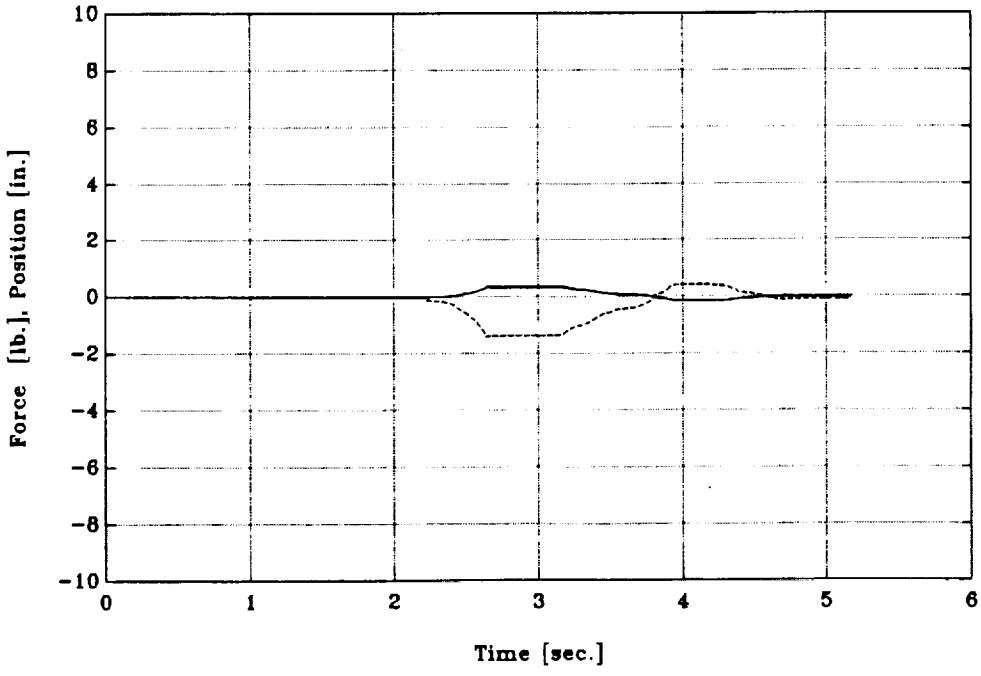

Figure B.8: Test A - Leg 2 Force History

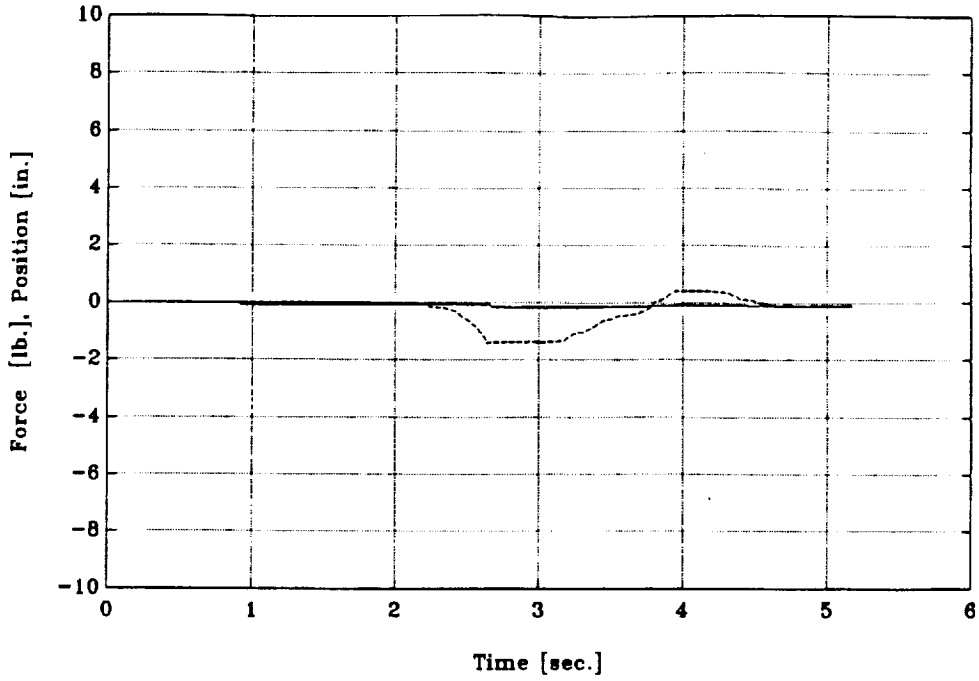

Figure B.9: Test A - Leg 3 Force History

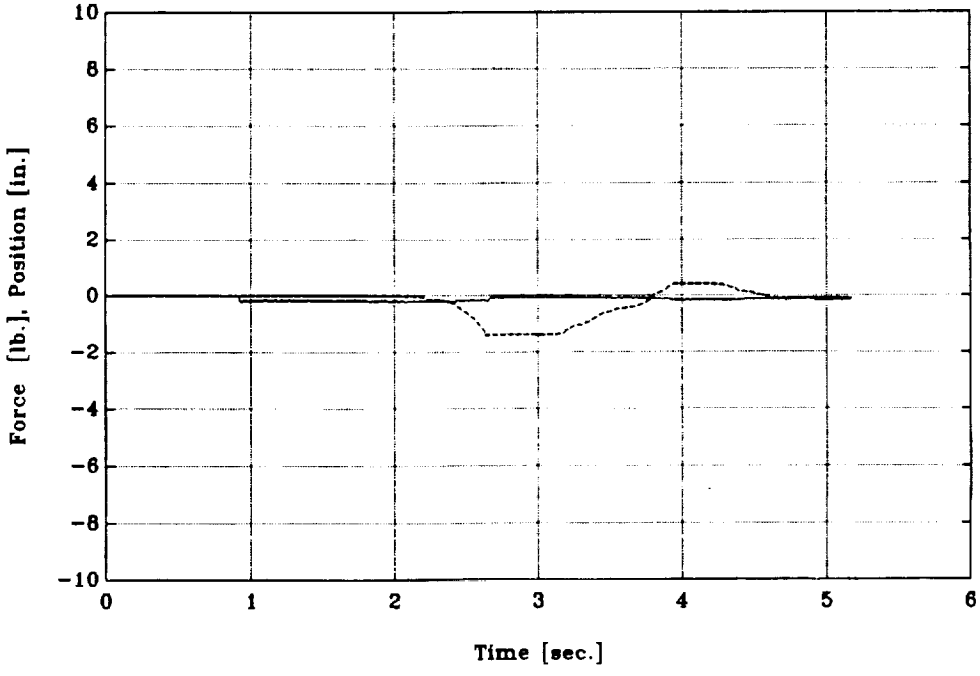

Figure B.10: Test A - Leg 4 Force History

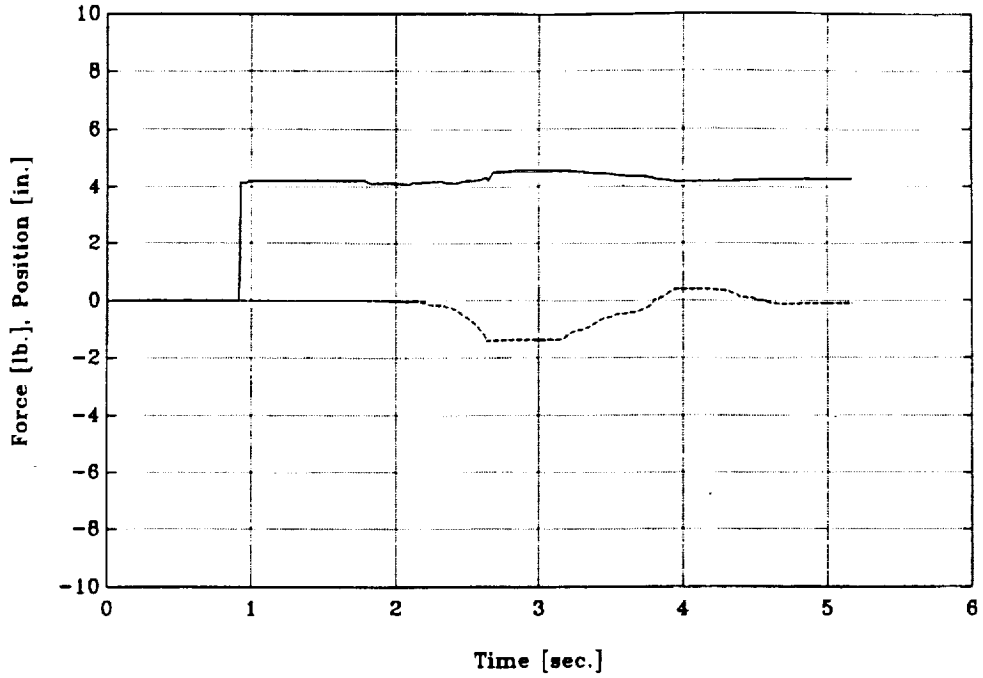

Figure B.11: Test A - Leg 5 Force History

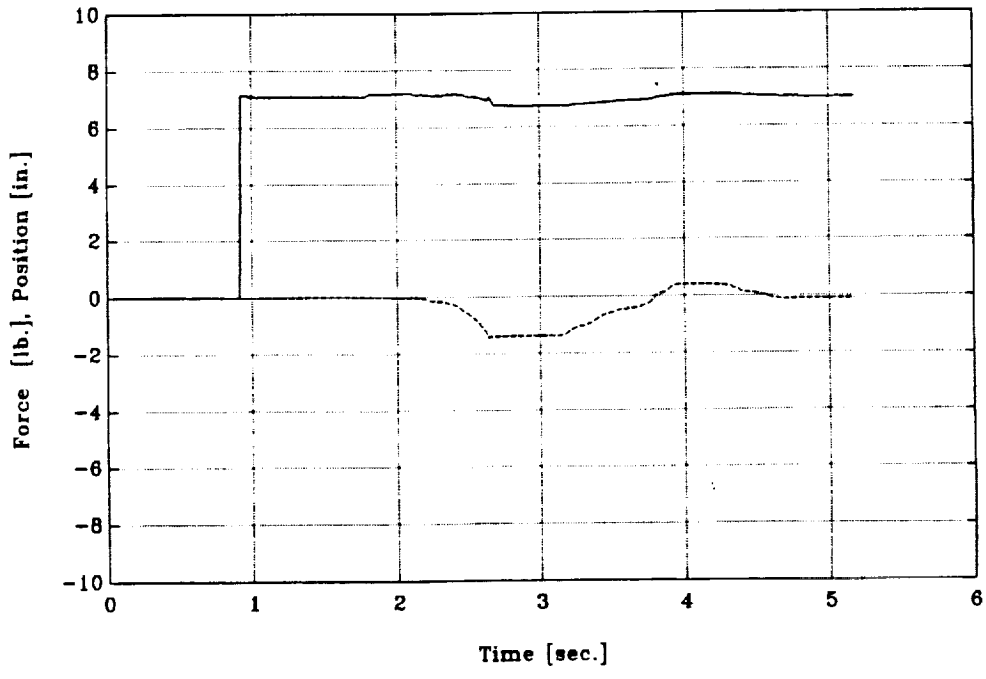

Figure B.12: Test A - Leg 6 Force History

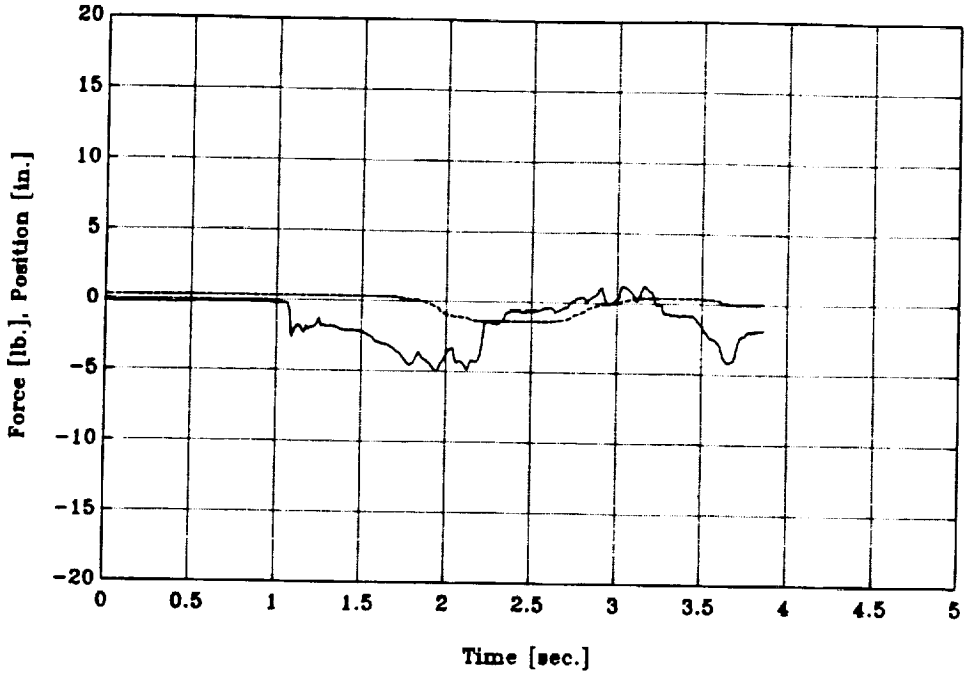

Figure B.13: Test B - Force Response in x

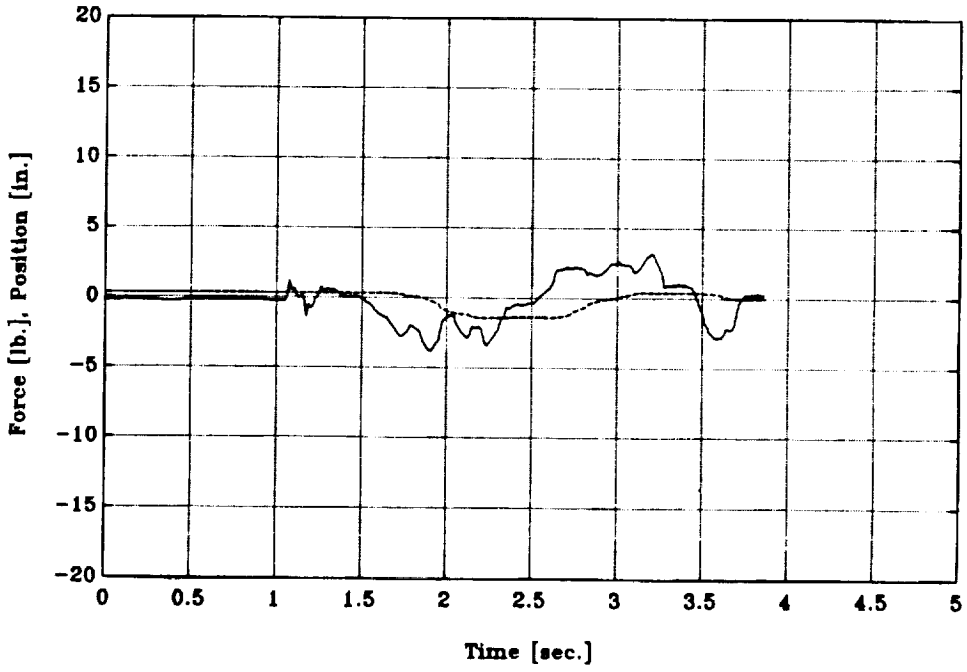

Figure B.14: Test B - Force Response in y

C-2

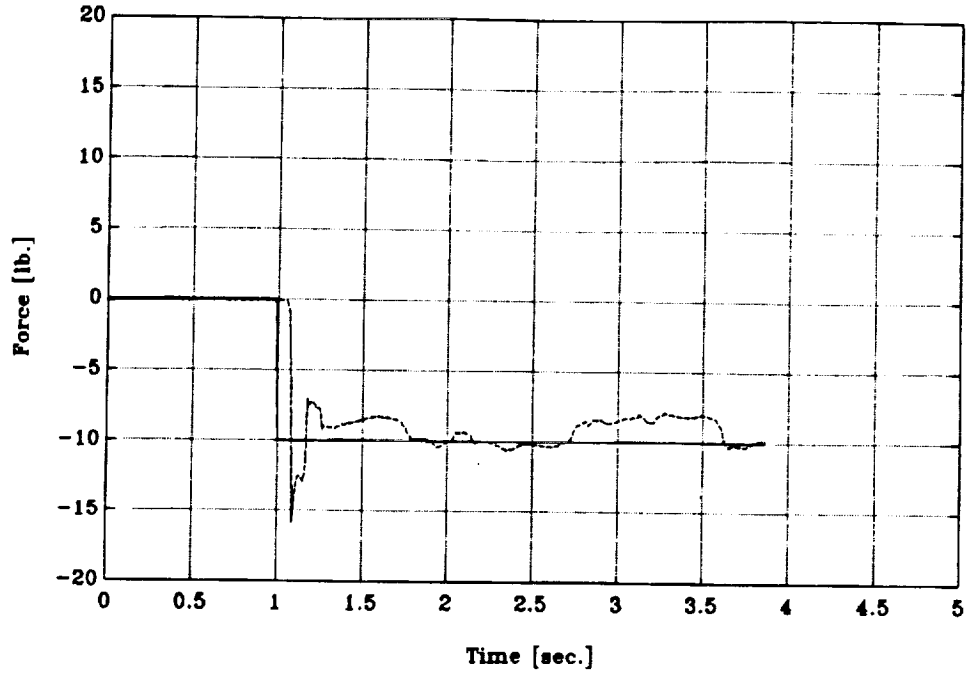

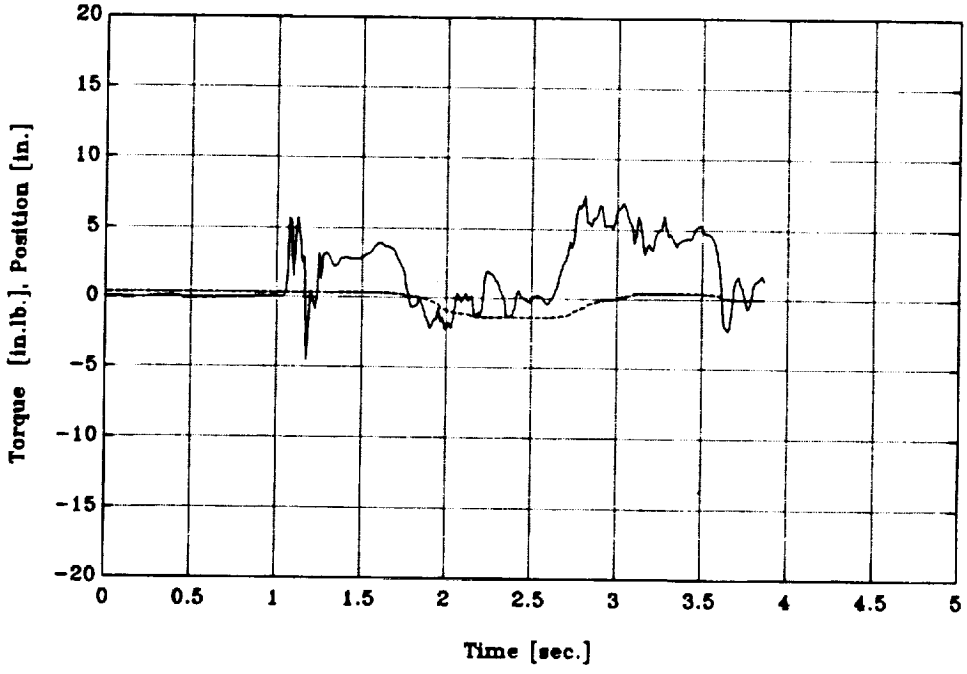

Figure B.16: Test B - Torque Response in x

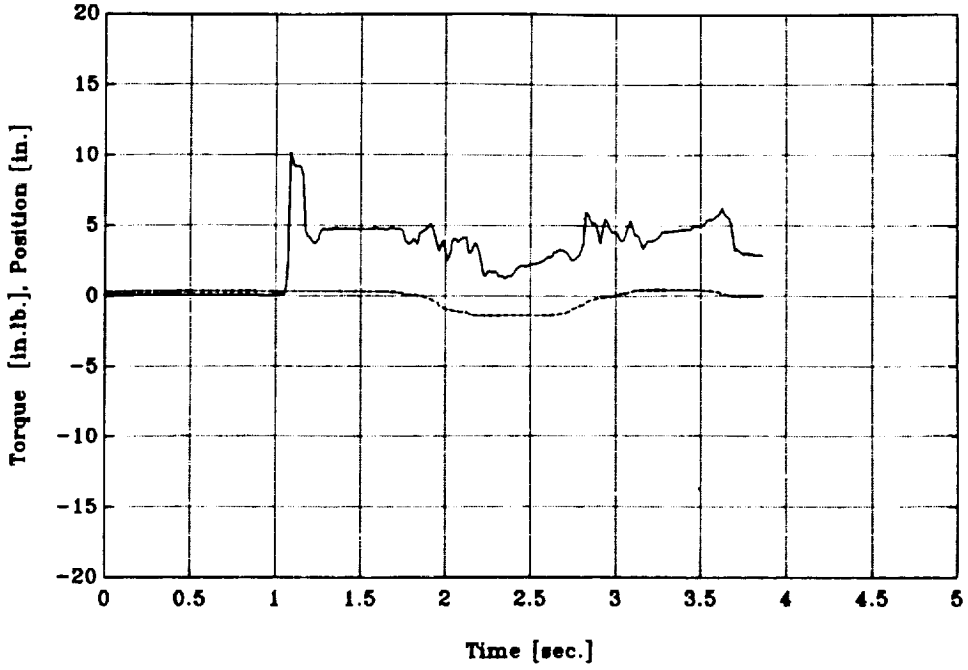

Figure B.17: Test B - Torque Response in y

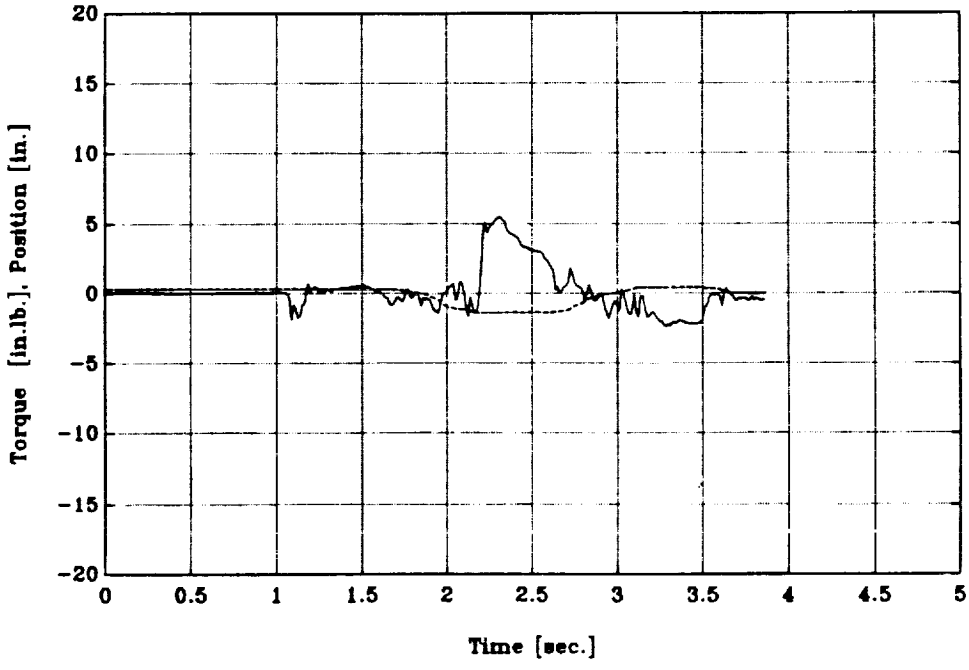

Figure B.18: Test B - Torque Response in z

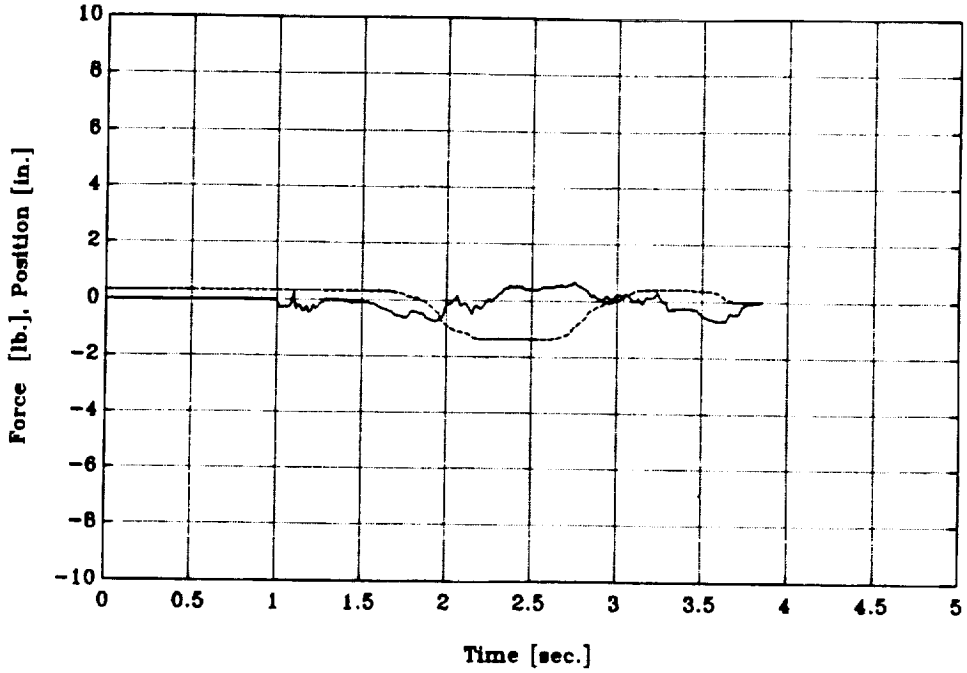

Figure B.19: Test B - Leg 1 Force History

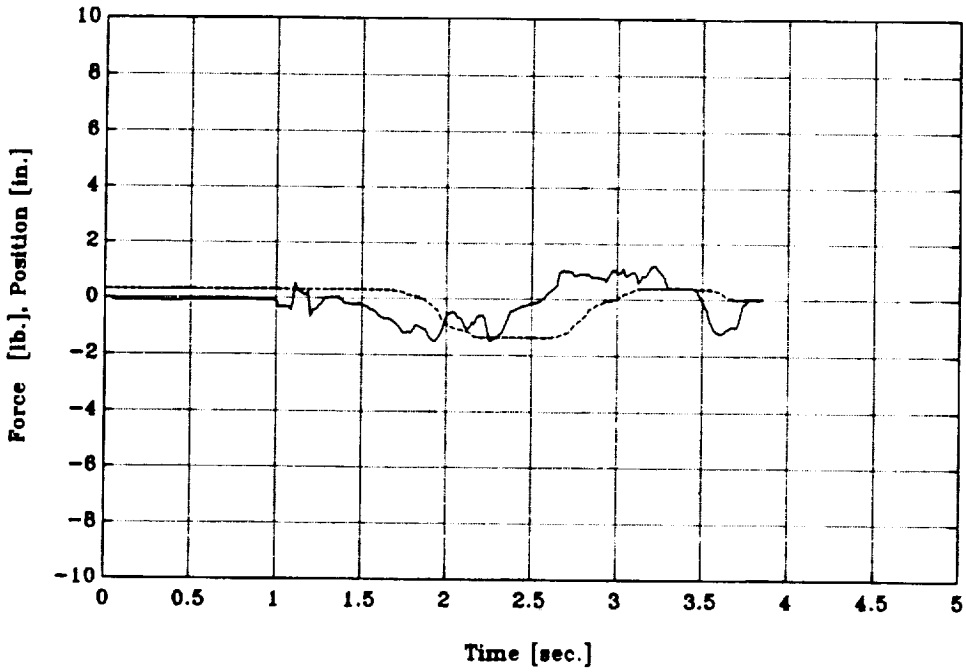

Figure B.20: Test B - Leg 2 Force History

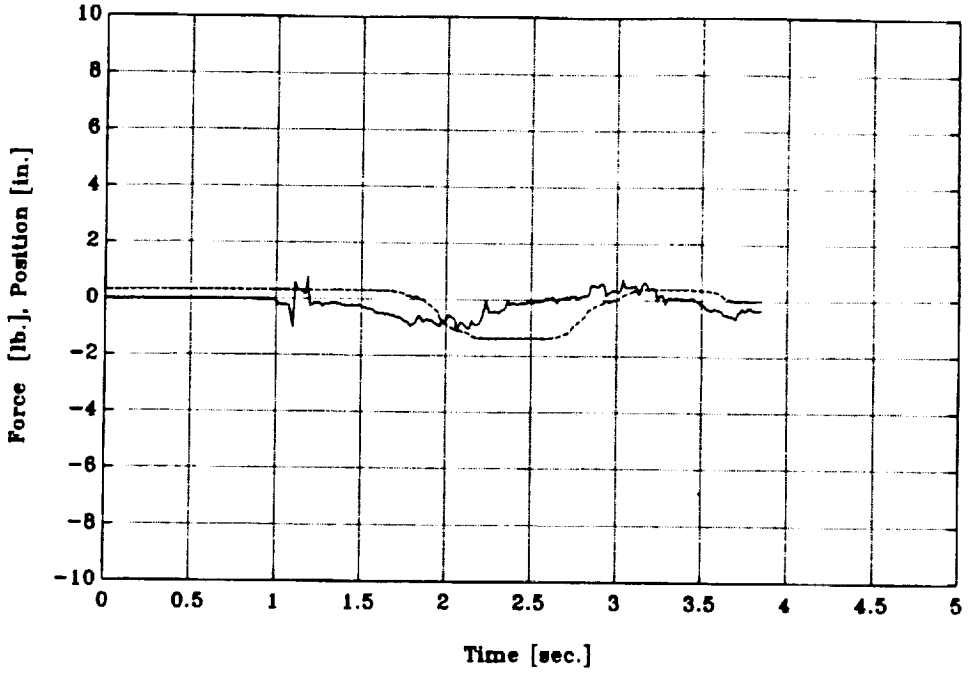

Figure B.21: Test B - Leg 3 Force History

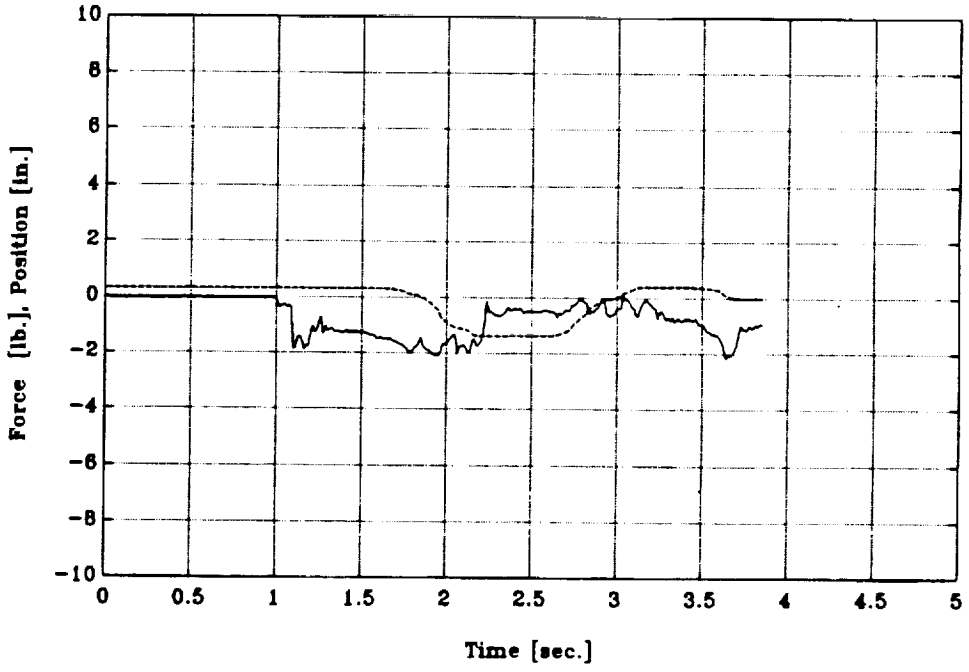

Figure B.22: Test B - Leg 4 Force History

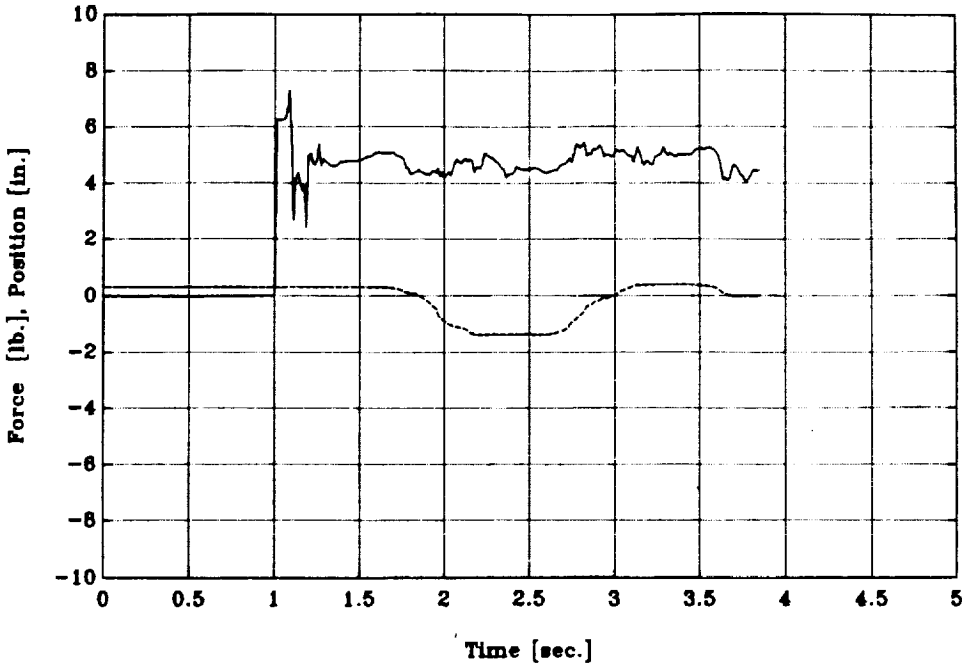

Figure B.23: Test B - Leg 5 Force History

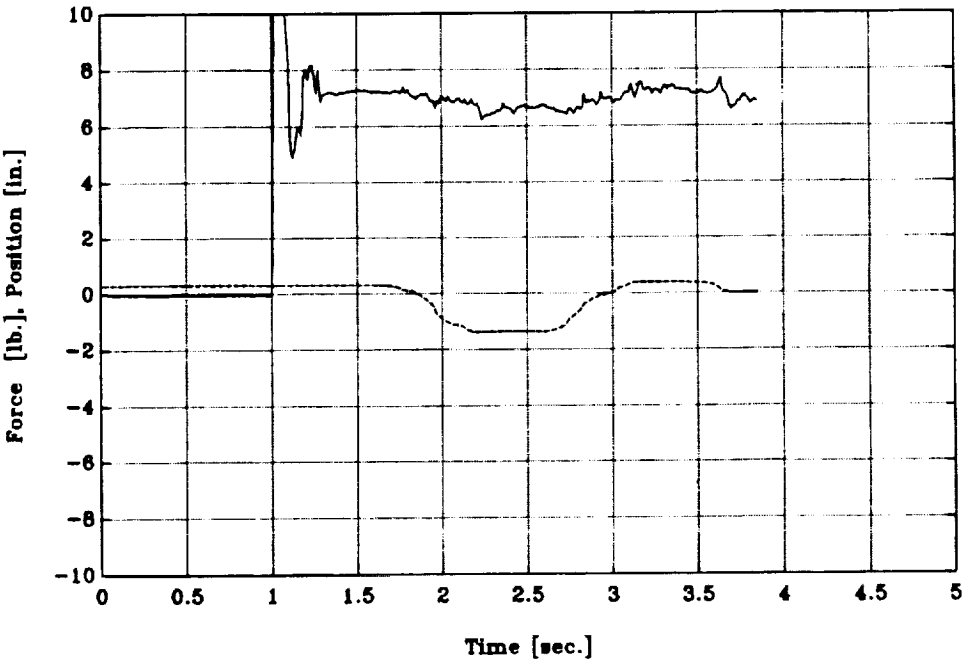

Figure B.24: Test B - Leg 6 Force History

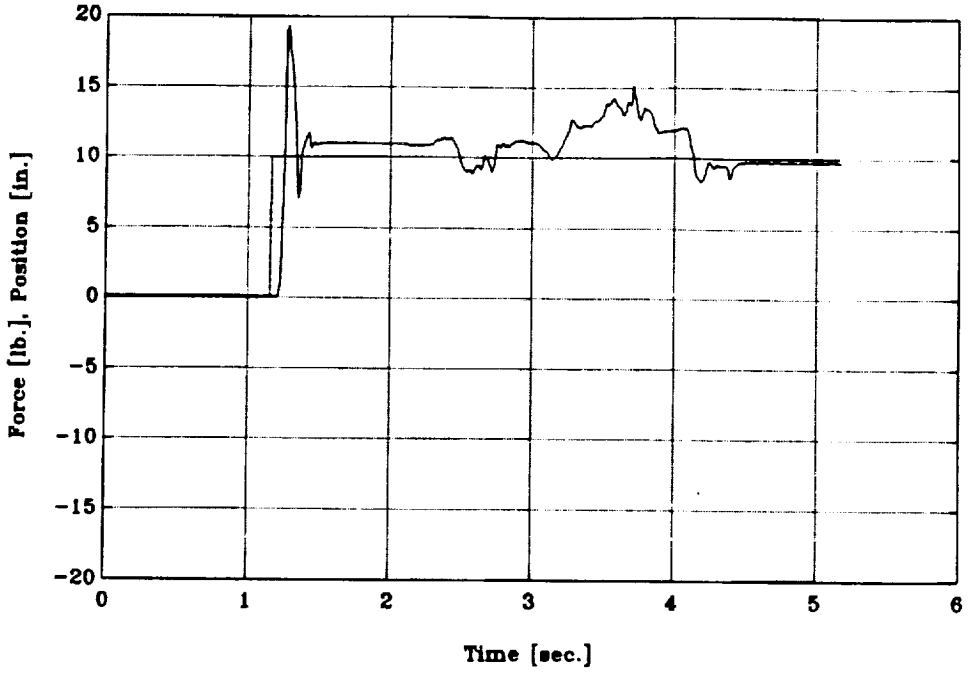

Figure B.25: Test C - Force Response in x

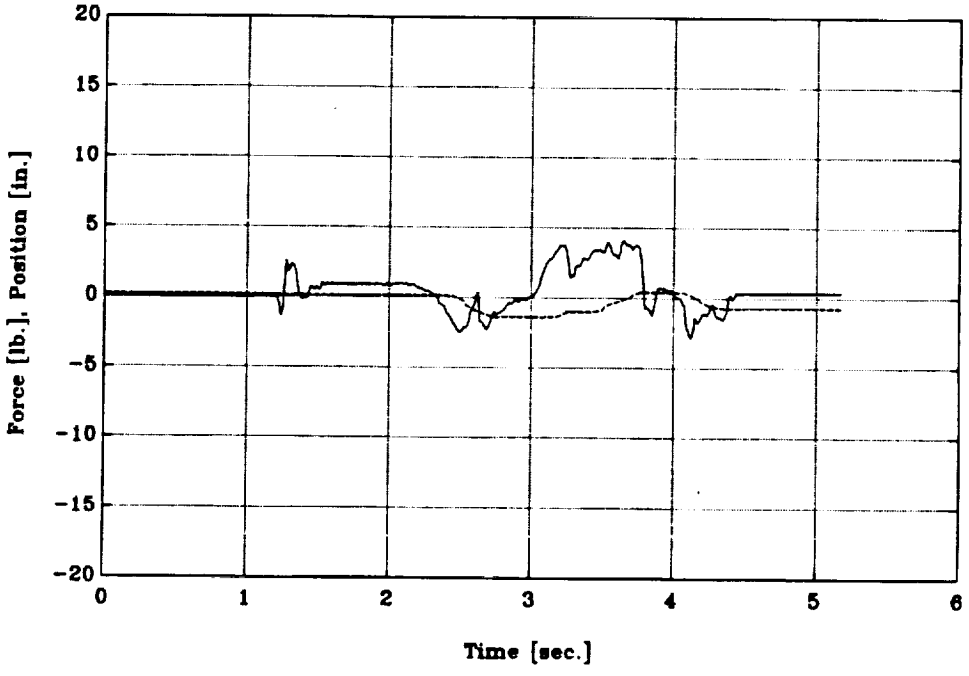

Figure B.26: Test C - Force Response in y

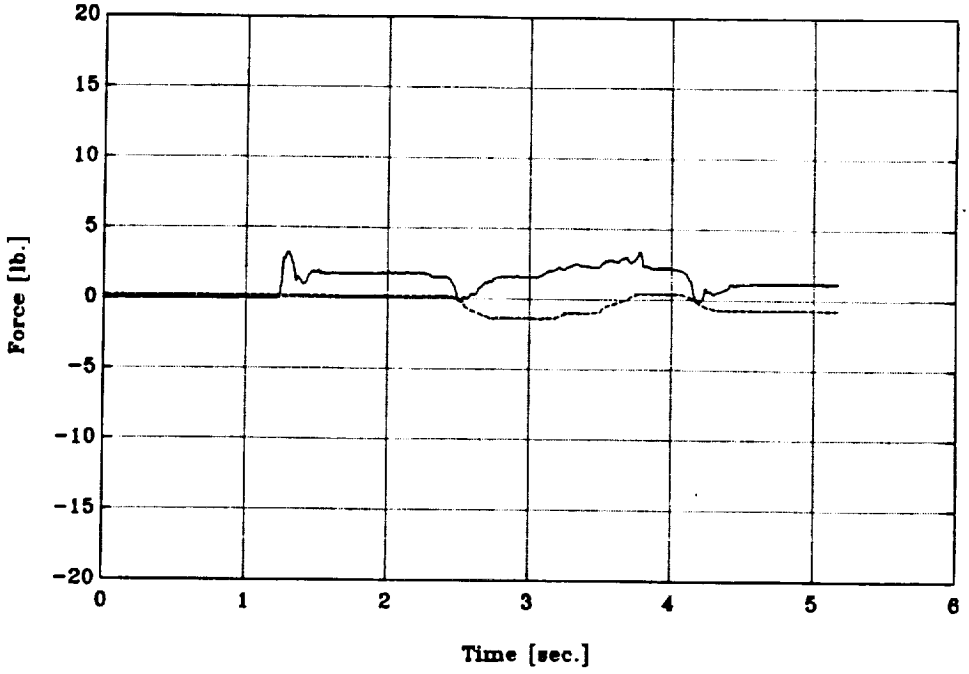

Figure B.27: Test C - Force Response in z

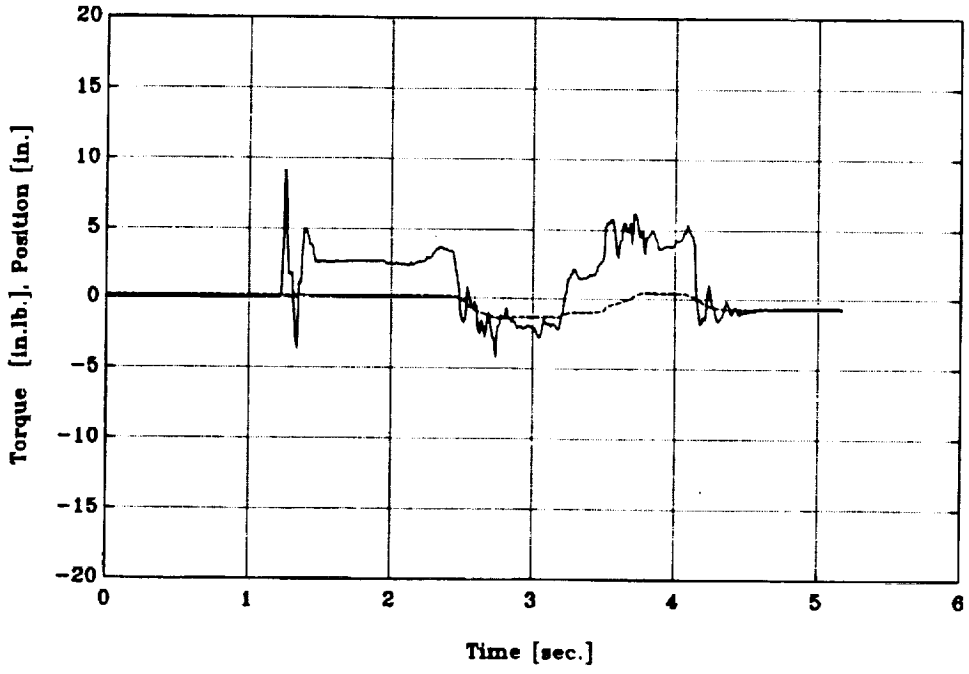

Figure B.28: Test C - Torque Response in x

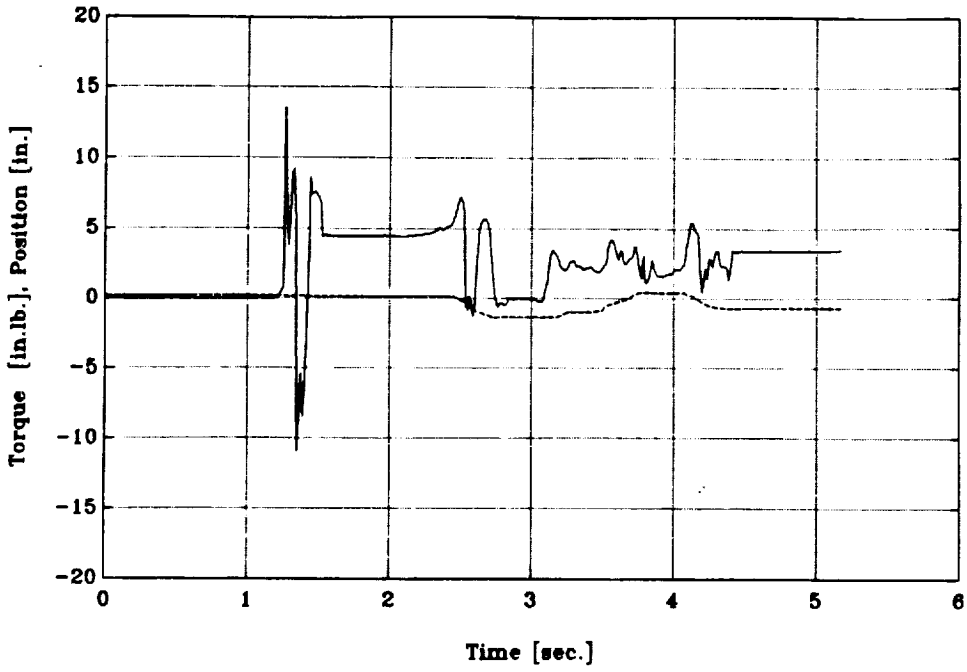

Figure B.29: Test C - Torque Response in y

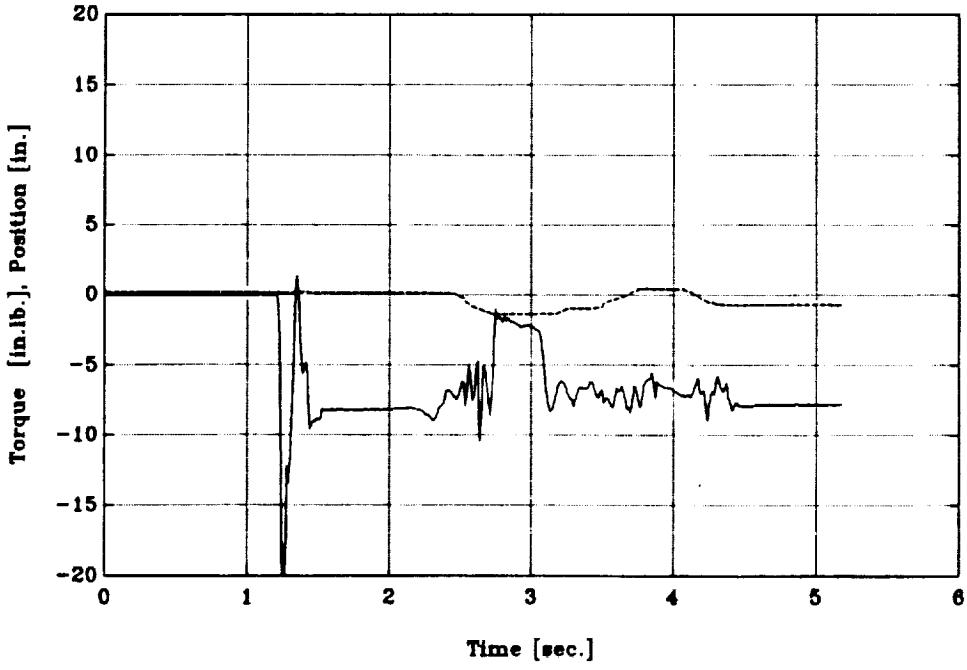

Figure B.30: Test C - Torque Response in z

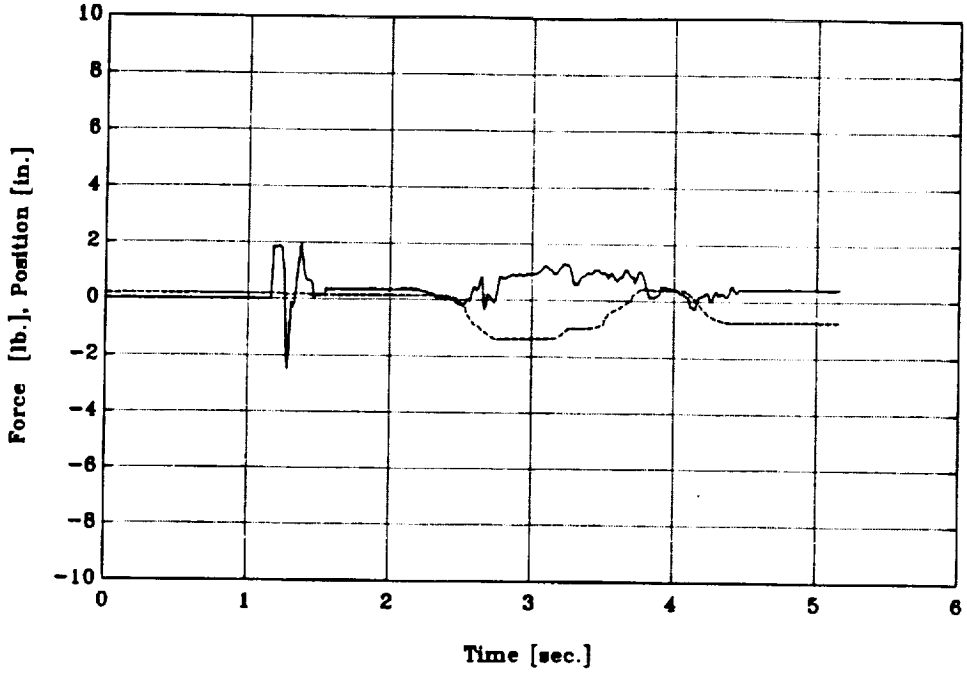

Figure B.31: Test C - Leg 1 Force History

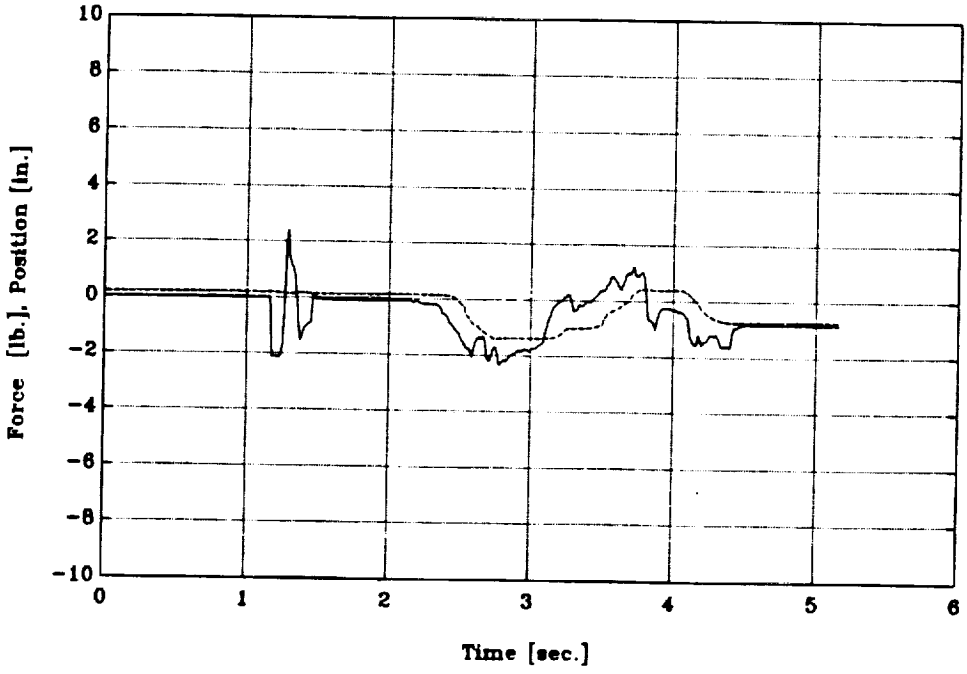

Figure B.32: Test C - Leg 2 Force History

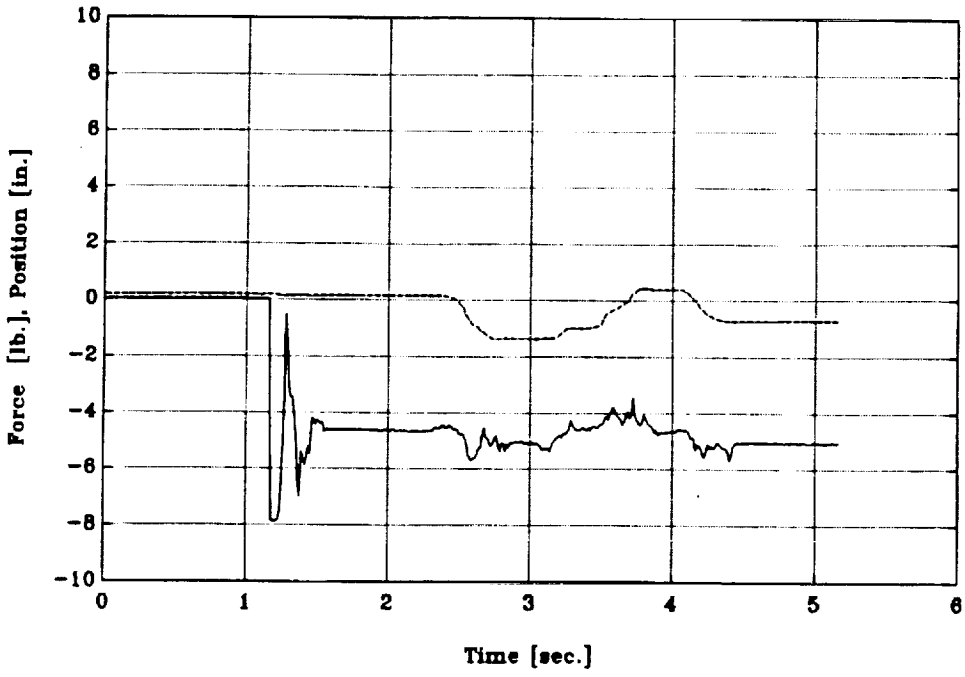

Figure B.33: Test C - Leg 3 Force History

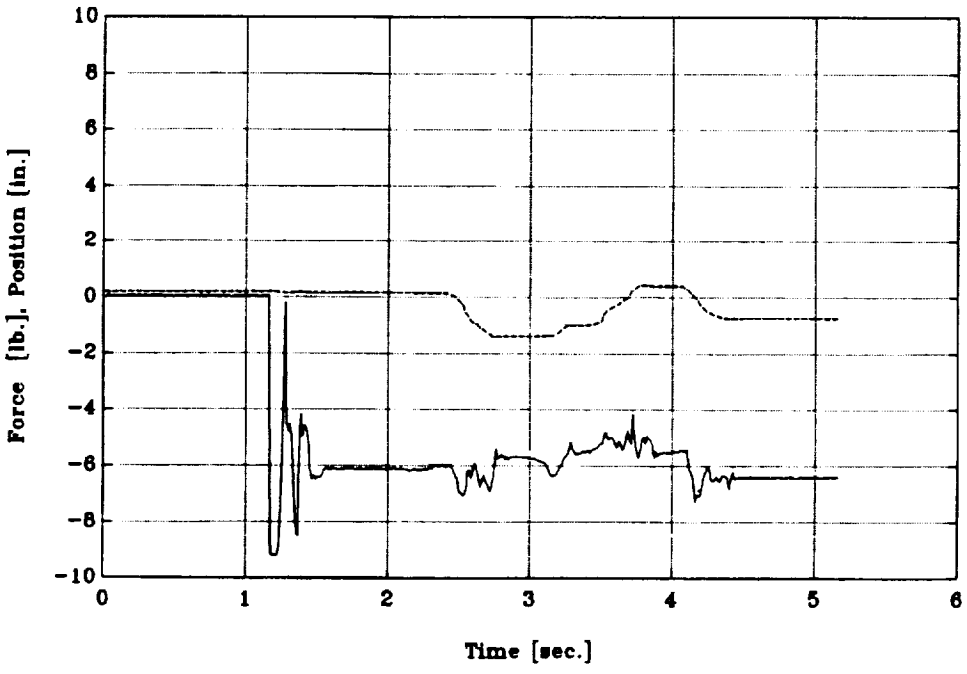

Figure B.34: Test C - Leg 4 Force History

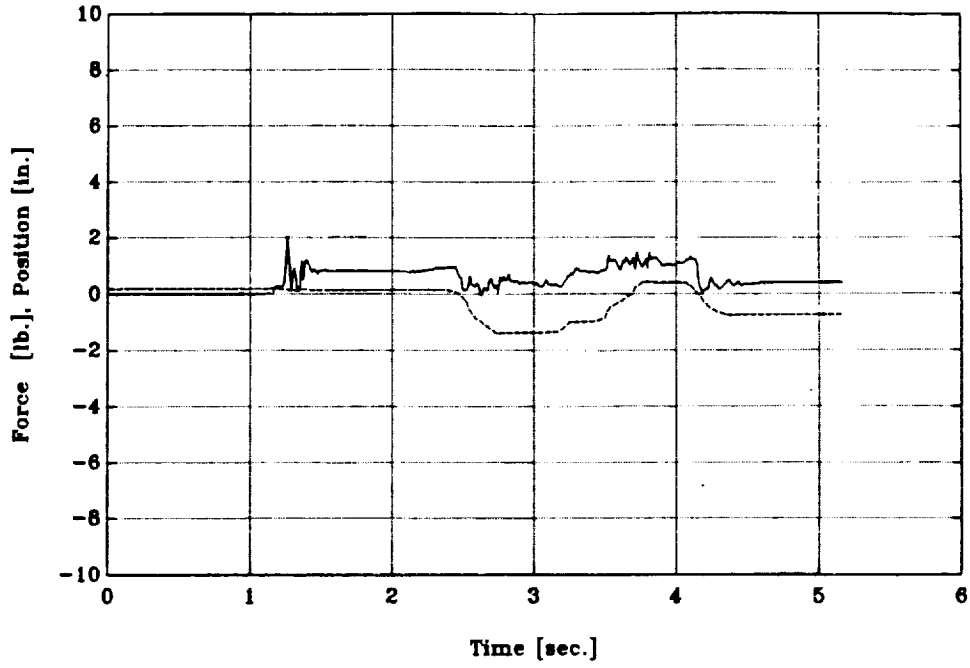

Figure B.35: Test C - Leg 5 Force History

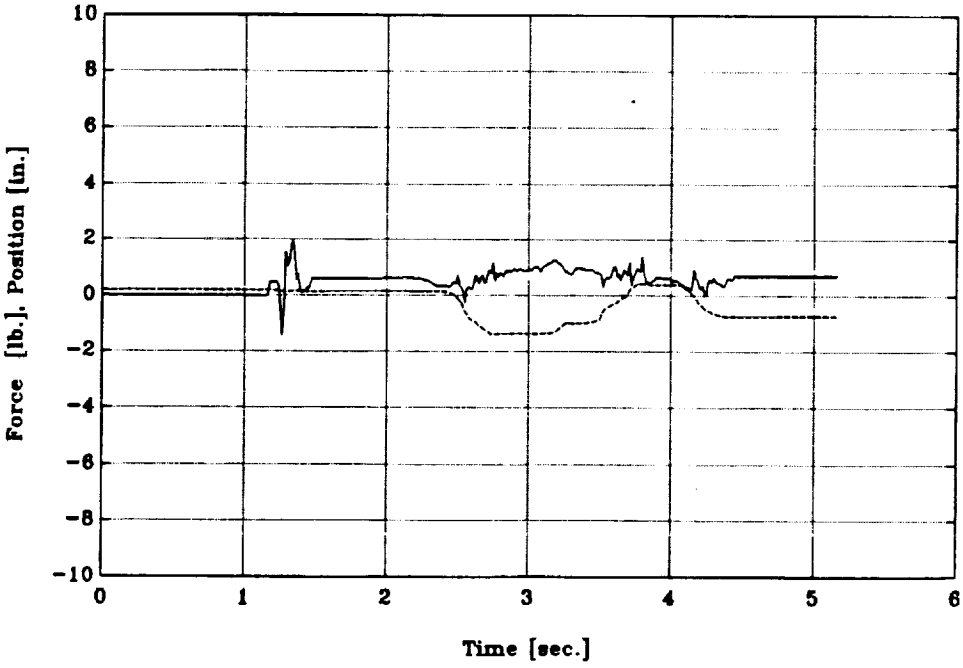

Figure B.36: Test C - Leg 6 Force History

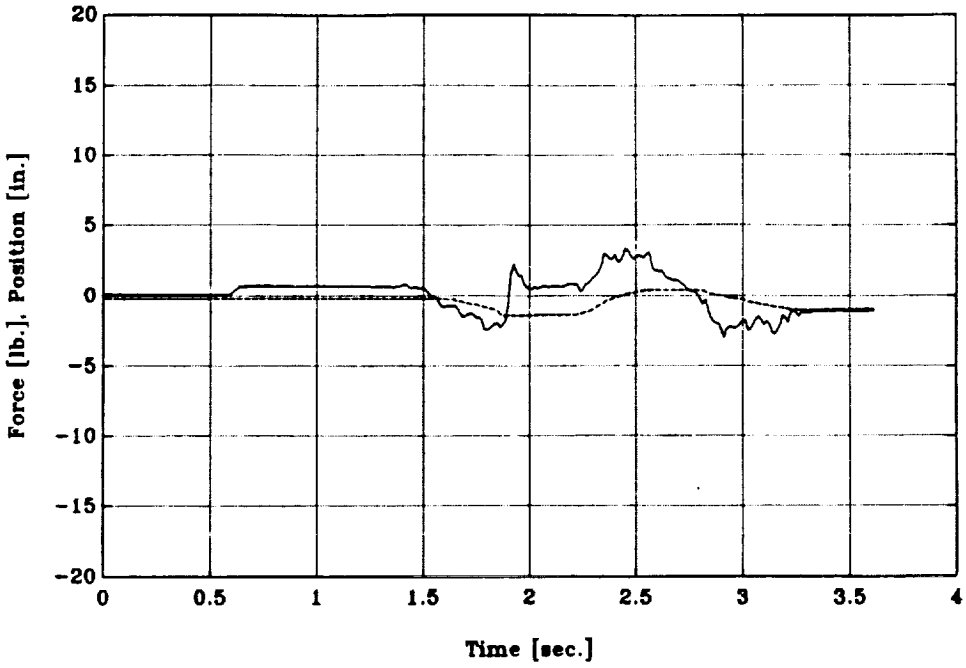

Figure B.37: Test D - Force Response in x

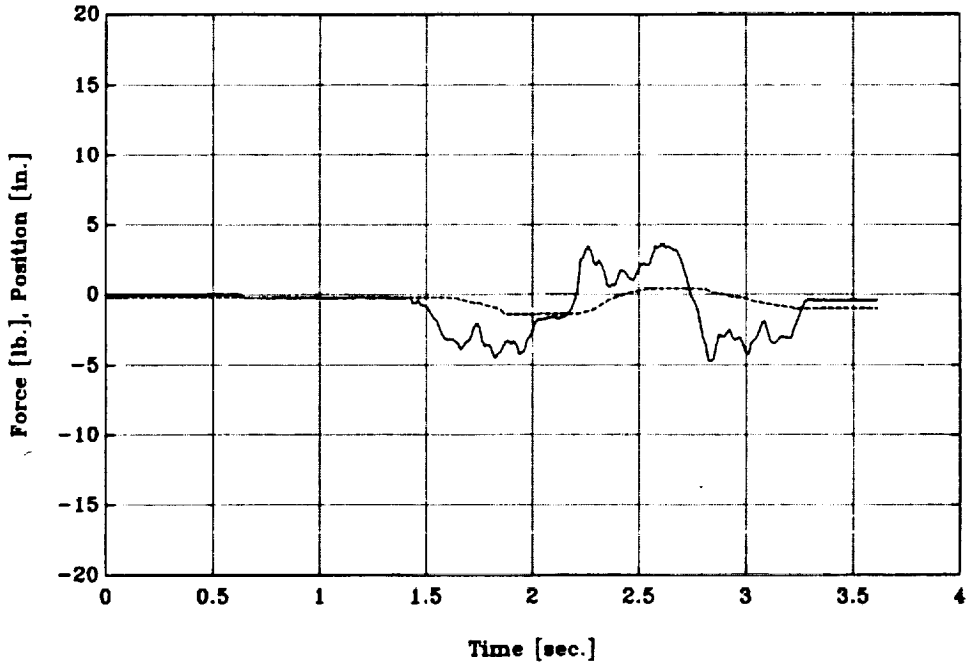

Figure B.38: Test D - Force Response in y

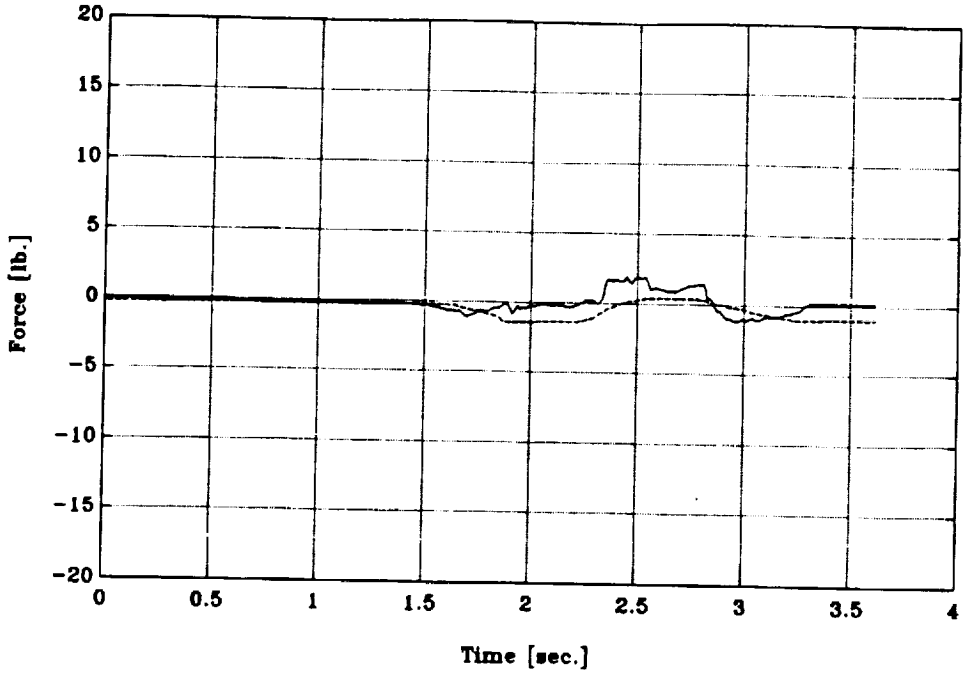

Figure B.39: Test D - Force Response in z

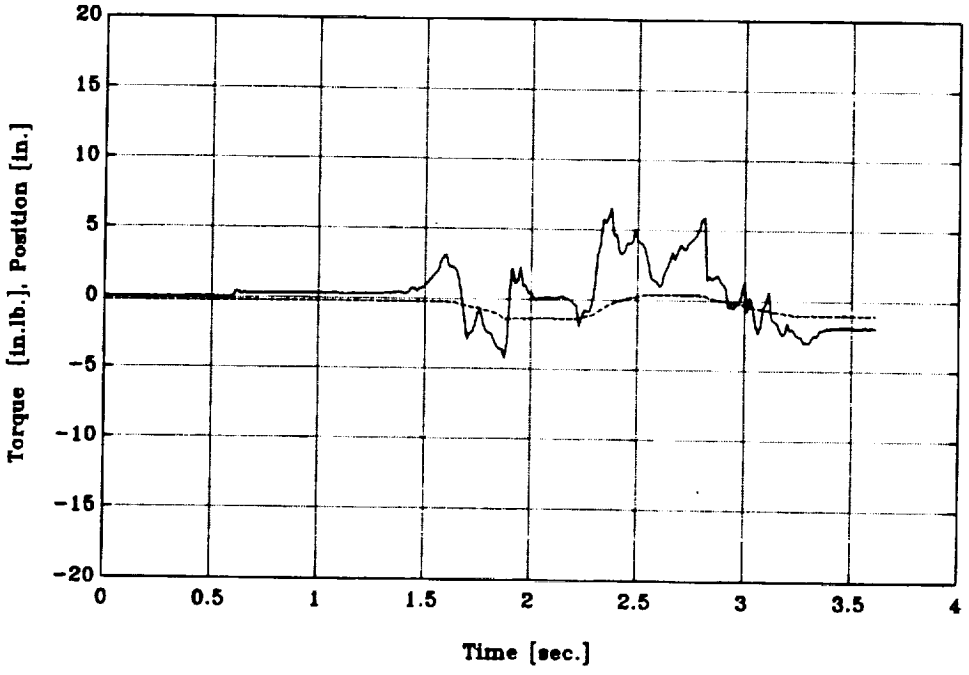

Figure B.40: Test D - Torque Response in x

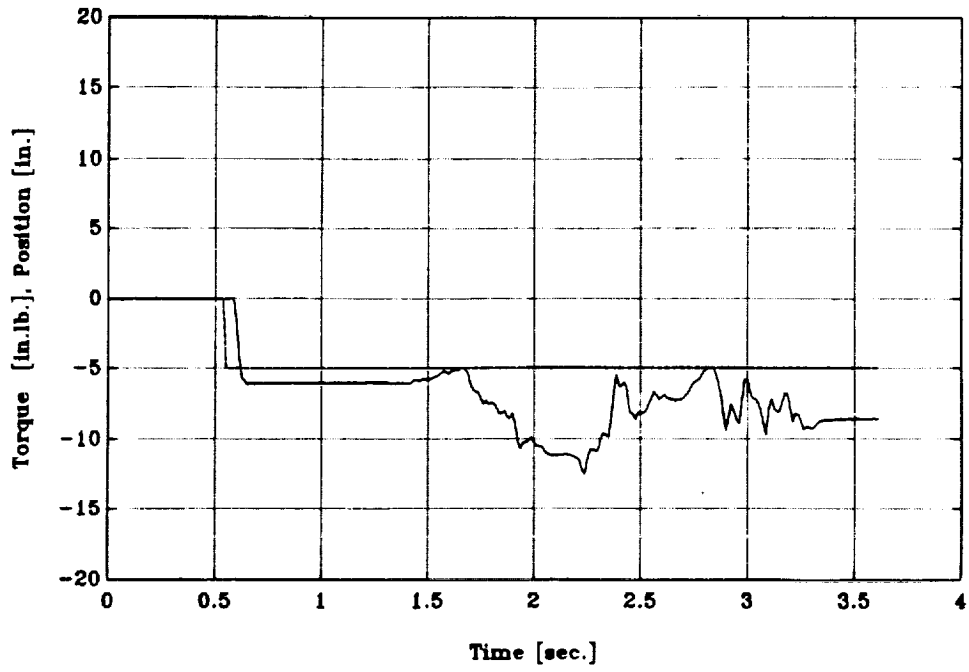

Figure B.41: Test D - Torque Response in y

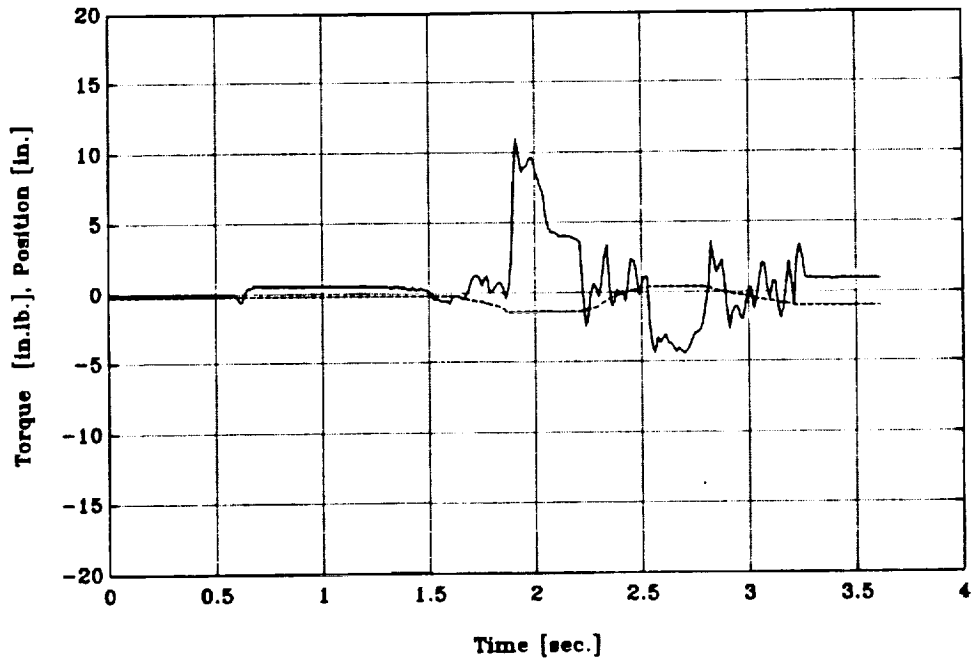

Figure B.42: Test D - Torque Response in z

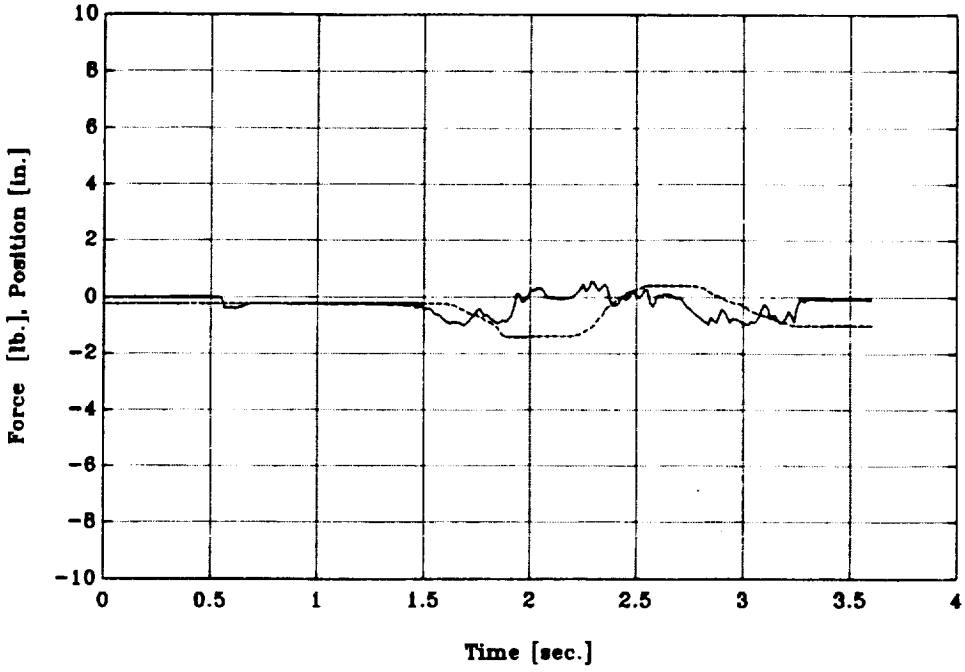

Figure B.43: Test D - Leg 1 Force History

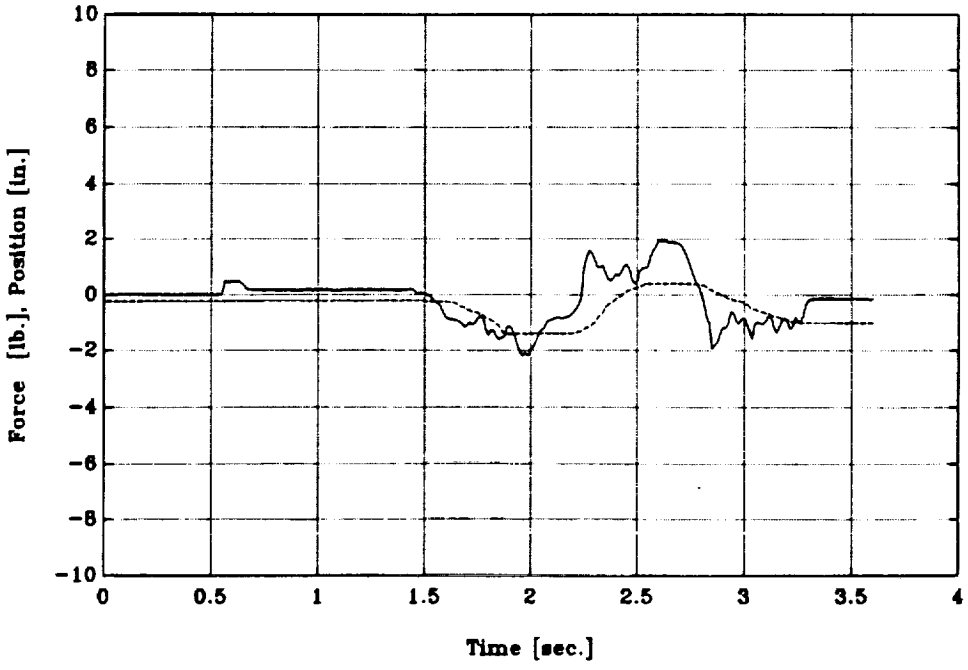

Figure B.44: Test D - Leg 2 Force History

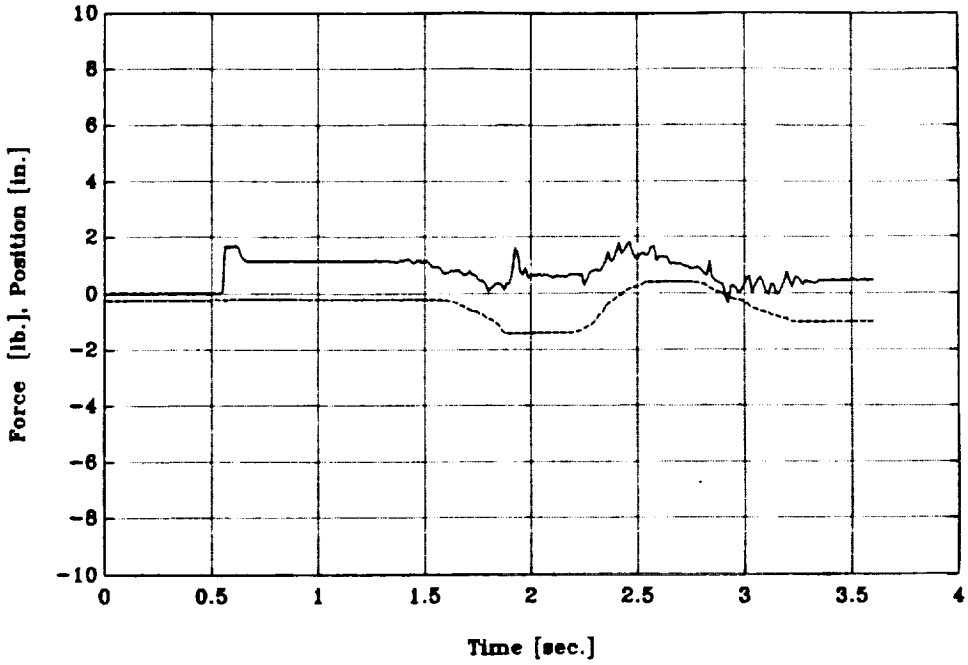

Figure B.45: Test D - Leg 3 Force History

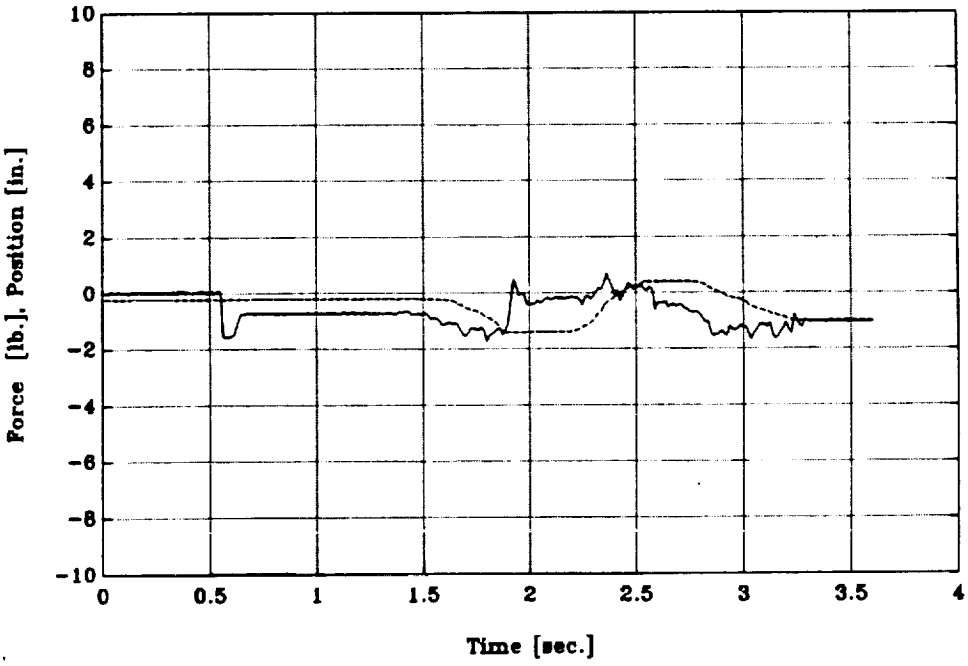

Figure B.46: Test D - Leg 4 Force History

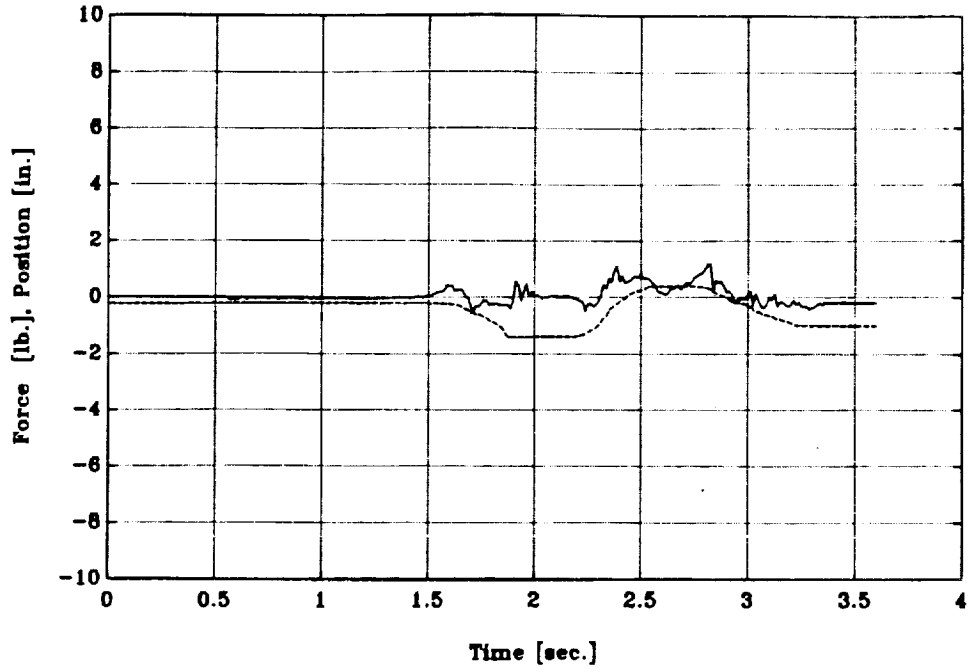

Figure B.47: Test D - Leg 5 Force History

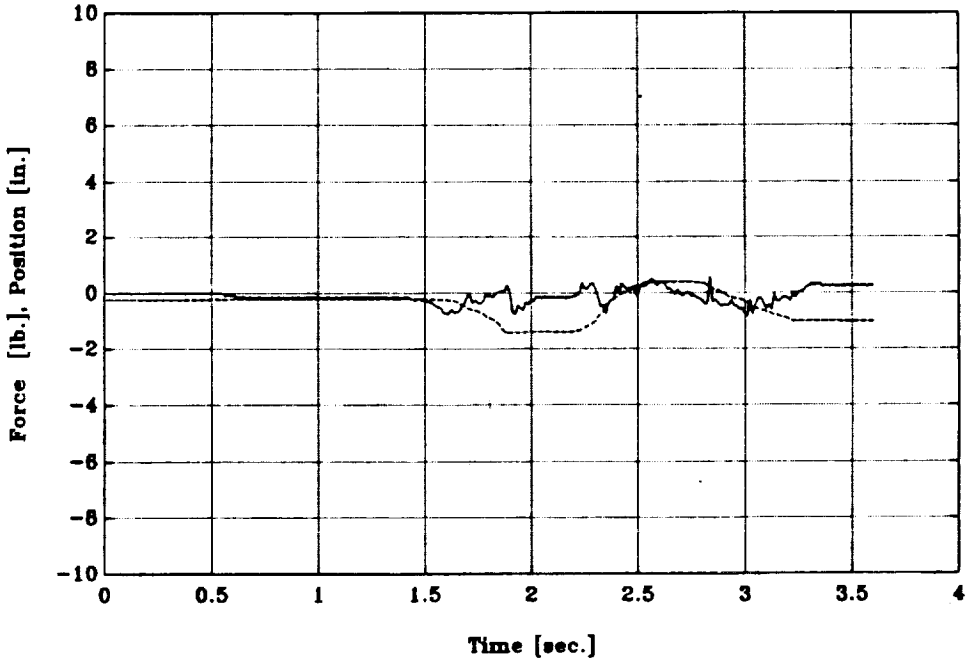

Figure B.48: Test D - Leg 6 Force History